FUNDAMENTAL MECHANISMS OF TRIBOLOGY AND THEIR IMPLICATIONS

(ONR Contract No. N00014-82-K-0520)

by
N. P. Suh, N. Saka and K. Komvopoulos

May 1989

REPORT DOCUMENTATION PAGE

1a. REPORT SECURITY CLASSIFICATION: Unclassified	1b RESTRICTIVE MARKINGS: None
2a. SECURITY CLASSIFICATION AUTHORITY: ------	3 DISTRIBUTION / AVAILABILITY OF REPORT: Unlimited
2b. DECLASSIFICATION / DOWNGRADING SCHEDULE: ------	
4. PERFORMING ORGANIZATION REPORT NUMBER(S): ------	5 MONITORING ORGANIZATION REPORT NUMBER(S)
6a. NAME OF PERFORMING ORGANIZATION: Massachusetts Institute of Technology; 6b OFFICE SYMBOL (If applicable): ---	7a NAME OF MONITORING ORGANIZATION: Office of Naval Research
6c. ADDRESS (City, State, and ZIP Code): 77 Massachusetts Avenue, Cambridge, MA 02139	7b ADDRESS (City, State, and ZIP Code): 800 North Quincy Street, Arlington, VA 22217-5000
8a. NAME OF FUNDING / SPONSORING ORGANIZATION: Office of Naval Research; 8b OFFICE SYMBOL (If applicable):	9 PROCUREMENT INSTRUMENT IDENTIFICATION NUMBER: -----
8c. ADDRESS (City, State, and ZIP Code): 800 North Quincy Street, Arlington, VA 22217-5000	10 SOURCE OF FUNDING NUMBERS

PROGRAM ELEMENT NO	PROJECT NO	TASK NO	WORK UNIT ACCESSION NO
N00014	-82-K	-0520	091-032

11 TITLE (Include Security Classification): Fundamental Mechanisms of Tribology and Their Implications

12 PERSONAL AUTHOR(S): Nam P. Suh, Nannaji Saka and Kyriakos Komvopoulos

13a TYPE OF REPORT	13b TIME COVERED	14 DATE OF REPORT (Year, Month, Day)	15 PAGE COUNT
Final technical paper	FROM 5/1/82 TO 1/31/86	30 May 1989	74

16. SUPPLEMENTARY NOTATION

17 COSATI CODES			18 SUBJECT TERMS (Continue on reverse if necessary and identify by block number)
FIELD	GROUP	SUB-GROUP	

19. ABSTRACT (Continue on reverse if necessary and identify by block number)

The objective of the proposed research was to create hard layers on metallic surfaces in boundary-lubricated sliding and to investigate their tribological behavior. In addition, the goal was to investigate the basic mechanism of friction of lubricated metallic surfaces.

We have investigated the following aspects: (a) Experimental investigation of the tribological behavior of metallic and coated surfaces in boundary lubrication and (b) Finite Element Analysis of friction and wear of the coated surfaces, and the delamination process at the interface. [illegible] Oxide [illegible] S. (Au)

20. DISTRIBUTION / AVAILABILITY OF ABSTRACT: ☒ UNCLASSIFIED/UNLIMITED ☐ SAME AS RPT ☐ DTIC USERS	21. ABSTRACT SECURITY CLASSIFICATION: Unclassified
22a. NAME OF RESPONSIBLE INDIVIDUAL: Dr Nannaji Saka	22b TELEPHONE (Include Area Code): (617)253-2227; 22c OFFICE SYMBOL: --

DD FORM 1473, 84 MAR — 83 APR edition may be used until exhausted. All other editions are obsolete.

FUNDAMENTAL MECHANISMS OF TRIBOLOGY AND THEIR IMPLICATIONS

Final Technical Report to
The Office of Naval Research

Contract No. N00014-82-K-0520

Nam P. Suh
Nannaji Saka
Kyriakos Komvopoulos

Tribology Research Program
Laboratory for Manufacturing and Productivity
School of Engineering
Massachusetts Institute of Technology
Cambridge, MA 02139

May 1989

Table of Contents

I. The Mechanisms of Friction in Boundary Lubrication 4

II. Plowing Friction in Dry and Lubricated Sliding 15

III. The Significance of Oxide Layers in Boundary Lubrication 28

IV. The Role of Hard Layers in Lubricated and Dry Sliding 40

V. Wear of Boundary-lubricated Metal Surfaces 49

The Mechanism of Friction in Boundary Lubrication

K. Komvopoulos
Mem. ASME

N. Saka

N. P. Suh

Department of Mechanical Engineering
Massachusetts Institute of Technology
Cambridge, Massachusetts 02139

The primary friction mechanism between boundary-lubricated sliding surfaces was investigated. Experiments were performed on well-polished aluminum, copper, and chromium using mineral oil lubricant. It was found that the prevailing boundary lubrication model, which is based on the adhesion between asperities and shearing of the lubricant film, cannot account for the formation of plowing grooves on polished surfaces. Scanning electron micrographs of the worn surfaces and surface profiles have shown that plowing is the dominant mechanism of friction in boundary lubrication. Theoretical analysis has shown that the coefficient of friction depends on the sharpness and the size of the entrapped wear debris or the surface asperities, and the interfacial "frictional" conditions. Reasonable agreement was obtained between theoretical and experimental friction coefficients.

I Introduction

More than sixty years ago, the phrase "Boundary Lubrication" was first introduced by Hardy. Hardy and Doubleday [1] postulated that when metallic surfaces in relative motion are separated by a thin lubricant film, friction is reduced due to the physico-chemical interactions between the sliding surfaces and the lubricant film. Consequently, the early investigations on boundary lubrication were primarily focused on such variables as molecular structure of the lubricant, environmental conditions, interfacial temperature, and physisorption and chemisorption which govern the adsorption of lubricants to solid surfaces.

Beeck et al. [2] suggested that long-chain polar molecules, when used to lubricate well-polished surfaces, form monomolecular layers by physical adsorption on metallic surfaces resulting in low friction. Bowden et al. [3] later reported that even on rough surfaces a molecular layer of soap provides effective lubrication. They emphasized that the first adsorbed monolayer was responsible for good lubrication, and that the lubricating properties depend on the chemical nature of the metallic surfaces. Bowden and Tabor [4] reported the importance of the molecular structure of the lubricant and the chain length on the friction force between boundary-lubricated surfaces. The physical properties of the lubricant film such as the film strength, contact angle, flash temperature, etc., were found to affect the friction force significantly [5, 6].

Campbell and Thurber [7] conducted experiments on steel surfaces lubricated with straight-chain hydrocarbons and observed that the environmental humidity plays a significant role in the mechanism of boundary lubrication. They hypothesized that the high friction coefficients obtained in a humid atmosphere were due to the weakly bonded and less strongly oriented lubricant molecules on an adsorbed water film. Godfrey [8, 9] stated that the important physical properties of the lubricant film are the shear strength, melting point and good adhesion to the surface, and that film formation may occur by physical or chemical adsorption. The various factors (such as atmosphere, temperature, liquid-solid interactions and chemical reactions) and their role in friction of boundary lubricated surfaces have also been reviewed by Campbell [10].

According to the prevailing boundary lubrication model, the friction force between boundary-lubricated surfaces is the weighted sum of the force necessary to shear the lubricant film, and that arising from the deformation of the surface asperities at the solid-to-solid contacts. Thus, the coefficient of friction, μ, is expressed as [3, 4]

$$\mu = \alpha\left(\frac{s_l}{p_m}\right) + (1-\alpha)\left(\frac{s_m}{p_m}\right) \quad 0 \le \alpha \le 1 \qquad (1)$$

where s_l is the shear strength of the lubricant film, s_m and p_m are the shear strength and the hardness of the softer metal respectively, and α is the proportion of the real contact area on which the lubricant adsorbs and separates the asperities.

Some basic limitations of the above boundary lubrication model are at once apparent. First, for a given set of lubricants and materials, the magnitudes of s_l, s_m, and p_m may be obtained, but the magnitude of the parameter α is not known *a priori* and, therefore, the coefficient of friction cannot be calculated directly from equation (1). Second, the boundary lubrication model predicts magnitudes for the coefficient of friction that frequently contradict the experimentally obtained friction coefficients. For example, when α reaches values close to zero, according to equation (1), $\mu \simeq s_m/p_m$. From the shear strength-hardness relationship for metals, the coefficient of friction in the limiting case is approximately equal to 0.16 which is lower than that measured in air as well as in inert atmospheres and vacuum. In order to explain this discrepancy, Rabinowicz [11] modified the ratio s_m/p_m in equation (1) by introducing the effect of the energy of adhesion. He stated that high friction coefficients may be

Contributed by the Tribology Division for publication in the JOURNAL OF TRIBOLOGY. Manuscript received at ASME Headquarters, December 7, 1984.

obtained when the ratio of the energy of adhesion to penetration hardness is high. Although this modification may explain qualitatively the experimentally obtained high friction coefficients, it cannot account for the formation of plowing grooves. In addition, the analysis considers two different modes of asperity interactions in order to obtain the normal and tangential forces and hence the coefficient of friction. The normal load was obtained by considering a hard cone indenting a softer surface while the tangential force was obtained by considering only the interfacial adhesion of flat asperities in contact. Such a separation of the modes of deformation at a single asperity contact is physically unrealistic.

In the past, much effort was also directed at the first term of equation (1). By definition, for well-lubricated surfaces α must assume values close to unity, and according to equation (1), $\mu \approx s_i/p_m$. The lowest reported coefficient of friction of boundary lubricated surfaces is about 0.04. Because the hardness, p_m, can vary by orders of magnitude, a value for μ for soft and hard materials within this range could only be produced if s_i is a function of the hydrostatic pressure, p. Indeed, Briscoe et al. [12] slid glass spheres over glass plates coated with a number of lubricants and observed that s_i increases with pressure in a roughly proportional manner. Later, Rabinowicz [13] suggested that at low hydrostatic pressures s_i is independent of the pressure, but at high pressures, s_i is proportional to the hydrostatic pressure and the ratio s_i/p_m has a value of 0.05.

Although the predictions of the first term of equation (1) appear to be in good agreement with the experimental results, there is a conceptual defect. It was assumed that plastic deformation of the metal surface occurs because of the normal load, and that the friction force arises only from shearing of the lubricant film. Such an argument is basically erroneous since the plastically deformed surface should also contribute, together with the lubricant, to friction during sliding.

A third limitation of the existing friction model is that it cannot explain the transition of the surface topography, and the variation of the friction force with sliding distance.

Numerous investigations have shown that the coefficient of friction undergoes significant changes before a steady state is reached. Recent experimental results have also shown that the coefficient of friction can assume different magnitudes when the stationary and moving specimens are reversed [14]. In order to explain the transitions of the friction coefficient with the distance slid, Suh and Sin [14] postulated that the coefficient of friction is not a material property but that it depends on the contribution of three friction mechanisms: deformation of surface asperities, plowing by wear particles entrapped at the interface and hard asperities, and adhesion. They suggested that the contribution of these friction mechanisms to the overall friction force depends not only on the sliding materials but also on the surface topography and the environment, and that the contribution by asperity deformation and plowing can be greater than that by adhesion.

It is apparent, therefore, that in addition to or in lieu of the adhesion between the asperities and the shear of the lubricant film between the sliding surfaces, some other mechanisms may occur concomitantly in boundary lubrication. Indeed, the plowing friction mechanism arising from the abrasive action of the wear debris may be important in the friction force. The purpose of this paper therefore is to identify the predominant friction mechanism in boundary lubricated sliding in light of experimental and analytical results.

II Experimental Materials and Procedures

A. Materials and Lubricant. Three metals were chosen for investigation: Pure aluminum (99.9994 percent), Oxygen Free High Conductivity (OFHC) copper (99.9994 percent), and electroplated chromium. The primary reason for this choice was the large range in the hardness of the three metals. Because the objective of this study is to investigate the fundamental friction mechanism when two lubricated metallic surfaces are sliding on each other, a relatively inert, additive-free mineral oil was used. The mineral oil consists primarily of naphthenic hydrocarbons and has the following physical properties as specified by the supplier. The density at 298 K is 0.89 g/cm^3, and the flash point temperature is 455 K. The kinematic viscosity at 310 K is 74 cSt and at 372 K it is 11 cSt.

B. Specimen Preparation.

(*a*) *Aluminum.* Disks (2.54 cm in diameter and approximately the same thickness) and cylindrical slider pins (0.635 cm in diameter with hemispherically shaped tips 0.889 cm in diameter) were used. After cutting and machining, the disk specimens were polished with 600-grit SiC abrasive paper. Then all the specimens were annealed at 673 K in argon for an hour. The annealed specimens were polished with 0.3 μm α-alumina and 0.05 μm γ-alumina to obtain a mirror finish. Then the specimens were cleaned with warm water and soap, rinsed with isopropyl alcohol and stored in a desiccator with Ca_2SO_4 at room temperature. Scanning electron micrographs obtained after polishing and rinsing the surfaces did not show any SiC or Al_2O_3 particles embedded on the surfaces (similar observations were also made for the copper and chromium surfaces after polishing). The hardness before annealing was found to be 294 MPa (30 kg/mm^2) and after annealing and polishing with alumina it was 186 MPa (19 kg/mm^2).

(*b*) *Copper.* As in the case of aluminum specimens, copper disks (2.54 cm in diameter and 1.27 cm thick) and cylindrical pins (sliders) (0.635 cm in diameter with hemispherically shaped tips of the same diameter) were used for the experiments. After machining the disk specimens from 2.54 cm diameter cold-worked rods, they were polished successively with 240, 320, and 600-grit SiC abrasive paper to obtain a smooth surface. The polished disks and the pins were then annealed at 673 K in argon for an hour to obtain a fully recrystallized structure which was free of residual stresses. The hardness after machining, and polishing with SiC abrasive paper was found to be 1,363 MPa (139 kg/mm^2), after annealing and polishing with 0.3 μm α-alumina and 0.05 μm γ-alumina it was 510 MPa (52 kg/mm^2). The specimens with mirror finish were cleaned with warm water and soap, and rinsed with isopropyl alcohol. Finally, they were stored in a desiccator with Ca_2SO_4 at room temperature to protect them from the adsorption of water vapor.

(*c*) *Chromium.* Disk specimens (2.54 cm in diameter and

Nomenclature

F = tangential force
L = normal force
h = groove depth
p = normal pressure
p_m = hardness
r = radius of spherical portion (or asperity)
s = shear stress
s_i = shear strength of lubricant film
s_m = shear strength
w = groove width
α = proportion of real contact area where the lubricant separates the surfaces
θ = angle between cone and the sliding direction
μ = coefficient of friction

Table 1 Experimental materials

Material	Hardness (MPa) Before annealing	Hardness (MPa) After annealing	Temperature of annealing (K)
Aluminum (99.9994%)	294 ± 52	186 ± 16	673
OFHC Copper (99.9994%)	1363 ± 53	510 ± 21	873
Chromium (125 μm, electroplated on AISI 1095 steel)	6590 ± 284		

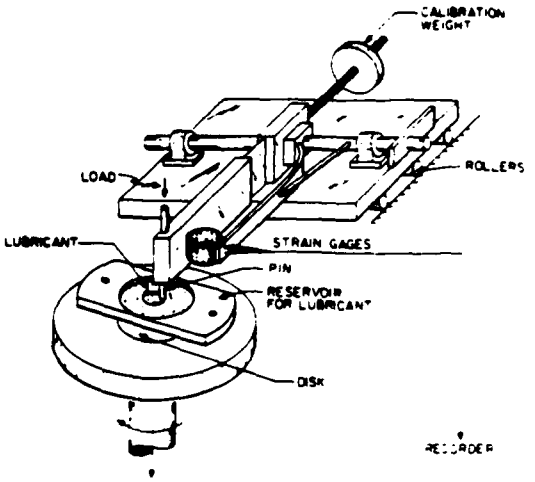

Fig. 1 Pin-on-disk experimental setup.

approximately 1.27 cm thick) were cut from AISI 1095 steel rods. Cylindrical pins (0.635 cm in diameter with hemispherically shaped tips of the same diameter) were prepared after cutting and machining AISI 1095 rods of equal diameter. After machining and cleaning, the steel specimens were polished with abrasive cloth to obtain a smooth surface. Then the steel specimens were electroplated with chromium, approximately 125 μm thick. After electroplating with chromium, in order to obtain a mirror finish, the disk and pin specimens were polished with 320 and 600-grit SiC abrasive paper and 0.3 μm α-alumina. The hardness of the AISI 1095 steel after machining was 3,501 MPa (357 kg/mm^2) while the hardness of the electroplated chromium on the steel specimens was 6,590 MPa (672 kg/mm^2). All the specimens were cleaned with warm water and soap, rinsed with isopropyl alcohol and stored in a desiccator with Ca_2SO_4 at room temperature.

Table 1 shows the experimental materials with their hardnesses before and after annealing, and the annealing temperatures.

C. Apparatus. The pin-on-disk geometry was used to conduct the friction and wear experiments. The experimental apparatus is shown in Fig. 1. The disk specimen was mounted firmly on a plate which was rotated at 4.5 rad/s (43 revolutions/min) and the pin was held stationary in a holder which was attached to a strain ring. A polymethylmethacrylate container was attached to the rotating disk to provide a reservoir for the lubricant during the lubricated tests. At the end of each experiment, the loose debris and mineral oil were removed by cleaning with warm water and isopropyl alcohol. All the tested specimens were cleaned with acetone in an ultrasonic vibrating container for a few minutes and then dried carefully before observing in the Scanning Electron Microscope. The experimental conditions are listed in Table 2. Some dry experiments under the same conditions were also conducted for comparison.

D. Friction and Wear Measurements. The tangential force was measured continuously by the strain gages mounted

Table 2 Test conditions

Load	2N (204g)
Angular speed	4.5 rad/s
Tangential speed	0.6 cm/s to 4.32 cm/s
Sliding distance	0.03m to 100m
Temperature	294 K
Lubricant	mineral oil*
Relative humidity	22 to 30%
Environment	laboratory air
*density at 298 K,	0.89 g/cm^3
viscosity at 310 K,	74 cSt
viscosity at 372 K,	11 cSt
flash point temperature	455 K

on the strain ring and by a recorder which was balanced and calibrated before each experiment. The continuously recorded tangential force was used to calculate the coefficient of friction for each experiment. For each material at least four experiments were conducted depending on the scatter in the data. For calculating the standard deviation in the coefficient of friction, the experimental data were assumed to follow a normal distribution.

The wear tracks were observed in a Scanning Electron Microscope (SEM). Because of very low wear rates in the lubricated experiments, a profilometer was used to trace the wear tracks normal to the sliding direction. For each experiment at least three profiles of the wear track at different locations were used for estimating the wear volume of the disk specimens. The wear volume of each pin was estimated based on the diameter of the circular worn surface and the radius of the hemispherical tips. For the calculation of the standard deviation in the wear rates and wear coefficients, the experimental values were assumed to follow again a normal distribution. Energy Dispersive X-ray Analyzer was used to check whether the AISI 1095 steel subsurface was exposed during the tests.

III Experimental Results

The friction coefficients of aluminum, copper, and chromium sliding on themselves for both dry and lubricated sliding conditions are shown in Fig. 2. In dry sliding the coefficient of friction has initially a low value and gradually increases until it reaches a maximum. Then it either drops or remains constant. In the case of aluminum, the coefficient of friction has a high initial value of 0.85 and after a sliding distance of approximately 2 m it reaches a maximum value of 1.2. Then it decreases rapidly to a steady value of 0.73. Unlike aluminum, copper shows a lower initial coefficient of friction of 0.3, but after a sliding distance of 3 m it reaches a maximum of 0.96 without changing as the distance slid increases. Like copper, chromium has a coefficient of friction initially about 0.3, but the maximum value is 0.77 which is reached after 2 m of sliding. Then it decreases gradually to a steady state value of 0.6.

When the metallic surfaces are lubricated, the coefficient of friction decreases substantially. Again, aluminum shows the highest initial coefficient of friction, but the steady state coefficients of friction for the three metals are almost the same. Aluminum has an initial coefficient of friction equal to

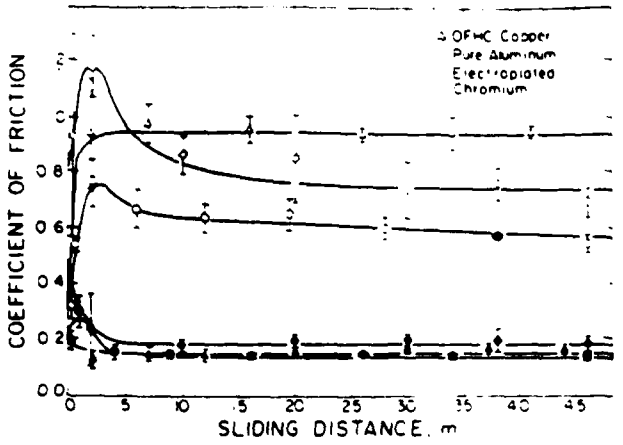

Fig. 2 Coefficient of friction versus sliding distance for aluminum, copper, and chromium sliding on themselves. The filled symbols represent lubricated experiments.

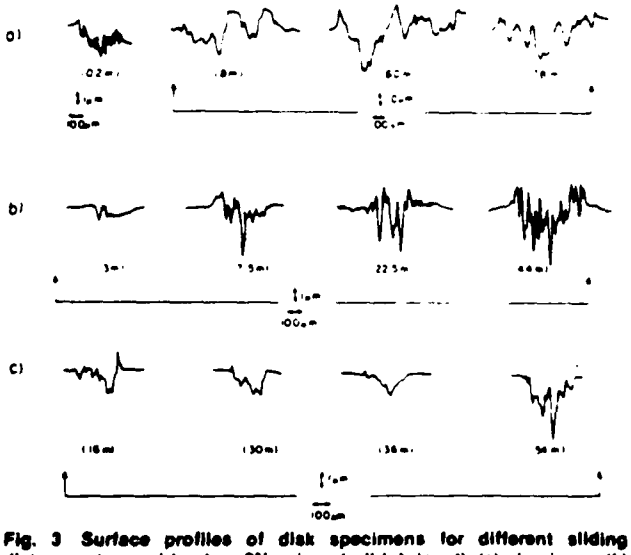

Fig. 3 Surface profiles of disk specimens for different sliding distances (normal load = 2N, mineral oil lubricant): (a) aluminum, (b) copper, and (c) chromium.

0.15 and rapidly reaches a maximum value of 0.45. After 5 m of sliding it reaches a steady state equal to 0.2. The coefficient of friction for copper assumes initially a magnitude equal to 0.1 and rapidly increases to a value equal to 0.18. The steady state value is about 0.17. Chromium shows an initial coefficient of friction equal to 0.13; after 0.5 m it reaches a maximum equal to 0.4 and then rapidly decreases to a steady state value, 0.15.

With the exception of the initial coefficient of friction of aluminum (unlubricated), the initial coefficient of friction for all the other cases lies between 0.1 and 0.3. This is in agreement with recent experimental observations [14].

Selected surface profiles of lubricated disk specimens are shown in Fig. 3. In the case of aluminum (Fig. 3, top row), the surface profiles of the wear tracks indicate that the roughness increases until a steady state is reached and then it remains the same. When the steady-state roughness is reached, grooves 10–30 μm deep have been formed. The middle row of Fig. 3 shows some characteristic surface profiles of copper disk specimens. The surface profiles again clearly show a drastic change of the initial surface topography. As sliding continues, deeper grooves are formed until a steady state is reached. However, in this case the depth of the plowing grooves remains below 4 μm. In Fig. 3, the bottom row shows the

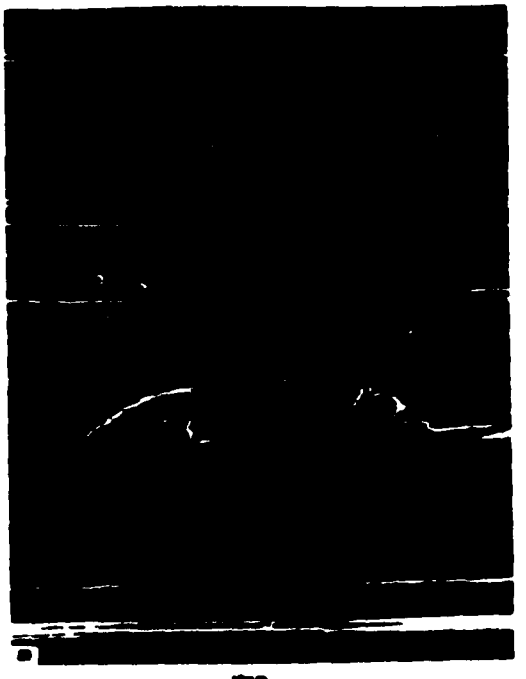

Fig. 4(a)

Fig. 4(b)

Fig. 4 Wear tracks of aluminum surfaces: (a) disk and (b) pin (lubricated experiment, 1 revolution (0.028m)).

profiles of the chromium disk specimens for selected lubricated experiments. The surface profiles of the chromium wear tracks indicate that the surface topography changes rather slowly with the sliding distance while the depth of the grooves remains below 2 μm. A comparison of the surface profiles shows that the groove depth and the width of the wear track decrease as the hardness of the material increases.

The steady-state coefficients of friction with the calculated wear rates and wear coefficients, together with their standard

Table 3 Experimental results*

Material	Coefficient of friction (steady state)	Wear rate (cm^3/cm)			Wear coefficient		
		Pin	Disk	Total	Pin	Disk	Total
Pure aluminum	0.20 ± 0.02	$(1.2 \pm 1.1) \times 10^{-8}$	$(3.4 \pm 2.2) \times 10^{-8}$	$(4.3 \pm 2.1) \times 10^{-8}$	$(3.3 \pm 3.1) \times 10^{-4}$	$(9.3 \pm 0.6) \times 10^{-4}$	$(1.2 \pm 0.6) \times 10^{-3}$
OFHC Copper	0.17 ± 0.02	$(3.7 \pm 1.8) \times 10^{-10}$	$(1.6 \pm 1.0) \times 10^{-9}$	$(2.0 \pm 1.1) \times 10^{-9}$	$(2.8 \pm 1.4) \times 10^{-5}$	$(1.2 \pm 0.8) \times 10^{-4}$	$(1.5 \pm 0.9) \times 10^{-4}$
Electroplated Chromium	0.15 ± 0.01	$(7.5 \pm 0.2) \times 10^{-11}$	$(6.5 \pm 2.0) \times 10^{-10}$	$(6.6 \pm 2.2) \times 10^{-10}$	$(7.4 \pm 0.2) \times 10^{-5}$	$(6.4 \pm 2.0) \times 10^{-4}$	$(6.5 \pm 2.1) \times 10^{-4}$

*Lubricated experiments

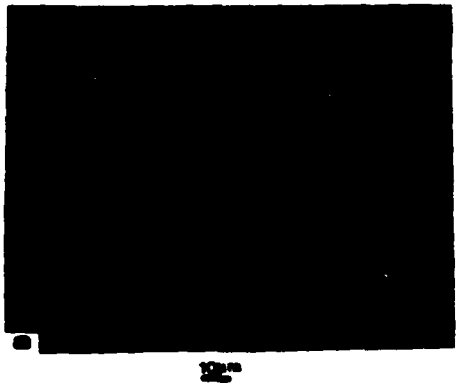

Fig. 5(a)

Fig. 5(b)

Fig. 5 Wear tracks of copper surfaces: (a) disk and (b) pin (lubricated experiment, 1 revolution (0.028m)).

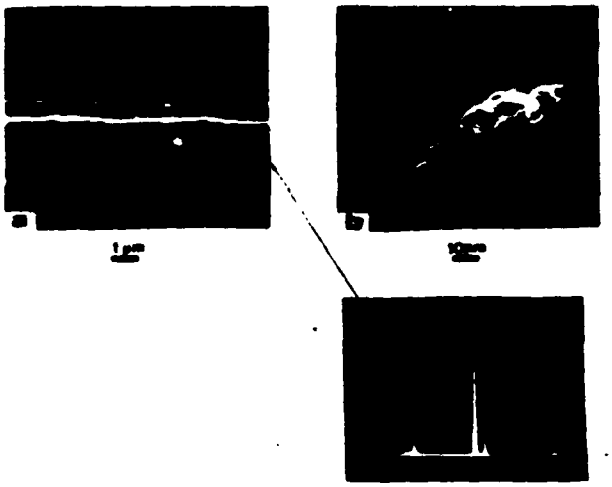

Fig. 6 Wear tracks of chromium surfaces: (a) disk and (b) pin (lubricated experiment, 1 revolution (0.028m)).

deviations, are shown in Table 3. The results indicate that the material hardness affects significantly the wear rate of the experimental materials, while the effect of hardness on the coefficient of friction, although noticeable, is marginal. However, the general trend that hard materials have low friction and wear seems to be followed also in boundary lubrication. The calculated wear rate and wear coefficient of aluminum are higher by an order of magnitude approximately than those for copper and chromium. These results are in agreement with the surface profiles of the wear tracks (Fig. 3).

In order to observe how the topography of the wear track changes during sliding, scanning electron micrographs of the worn surfaces were obtained as a function of the distance slid. Although extremely smooth surfaces were used in the experiments, plowing grooves were formed on the sliding surfaces immediately. The number of the plowing grooves and the width of the wear tracks were found to increase with the distance slid until a steady state was reached. Figures 4-6 show the worn surfaces of aluminum, copper and chromium disk and pin specimens, respectively, after one revolution. Plowing grooves have been formed on all the surfaces indicating that plowing takes place from the very beginning of sliding. A comparison of the worn surfaces shown in Figs. 4-6, shows that the number of plowing grooves decreases as the hardness of the material increases. Material adherence on the surfaces can also be seen, especially in Figs. 4(a) and 6(b). Some typical wear tracks after a large number of revolutions are shown in Figs. 7-9. In all cases the surfaces have been plastically deformed and many plowing grooves have been formed on both surfaces. Figure 7 shows that the aluminum disk and pin specimens suffered extensive surface damage and numerous plowing grooves have been formed especially on the pin surface. Figure 8 shows, in contrast with aluminum, that the copper surfaces have been less plastically deformed, but fine plowing grooves have been formed. It can be seen that the ridges of some plowing grooves have been ruptured and many microchips have been formed. Figure 9 shows the plastically deformed surfaces of two chromium specimens. Plowing grooves are noticeable on the disk specimen and material adherence on the pin surface can be seen. Rupture of ridges and formation of microchips can also be seen on the disk surface similar to what was found on the copper disk surface (Fig. 8(a)). A comparison of the worn surfaces shown in Figs. 7-9 indicates that the number of relatively large plowing grooves and the width of the wear track decrease as the hardness of the metal increases. This observation is consistent with the estimated wear rates for the three metals (Table 3) and the surface profiles (Fig. 3).

20μm

Fig. 7(a)

100μm

Fig. 7(b)

Fig. 7 Wear tracks of aluminum surfaces: (a) disk and (b) pin (lubricated experiment, 1,880 revolutions (31.8m)).

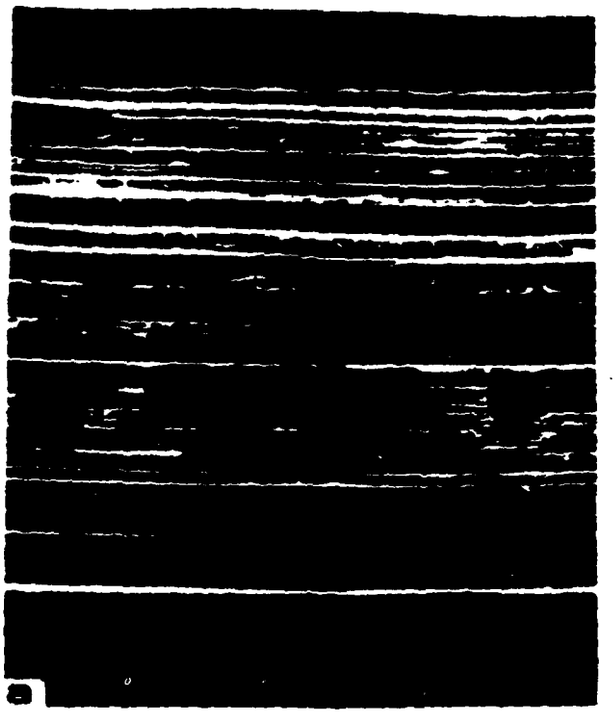

20μm

Fig. 8(a)

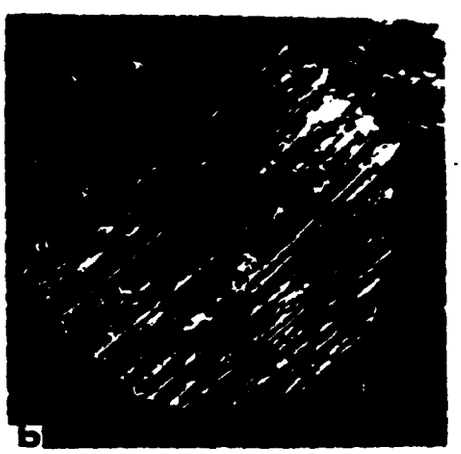

50μm

Fig. 8(b)

Fig. 8 Wear tracks of copper surfaces: (a) disk and (b) pin (lubricated experiment, 2,140 revolutions (32m)).

IV Discussion

The experimental results of this investigation clearly demonstrate the significance of the plowing mechanism of friction in boundary lubrication. The drastic changes the surface topography undergoes, as evident from the surface profiles and the scanning electron micrographs, can be explained only by the plowing friction mechanism. The fact that plowing grooves were found on extremely well-polished surfaces at the onset of sliding, emphasizes the role of the wear particles in friction. Because the wear particles could be harder, due to work hardening, than the metal surfaces from which they are formed, they indent and plow both surfaces, as the surfaces slide past each other, forming grooves and further wear debris. The new wear particles when entrapped at the interface cause progressive damage to the metal surfaces by further plowing. However, some of the wear particles can be extruded from the wear track and pushed away from the interface.

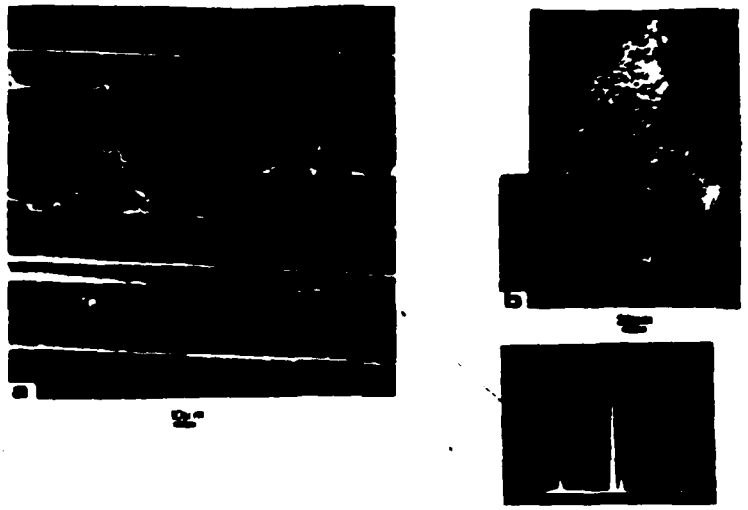

Fig. 9 Wear tracks of chromium surfaces: (a) disk and (b) pin (lubricated experiment, 1,920 revolutions (54.4m)).

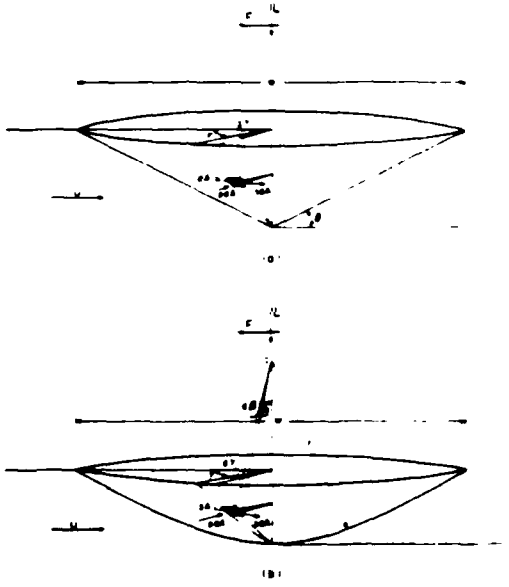

Fig. 10 Idealized models of wear debris: (a) cone and (b) sphere.

Plowing can also occur from fragmentation of the ridges formed along the sides of the plowing grooves and from material transferred and strongly adhered to the surfaces. In this case, the transferred fragment can act as a hard abrasive grain and plow the surface from which it was transferred.

In order to calculate the coefficient of friction due to plowing, it is assumed that the entrapped wear particles are either conical or spherical. The experimentally obtained coefficients of friction are then compared with those obtained from the conical and spherical models to estimate the contribution of the plowing mechanism to the total friction force.

Bowden et al. [15] were among the first who attempted to model the plowing mechanism in dry sliding. Assuming a spherical or a cylindrical shape for the hard asperity, they obtained simple expressions for the plowing force. Bowden et al. found that when a small hemispherical slider of steel slides on unlubricated indium, plowing accounts for as much as one-third of the total friction. Theoretical calculations for such simple shapes as cones, spheres and pyramids have also been made by many investigators [16–18], and the experimental results agree fairly closely with the predictions of these models [17].

For a conical asperity (Fig. 10(*a*)), the normal and tangential forces acting on an elemental area, dA, respectively, are

$$dL = p\cos\theta\, dA \tag{2}$$

$$dF = p\sin\theta\cos\gamma\, dA + s\sin\gamma\, dA \tag{3}$$

where $dA = \sec\theta\, r\, dr\, d\gamma$, and p and s are the normal pressure and the shear stress, respectively, acting on the elemental area as the cone plows. Integration of equations (2) and (3) over the front half of the conical surface where contact occurs yields the total normal and tangential forces, respectively, as

$$L = \frac{\pi w^2}{8} p \tag{4}$$

$$F = \frac{w^2}{4} p\left[\tan\theta + \left(\frac{s}{p}\right)\sec\theta\right] \tag{5}$$

where w is the diameter of indentation. The coefficient of friction can be obtained, by dividing equation (5) by equation (4), as

$$\mu = \frac{2}{\pi}\left[\tan\theta + \left(\frac{s}{p}\right)\sec\theta\right] \tag{6}$$

For a spherical asperity (Fig. 10(*b*)) the normal and tangential forces acting on an infinitesimal area, dA, can be expressed as

$$dL = p\cos\beta\, dA \tag{7}$$

$$dF = p\sin\beta\cos\gamma\, dA + s\sin\gamma\, dA \tag{8}$$

where $dA = r^2\sin\beta\, d\beta\, d\gamma$, and r is the radius of the sphere. Integrating the above two equations over the front half of the sphere where contact occurs, the total normal and tangential forces can be expressed as

$$L = \frac{\pi w^2}{8} p \tag{9}$$

$$F = pr^2\left[\sin^{-1}\left(\frac{w}{2r}\right) - \left(\frac{w}{2r}\right)\left\{1 - \left(\frac{w}{2r}\right)^2\right\}^{1/2}\right] + 2sr^2\left[1 - \left\{1 - \left(\frac{w}{2r}\right)^2\right\}^{1/2}\right] \tag{10}$$

The coefficient of friction is obtained, by dividing equation (10) by equation (9), as

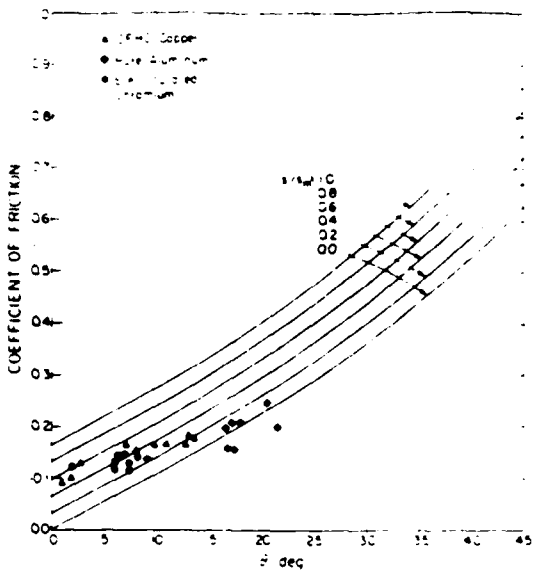

Fig. 11 Coefficient of friction for a conical asperity as a function of the angle θ for different boundary "frictional" conditions. Points represent experimental data obtained from lubricated experiments with aluminum, copper, and chromium sliding on themselves.

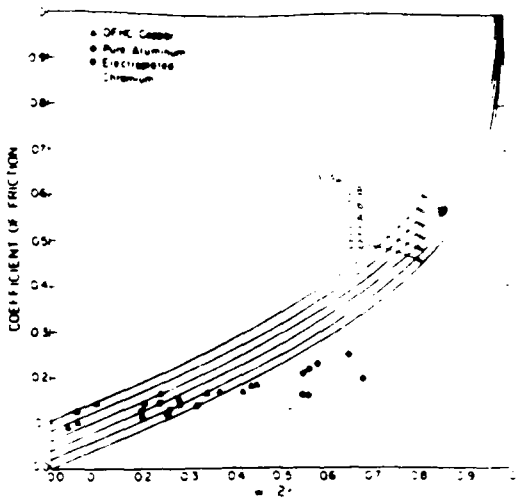

Fig. 12 Coefficient of friction for a spherical asperity as a function of the ratio of groove width to diameter of sphere for different boundary "frictional" conditions. Points represent experimental data obtained from lubricated experiments with aluminum, copper, and chromium sliding on themselves.

$$\mu = \frac{2}{\pi}\left(\frac{2r}{w}\right)^2\left[\sin^{-1}\left(\frac{w}{2r}\right) - \left(\frac{w}{2r}\right)\left\{1-\left(\frac{w}{2r}\right)^2\right\}^{1/2} + 2\left(\frac{s}{p}\right)\left[1-\left\{1-\left(\frac{w}{2r}\right)^2\right\}^{1/2}\right]\right] \quad (11)$$

where w is the diameter of indentation.

It is reasonable to assume that the normal pressure p is approximately equal to the hardness, p_m, of the material being plowed which is equal to $6s_m$, where s_m is the shear strength. Using this assumption, equations (6) and (11) may be rewritten as

$$\mu = \frac{2}{\pi}\left[\tan\theta + \frac{1}{6}\left(\frac{s}{s_m}\right)\sec\theta\right] \quad (12)$$

$$\mu = \frac{2}{\pi}\left(\frac{2r}{w}\right)^2\left[\sin^{-1}\left(\frac{w}{2r}\right) - \left(\frac{w}{2r}\right)\left\{1-\left(\frac{w}{2r}\right)^2\right\}^{1/2} + \frac{1}{3}\left(\frac{s}{s_m}\right)\left[1-\left\{1-\left(\frac{w}{2r}\right)^2\right\}^{1/2}\right]\right] \quad (13)$$

Depending on the interfacial conditions the ratio s/s_m can assume values between zero and unity. For "ideal" interfacial lubrication, the interfacial shear stress, s, is the shear strength of the lubricant film, s_l, which is very small in comparison to the metal shear strength, s_m. In this case, the ratio s/s_m approaches a value close to zero and equations (12) and (13) can be rewritten as

$$\mu = \frac{2}{\pi}\tan\theta \quad (14)$$

$$\mu = \frac{2}{\pi}\left(\frac{2r}{w}\right)^2\left[\sin^{-1}\left(\frac{w}{2r}\right) - \left(\frac{w}{2r}\right)\left\{1-\left(\frac{w}{2r}\right)^2\right\}^{1/2}\right] \quad (15)$$

On the other hand, for dry sliding conditions, cold welding at the interface takes place and the interfacial shear stress, s, approaches the shear strength of the metal, s_m, and the ratio s/s_m has a value equal to one. The friction curves obtained from equations (12) and (13) and for s/s_m equal to 0 and 1 represent extreme values; in reality it assumes an intermediate value.

Figure 11 shows several friction curves obtained from equation (12) (conical asperity) as a function of the angle θ and for different interfacial "frictional" conditions. It can be seen that the experimental points fall closer to the bottom friction curves. Figure 12 shows the friction curves obtained from equation (13) (spherical asperity) as a function of the ratio $w/2r$ for different interfacial "frictional" conditions (similar to those for the conical asperity). The experimental points again fall closer to the bottom friction curves. Both models clearly show that the experimental points fall closer to the lower curve (i.e., the $s/s_m = 0$ curve). (The experimental values of θ and $w/2r$ were obtained from the surface profiles as shown in the Appendix.) A comparison between Figs. 11 and 12 shows that in the case of large wear particles (i.e., large magnitudes of θ or $w/2r$) the conical model is in better agreement with the experimental results. This may be an indication that large wear particles are rough and angular in contrast to small wear particles which may be smooth and round and thus can be idealized as spheres. The most important result of this analysis, however, is that the coefficient of friction as predicted by the conical and spherical models is in good agreement with the experimental results. Table 4 lists the steady state values of θ and $w/2r$, obtained from lubricated experiments, the calculated friction coefficients from equations (12) and (13) for $s/s_m = 0.1$, which is a reasonable assumption for boundary lubricated surfaces, and the experimental coefficients of friction. The agreement between theoretical and experimental friction coefficients is reasonably good.

The analysis performed above using conical and spherical models to estimate the coefficient of friction considers the transition of the surface topography and the size of the wear particles in addition to the shear strength of the solid surfaces and the lubricant film. Both models give good estimates for the coefficient of friction and also explain semi-quantitatively the variation of the friction coefficient with the size of the wear particles and/or the surface roughness and the effect of the lubricant on the coefficient of friction through the interfacial friction conditions (i.e., magnitude of s/s_m).

It is well known that when a lubricant is introduced at the interface of two sliding surfaces, wear is reduced by orders of magnitude. Experimental results under dry sliding conditions verify the above statement. Indeed, it was found that the wear rates of aluminum and copper under dry conditions were both

Table 4 Theoretical and experimental coefficients of friction*

Material	Theoretical coefficient of friction				Experimental coefficient of friction
	Conical model		Spherical model		
	θ (deg)	Coefficient of friction ($s/s_m = 0.1$)	$w/2r$	Coefficient of friction ($s/s_m = 0.1$)	
Pure aluminum	19 ± 2	0.23 ± 0.04	0.62 ± 0.05	0.31 ± 0.03	0.20 ± 0.02
OFHC Copper	11 ± 2.5	0.14 ± 0.04	0.37 ± 0.08	0.17 ± 0.04	0.17 ± 0.02
Electroplated chromium	6 ± 0.7	0.08 ± 0.02	0.23 ± 0.02	0.11 ± 0.02	0.15 ± 0.01

*Steady state values

Table 5 Parameters of surface topography and friction coefficients at steady state

Material	Groove depth (μm)	θ (deg)	$w/2r$	Experimental coefficient of friction
Dry experiments				
Pure aluminum	10-60	29 ± 3	0.83 ± 0.05	0.73 ± 0.04
OFHC Copper	5-30	16 ± 2	0.53 ± 0.06	0.96 ± 0.02
Electroplated chromium	2-3	7 ± 1	0.23 ± 0.04	0.60 ± 0.03
Lubricated experiments				
Pure aluminum	10-30	19 ± 2	0.62 ± 0.05	0.20 ± 0.02
OFHC Copper	<4	11 ± 2.5	0.37 ± 0.08	0.17 ± 0.02
Electroplated chromium	<2	6 ± 0.7	0.23 ± 0.02	0.15 ± 0.01

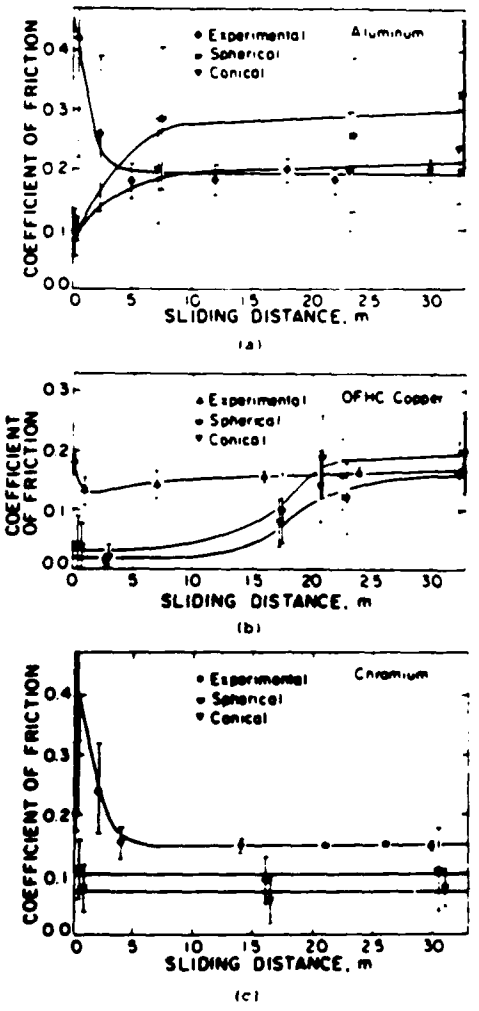

Fig. 13 Experimental and calculated plowing friction coefficients versus sliding distance obtained from lubricated experiments: (a) aluminum on aluminum, (b) copper on copper, and (c) chromium on chromium.

of the order of 10^{-7} cm^3/cm while for chromium it was 10^{-8} cm^3/cm, and the wear coefficients for aluminum, copper and chromium were of the order of 10^{-3}, 10^{-4}, and 10^{-5}, respectively. It is clear that the above wear rates and wear coefficients are by one or two orders of magnitude higher than those of the lubricated experiments (Table 3). In addition, profiles of surfaces slid without lubricant showed that the surface roughness was larger, at least by a factor of two, compared to the roughness of the lubricated experiments. Table 5 lists the range of the groove depths, the steady state magnitudes of θ and $w/2r$, and the steady state coefficients of friction, for both dry and lubricated experiments. It is clear that lubrication of the sliding surfaces reduces the magnitudes of θ, $w/2r$, and s/s_m, resulting in low coefficients of friction. Figures 11 and 12 also demonstrate the validity of these remarks.

An interesting observation regarding the magnitude of the friction coefficient can be made on the basis of Figs. 11 and 12. The experimental results from the lubricated experiments fall close to the friction curve that corresponds to $s/s_m = 0$, the curve for which adhesion at the interface vanishes. This implies that the contribution of the first part of equations (12) and (13) (i.e., equations (14) and (15)) to the total friction coefficient in lubricated sliding is in general more significant than the contribution of the second part for all values of θ and $w/2r$. Equations (14) and (15) represent the friction arising from plowing of the subsurface, while the remaining second part of equations (12) and (13) represent that due to the interfacial adhesion.

To investigate the contribution of the plowing mechanism as a function of the distance slid, equations (14) and (15) were used to obtain estimates for the plowing friction coefficient and were then compared with the experimental values. The calculated plowing friction terms from the conical and spherical models and the experimental coefficient of friction are shown in Fig. 13. Figure 13(*a*) shows the calculated plowing friction curves together with the experimental curves obtained from lubricated experiments conducted on aluminum. Both the conical and spherical models show that the plowing mechanism is responsible for most of the friction force. Although initially the plowing mechanism contributes only 20 percent to the total friction, in the steady state approximately 90 percent of the total friction force is due to the plowing mechanism. Figure 13(*b*) shows the friction curves

obtained from the conical and spherical models together with the experimental friction curve obtained from experiments on copper. During the early stage, the plowing term accounts for 20 to 25 percent of the total friction force. When a distance of approximately 20 m is slid, the magnitude of the plowing term reaches 80 to 95 percent of the total friction force. Figure 13(c) shows the calculated plowing friction curves together with the experimental curve for chromium. The spherical model shows that 50 to 80 percent of the total friction is responsible for the plowing action while the conical model shows that the contribution of the plowing term to the total friction force is between 40 to 60 percent. Figure 13 clearly demonstrates that for boundary lubricated surfaces plowing is always the governing friction mechanism while adhesion between the asperities and shearing of the lubricant film have minor contributions.

Nevertheless, if plowing of the sliding surfaces vanishes, the plastically deformed volume should be reduced substantially, resulting in a very low coefficient of friction. Coating the surfaces with very hard layers will prevent plowing resulting in only elastic deformations. In this case the friction coefficient will be, $\mu = s_i(p)/p$, where $s_i(p)$ indicates that s_i is a function of the hydrostatic pressure p. Under these conditions μ can be reduced close to 0.05 [13].

The analysis based on the conical or spherical shapes of the wear particles is a simplification of the problem since the wear particles are not necessarily of a simple geometrical shape. Further, the velocity field of the material being plowed is arbitrarily chosen. The assumption that the material flows around the plowing asperity in planes parallel to the sliding surface is not quite correct. Moreover, the stresses at the surfaces of the cone and sphere are also arbitrarily assumed to have independent hydrostatic and tangential components. A more rigorous analysis based on a slip-line field is required. Although an improvement for the estimation of the plowing friction force is desirable, the main conclusion of this investigation will still remain the same, i.e., plowing is the predominant friction mechanism in boundary lubrication, while adhesion and shearing of the lubricant film are secondary.

V Conclusions

The major conclusions of this investigation are as follows:

(1) The primary steady state friction mechanism in boundary lubrication is plowing. Shear of the lubricant film between the sliding surfaces and adhesion between the asperities, although may occur, contribute less than plowing to the overall friction force.

(2) The friction model proposed in this paper for boundary lubrication accounts for the formation of plowing grooves. Both conical and spherical models show that the coefficient of friction depends on the sharpness and the size of the entrapped wear debris and the surface asperities, and the interfacial "frictional" conditions, i.e., θ, $w/2r$ and s/s_m, respectively. Reasonably good agreement between theoretical and experimental friction coefficients was obtained.

(3) The hardness of the sliding surfaces affects the plowing friction mechanism. It was found that soft materials, such as aluminum, suffered more plowing than hard materials (e.g., chromium). In any case, the plowing component contributes mostly to the total coefficient of friction.

(4) The contribution of the plowing friction mechanism to the overall friction depends also on the magnitude of the interfacial adhesion (i.e., the s/s_m ratio). The analysis has shown that for very low values of θ and $w/2r$ (i.e., for flat asperities and small wear particles) the friction force may arise primarily from adhesion and shear of the lubricant film at the solid-to-solid contacts.

Acknowledgments

This work was done under the sponsorship of the Office of Naval Research, Contract N00014-82-K-0520. The personal support of Dr. A. W. Ruff and Dr. R. S. Miller is greatly appreciated.

References

1 Hardy, W. B., and Doubleday, I., "Boundary Lubrication—The Paraffin Series," *Proc. Roy. Soc. A*, Vol. 102, 1922, pp. 550–574.

2 Beeck, O., Givens, J. W., and Smith, A. E., "On the Mechanism of Boundary Lubrication I. The Action of Long-Chain Polar Compounds," *Proc. Roy. Soc. A*, Vol. 177, 1940, pp. 90–102.

3 Bowden, F. P., Gregory, J. N., and Tabor, D., "Lubrication of Metal Surfaces by Fatty Acids," *Nature*, Vol. 156, 1945, pp. 97–101.

4 Bowden, F. P., and Tabor, D., *The Friction and Lubrication of Solids*, Clarendon Press, Oxford, 1958, pp. 176–199.

5 Boyd, J., and Robertson, B. P., "The Friction Properties of Various Lubricants at High Pressures," *Trans. ASME*, Vol. 167, 1945, pp. 51–59.

6 Appeldoorn, J. K., "Physical Properties of Lubricants," Chapter 8, *Boundary Lubrication: An Appraisal of World Literature*, Eds. Ling, F. F., Klaus, E. E., and Fein, R. S., ASME, New York, 1969, pp. 133–144.

7 Campbell, W. E., and Thurber, E. A., "Studies in Boundary Lubrication—II. Influence of Adsorbed Moisture Films on Coefficient of Static Friction Between Lubricated Surfaces," *Trans. ASME*, Vol. 70, 1945, pp. 401–408.

8 Godfrey, D., "Boundary Lubrication," *Proc. Int. Symp. on Lubr. and Wear*, Houston, Texas, 1963, pp. 283–306.

9 Godfrey, D., "Boundary Lubrication," *Interdisciplinary Approach to Friction and Wear*, NASA SP-181, 1968, pp. 335–384.

10 Campbell, W. E., "Boundary Lubrication," Chapter 6, *Boundary Lubrication: An Appraisal of World Literature*, Eds. Ling, F. F., Klaus, E. E., and Fein, R. S., ASME, New York, 1969, pp. 87–117.

11 Rabinowicz, E., *Friction and Wear of Materials*, John Wiley, New York, 1965, pp. 29–31, 65–67, 198–219.

12 Briscoe, B. J., Scruton, B., and Willis, F. R., "The Shear Strength of Thin Lubricant Films," *Proc. Roy. Soc. A*, Vol. 333, 1973, pp. 99–114.

13 Rabinowicz, E., "Friction—Especially Low Friction," *Fundamentals of Tribology*, Eds. Suh, N. P., and Saka, N., The MIT Press, Cambridge, MA, 1980, pp. 351–364.

14 Suh, N. P., and Sin, H.-C., "The Genesis of Friction," *Wear*, Vol. 69, 1981, pp. 91–114.

15 Bowden, F. P., Moore, A. J. W., and Tabor, D., "The Ploughing and Adhesion of Sliding Metals," *J. of Applied Physics*, Vol. 14, 1943, pp. 80–91.

16 Goddard, J., and Wilman, H., "A Theory of Friction and Wear during the Abrasion of Metals," *Wear*, Vol. 5, 1962, pp. 114–135.

17 Hisakado, T., "On the Mechanism of Contact between Solid Surfaces," *Bull. JSME*, Vol. 13, No. 55, 1970, pp. 129–139.

18 Tzukizoe, T., and Sakamoto, T., "Friction in Scratching without Metal Transfer," *Bull. JSME*, Vol. 18, No. 115, 1975, pp. 65–72.

APPENDIX

Calculation of θ and $w/2r$ From Surface Profiles

The experimental values of θ and $w/2r$ in Figs. 11 and 12

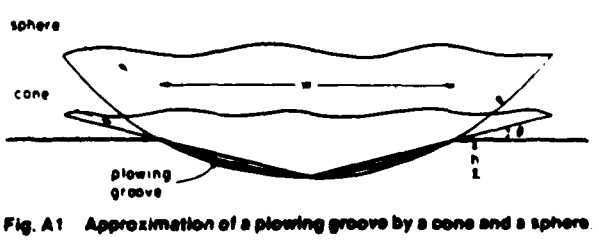

Fig. A1 Approximation of a plowing groove by a cone and a sphere

were obtained from the surface profiles. It was assumed that groove formation resulted from the plowing action of conical or spherical wear particles and or surface asperities. Figure A1 shows schematically a plowing groove formed by a conical or a spherical wear particle.

For each groove, the width, w, and the depth, h, were measured by a profilometer and the magnitude of θ was obtained from the relation

$$\theta = \tan^{-1}(2h/w) \tag{A.1}$$

Using equation (A.1) several values of θ were calculated based on measurements taken from at least four profiles of the same wear track, but at different locations and always normal to the direction of sliding. The values of θ so calculated were assumed to follow a normal distribution, and a mean value and the standard deviation for θ were obtained. It was also assumed that θ was the same both in the direction of sliding and in the transverse direction. Thus, the mean value of θ, as obtained from several profiles of the same wear track, and the corresponding coefficient of friction recorded just before the experiment was interrupted, were used to plot the experimental data in Fig. 11.

If the shape of the groove section is approximated by an arc (which is a reasonable assumption for shallow grooves) as shown in Fig. A1, then it can be assumed that groove formation resulted from plowing by spherical wear particles (or surface asperities). In this case the measured values of w and h were used again to calculate the ratio $w/2r$ as following (see Fig. A1)

$$r^2 = (r-h)^2 + (w/2)^2$$

or

$$2r = h + \frac{w^2}{4h}$$

or

$$\frac{w}{2r} = 2\left[\frac{2h}{w} + \frac{w}{2h}\right]^{-1} \tag{A.2}$$

Using equation (A.2) and following the same procedure as for the calculation of θ, a mean value and a standard deviation for $w/2r$ were obtained for each experiment and assumed to be the same both in the direction of sliding and in the transverse direction. The experimental points in Fig. 12 were then plotted based on the obtained mean values of $w/2r$ and the recorded coefficient of friction before sliding was interrupted.

Plowing Friction in Dry and Lubricated Metal Sliding

K. Komvopoulos
Mem. ASME

N. Saka

N. P. Suh

Department of Mechanical Engineering,
Massachusetts Institute of Technology,
Cambridge, Mass. 02139

Experimental evidence for plowing under dry and lubricated sliding conditions is presented and analytical expressions for the coefficient of friction due to plowing are obtained. The theoretical friction coefficient was found to be a function of the sharpness of the hard asperities, the interfacial "friction" conditions and the shape of the plastic zone. The agreement between theoretical and experimental friction coefficients from lubricated sliding and cutting experiments was remarkably good. The discrepancy between theory and experiment in the case of dry sliding between like metals was shown to be due to plastic deformation of the asperities. Consequently, a different model for plowing was proposed for the case of dry sliding between like metals which produced estimates for the coefficient of friction in fair agreement with the experimental results.

1 Introduction

In recent years it has become increasingly clear that plowing by hard asperities and wear debris plays a predominant role in sliding friction. Numerous investigations have shown that the coefficient of friction is not a material property, and that it depends on parameters such as the surface roughness, the size of the wear debris and the environmental conditions. For example, Suh and Sin [1] in their interpretation of the variation of the magnitude of the coefficient of friction with the distance slid proposed that the friction coefficient must be expressed as the sum of three components: asperity deformation, plowing by wear particles entrapped between the sliding surfaces or by hard asperities, and adhesion. In the same investigation it was also shown that the contribution of plowing to the overall friction force in dry sliding could be greater than that due to adhesion. Furthermore, recent work in boundary lubrication has shown that plowing is the prevailing mechanism of friction, while adhesion between the asperities and shearing of the lubricant film have secondary effects [2].

The significance of the wear debris in friction was pointed out long ago by Cocks, who performed experiments with copper riders sliding slowly on drums made of copper and indium [3-5]. He observed that soon after sliding starts wear debris agglomerates and forms large wear particles (wedges) between the contacting surfaces and separates the surfaces. Cocks suggested that some sort of plowing action plays an important role in the sliding friction, and that a reexamination of the idealized cold welding between the asperities and the elastic-plastic deformation of the junctions was necessary. Later, he observed that wear particle agglomeration, wedge formation and surface separation occurred also with flat metallic surfaces of different hardnesses [6]. Cocks postulated that when sliding begins, shearing does not occur at the original interface but that it actually takes place in a direction slightly inclined to the surfaces [7]. The observed mode of shearing in his experiments was primarily a continuous extrusion process, somewhat similar to the process of chip formation in the machining of ductile metals. Antler [8] also observed separation of the sliding surfaces due to wear debris agglomeration at the interface. Hardness measurements indicated that the formed wedges were significantly harder than the metal surfaces from which they were formed. He suggested an analogy between the plowing action of the agglomerated work-hardened wear debris at the interface and the built-up edge in metal cutting.

A good deal of effort has been devoted in the past to derive analytical expressions for the friction coefficient due to plowing. The shape of the wear particles and the asperities were approximated as spheres, cones, pyramids, etc., and expressions for the plowing component of friction were obtained. Bowden et al. [9] in one of their early studies on friction obtained simple expressions for the plowing friction force for spherical and cylindrical hard sliders of steel sliding on a soft surface like indium. Goddard and Wilman [10] later showed for spherical particles that the plowing friction term is a function of the groove width to particle diameter ratio and that the coefficient of friction can assume values between zero and one. Hisakado [11] has shown that theoretical predictions based on conical, spherical and pyramidal models for the wear debris were in fair agreement with those obtained from abrasion experiments. Recently, Suh et al. [12] explained the variation of the coefficient of friction with grit diameter in abrasion using a cone with hemispherical tip for the abrasive particles. Based on this model, they explained semi-quantitatively the transition from cutting to sliding mode in abrasion.

Although such analyses yield good estimates for the plowing coefficient of friction, they make use of rather simplistic assumptions. For example, the assumption that the material being plowed flows around the abrasive particles in planes parallel to the surface leaving behind grooves of the

Contributed by the Tribology Division of THE AMERICAN SOCIETY OF MECHANICAL ENGINEERS and presented at the ASME/ASLE Tribology Conference, Atlanta, Ga., October 8-10, 1985. Manuscript received by the Tribology Division, April 29, 1985. Paper No. 85-Trib-22.

Table 1 Experimental results

Material	Hardness (MPa)	Dry Experiments Coefficient of Friction (steady state)	Dry Experiments Groove depth (μm)	Lubricated Experiments Coefficient of Friction (steady state)	Lubricated Experiments Groove depth (μm)
Pure Aluminum	186 ± 16[a]	0.73 ± 0.04	10–60	0.20 ± 0.02	5–20
OFHC Copper	510 ± 21[b]	0.96 ± 0.02	5–35	0.17 ± 0.02	1–2
Pure Titanium	3026 ± 131	0.48 ± 0.02	1–6	0.46 ± 0.01	0.5–4
AISI 1095 Steel	3500 ± 451	0.50 ± 0.08	0.5–4	0.12 ± 0.004	< 0.5
Chromium (125 μm, electroplated on AISI 1095 steel)	6590 ± 284	0.58 ± 0.03	1–2	0.15 ± 0.01	< 1

[a]Annealed at 673 K for 1 hr in argon.
[b]Annealed at 873 K for 1 hr in argon.

same cross section may be correct in the abrasion of very soft metals (e.g., indium and lead), but in general it is unrealistic. Experimental results show that the plowed metal does not necessarily flow in parallel planes, but that it deforms in a more complicated way resulting in ridges and wear debris formation. Further, it was also assumed that the reaction stresses at the interface of the hard abrasive and the metal being plowed are a normal pressure and a shear stress, and that they are constant everywhere. Although equilibrium is satisfied at the interface, the assumed stresses may not satisfy equilibrium at each location within the deforming soft metal ahead of the abrasive particle. Moreover, it is not certain whether the stress components satisfy the yield criterion in the plastically deformed region. It is apparent, therefore, that an analysis which accounts for the shape of the plastic zone ahead and below the hard abrasive, and the correct state of stresses and boundary conditions, may provide a better solution. Such an analysis can be performed using the slip-line field theory [13–15].

Green [16] was the first to analyze the plastic deformation of asperity junctions in dry sliding under combined normal and shear stresses using the slip-line field theory. He estimated the forces for both strong and weak junctions using simple shapes for the junctions. However, Green's analysis is appropriate only for obtaining the friction component due to deformation of the asperities. A different slip-line geometry is necessary for plowing.

The different regimes of friction have also been studied by Challen and Oxley [17] who proposed three models using the slip-line field theory. The first model, "rubbing model," was based on a slip-line field similar to that proposed by Green [16] for weak junctions and Rowe and Wetton for metal grinding [18]. The "rubbing model" is appropriate for predicting the friction component due to asperity deformation, for it assumes that no wear takes place. The second model, "wear model," assumes that wear particles can be formed by plastic deformation and fracture of the softer asperities, but the proposed slip-line field does not satisfy the kinematic constraints on the problem. The third model, "cutting model," predicts friction coefficients and wear rates higher than the previous two models. The proposed slip-line field is similar to that proposed by Lee and Shaffer [19] for machining. However, the assumed slip-line is unrealistic since the change in direction of a plastically deforming element of the workpiece is assumed to take place abruptly after crossing the shear plane. Moreover, the slip-line network does not

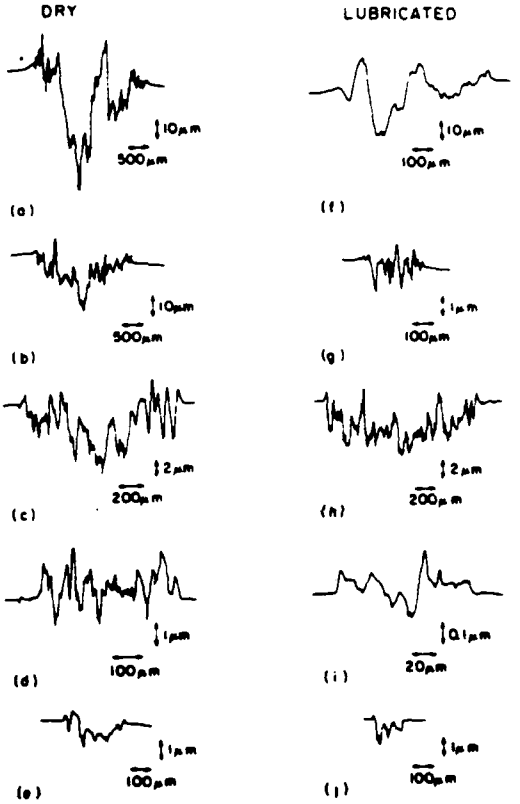

Fig. 1 Surface profiles of disk specimens from dry (first column) and lubricated (second column) pin-on-disk experiments with metals slid on themselves (normal load = 2N, mineral oil lubricant, in air). (a) aluminum (30 m), (b) copper (40.7 m), (c) titanium (58.8 m), (d) AISI 1095 steel (58.4 m), (e) chromium (32.9 m), (f) aluminum (23.5 m), (g) copper (31.6 m), (h) titanium (62.7 m), (i) AISI 1095 steel (72.2 m) and (j) chromium (38.2 m). (Numbers in parentheses indicate the distance slid.)

Nomenclature

F_x = horizontal force
F_y = vertical force
f = ratio of interfacial shear strength to shear strength of deformed soft surface
k, k_s, k_i = shear strengths
m = shear strength (hardness) ratio of soft surface to hard asperity
p = hydrostatic pressure
s, s_i = interfacial shear strength
Φ = shear angle in Henky's equations
α, α_c = semi-asperity angles
δ = angle in hodograph
$\eta_1, \eta_2, \eta_3, \eta_h, \eta_s$ = "friction" angles
θ, ϕ = angles in slip-line field
μ = coefficient of friction
$\sigma_I, \sigma_{II}, \sigma_{III}$ = principal stresses
σ_n = normal stress
σ_t = tangential stress

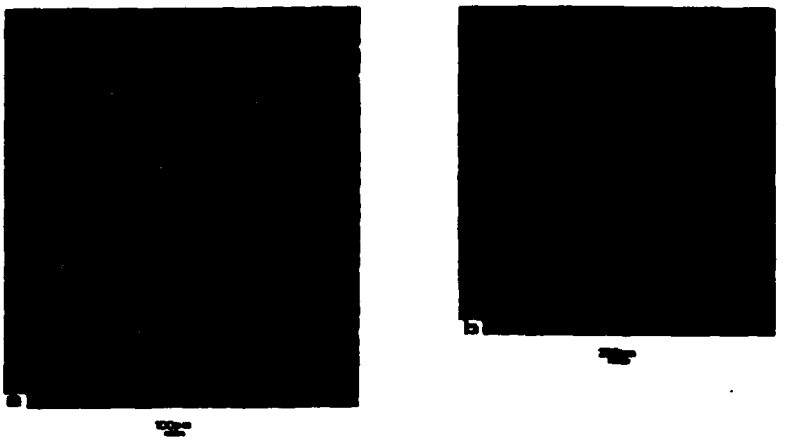

Fig. 2 Wear tracks of aluminum surfaces: (a) disk and (b) pin (dry experiment in air, normal load = 2N, sliding distance = 30 m)

account for the plastically deformed material sufficiently ahead of the shear plane.

Recently, Abebe and Appl [20] have proposed a slip-line field for metal cutting with negative rake angles. The proposed deformation field assumes chip formation and built-up-edge at the nose of the cutting tool and it represents fairly well that observed in cutting. It was found that the ratio of the horizontal to vertical cutting forces decreases as the rake angle becomes more negative, and that the ratio of the chip thickness to the depth of cut is always greater than one. The proposed slip-line model can be extended to plowing friction problems, for it accounts for wedge formation due to material transfer from the plowed surface, and the formation of a ridge ahead of the plowing hard asperity due to material pile-up. Furthermore, shear of the plastically deformed metal is assumed to occur within a shear zone and not simply along a shear plane as in the previous models [17].

The purpose of the present study is to obtain an analytical solution for the plowing friction coefficient based on a model that represents fairly well the plowing process. The dependence of the friction coefficient on such important parameters as the sharpness of the asperities, the shape of the plastic zone and the interfacial "friction" conditions is also examined. In addition, experimental evidence for plowing in both dry and lubricated sliding is presented and the range of application of the theoretical model is discussed.

2 Experimental Evidence for Plowing in Dry and Lubricated Sliding

Dry and lubricated experiments conducted on pure aluminum, OFHC copper, pure titanium, AISI 1095 steel and chromium have shown that plowing grooves form on the surfaces. The experimental apparatus, which was a pin-on-disk tester, the methods of preparing the samples and the experimental conditions and procedures have been described in detail in a previous publication [2]. Although the specimens were polished to mirror-like finish, grooves have formed on the sliding surfaces at the very beginning of sliding. As sliding continued, more wear debris and deeper plowing grooves have appeared. Surface profiles and scanning electron micrographs clearly showed the transitions of the surface topography, especially in the early stages of sliding. In both dry and lubricated experiments the surface profiles indicated that the roughness and the width of the wear tracks increase with sliding distance until a steady-state is reached. The grooves formed in the dry experiments were always deeper and wider than those of the lubricated experiments.

Selected profiles of worn surfaces from dry and lubricated

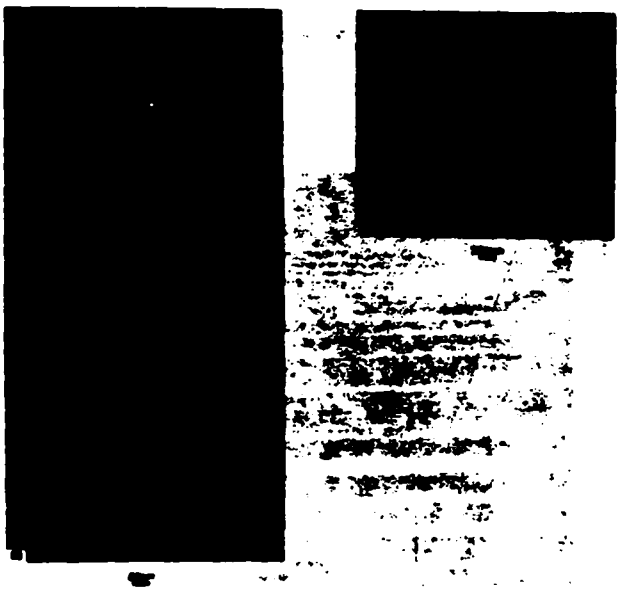

Fig. 3 Wear tracks of copper surfaces: (a) disk and (b) pin (dry experiment in air, normal load = 2N, sliding distance = 30 m)

experiments are shown in Fig. 1. In the case of dry sliding (Fig. 1, first column) grooves 10-60 μm deep were formed on aluminum, 5-35 μm on copper, 1-6 μm on titanium, 0.5-4 μm on steel and 1-2 μm on chromium. The profiles of the wear tracks of the lubricated experiments (Fig. 1, second column) show that lubrication reduces the depth and width of the plowing grooves significantly. The groove depth for lubricated aluminum was in the range 5-20 μm while the grooves formed on the other metals were less deep. In particular, the depth of the grooves formed on copper was 1-2 μm, on titanium it was 0.5-4 μm and on steel and chromium it was less than 0.5 and 1 μm, respectively. In addition, the width of the wear tracks is much smaller in the lubricated experiments than in the dry experiments. The effect of the material hardness on the surface topography and the coefficient of friction is also noticeable. The surface roughness and the friction coefficients were significantly smaller under lubricated sliding conditions except in the case of titanium where lubrication was not effective. The general trend for lower friction coefficients when hard materials are slid on themselves is evidently followed. The hardness of the tested metals, the steady state coefficient of friction and the range of the groove depths are listed in Table 1.

The transition of the surface topography was also studied

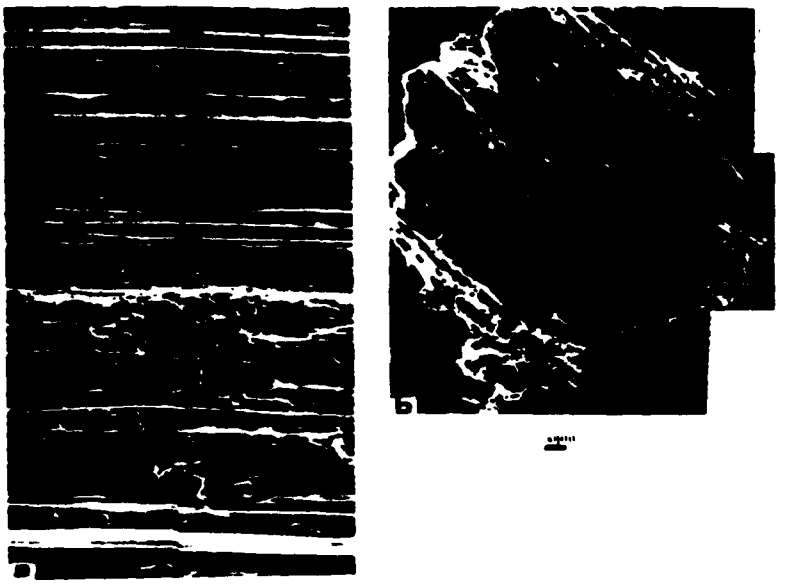

Fig. 4 Wear tracks of aluminum surfaces: (a) disk and (b) pin (lubricated experiment (mineral oil), normal load = 2N, sliding distance = 83.5 m)

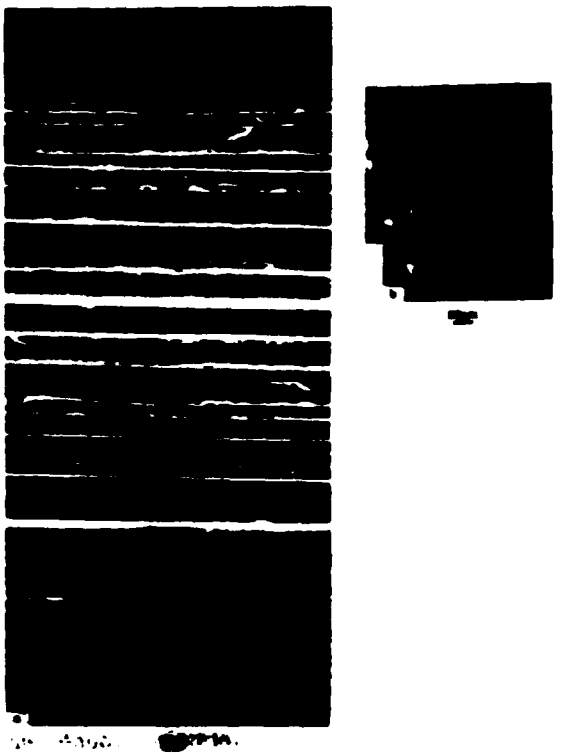

Fig. 5 Wear tracks of copper surfaces: (a) disk and (b) pin (lubricated experiment (mineral oil), normal load = 2N, sliding distance = 44 m)

with a scanning electron microscope. Several micrographs of the wear tracks as a function of the distance slid were obtained. Some characteristic micrographs of the wear tracks of three of the tested metals are shown in Figs. 2-6. The topographies of worn aluminum and copper surfaces from dry experiments are shown in Figs. 2 and 3, respectively. It can be seen that plastic deformation took place as a result of sliding, and that many plowing grooves have formed on all of the surfaces. Figures 4-6 show some typical wear tracks on aluminum, copper and chromium from the lubricated experiments. As in the dry experiments, the surfaces have plastically deformed and many grooves have formed. However, the width of the wear tracks and the plowing grooves are substantially smaller than those of the dry experiments. This reduction is especially noticeable for aluminum and copper wear tracks (Figs. 2-5).

These experimental observations clearly demonstrate the significance of the plowing friction mechanism in both dry and lubricated sliding. The variation of the surface topography and the formation of wear grooves during sliding can be primarily associated with the plowing action of wear debris entrapped between the sliding surfaces or with plowing by work-hardened asperities.

3 Analysis and Discussion

3.1 The Analytical Model. When a hard asperity, or a hard wear particle entrapped at the interface, slides on a softer surface, plastic deformation of the soft material occurs due to plowing or microcutting. A material element ahead of the hard asperity is undeformed, but as it approaches the plowing particle extensive shearing and microchip formation occur. The sheared material may produce a new wear particle or it may adhere strongly to the surface of the hard asperity resulting in the formation of a rigid stagnant region (dead zone) in front of the plowing edge, in accord with the experimental evidence reported by Cocks [3-7] and Antler [8]. The similarity between sliding and machining has been discussed in the past. For example, the process of formation of a built-up edge and a frontal bulge (or prow) in metal grinding or cutting could be extended to the sliding problem where material transferred and strongly adhered to the surface asperities may act as a built-up edge deforming plastically the surfaces and resulting in ridge and wear debris formation. Rowe and Wetton [18], in their analyses for metal grinding, emphasized the similarity between grinding and sliding and suggested that the proposed slip-line model, which accounts for the formation of a frontal bulge ahead of the abrasive grit, could be assumed for modeling material pile-up in front of the plowing asperities in sliding. Experiments conducted with diamond cones traversed on copper indicated that as sliding proceeded, material removed from the plowing

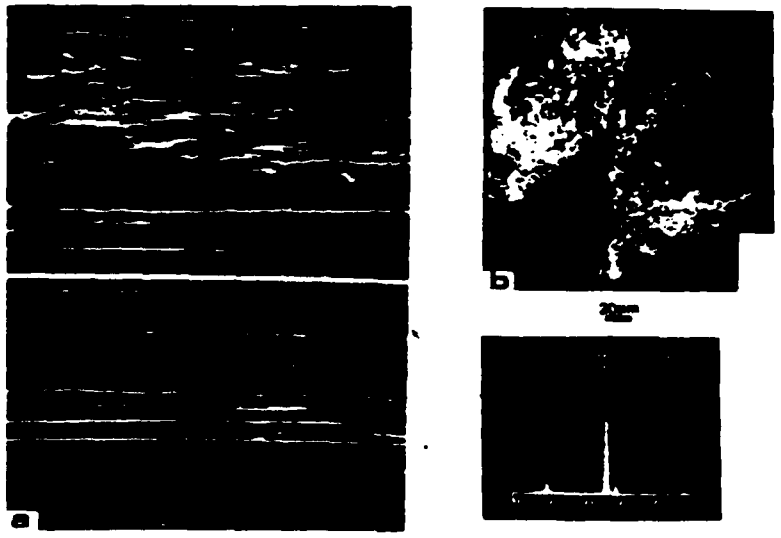

Fig. 6 Wear tracks of chromium surfaces: (*a*) disk and (*b*) pin (lubricated experiment (mineral oil), normal load = 2N, sliding distance = 16 m)

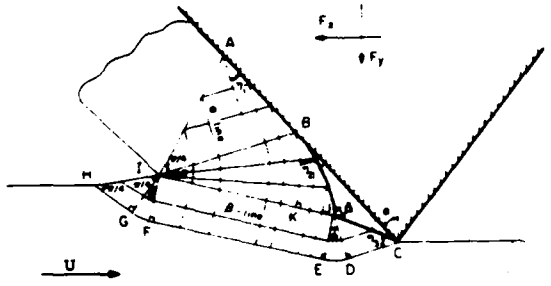

Fig. 7 Plastic deformation due to plowing by a hard asperity (or wear particle)

grooves was eventually piled up and a prow, termed ridge, was formed ahead of the diamond rider [21]. It is essential, therefore, that a slip-line field which may account for this experimental evidence must be used for analyzing the plowing friction mechanism.

A slip-line field with these features is shown in Fig. 7. The proposed field is similar to the one given for metal cutting with negative rake angle tools [20]; however the solution of the present study is based on different assumptions. In reference [20], it was proposed that the shear stress is a function of the real area of contact and the normal stress due to the high normal pressures. In the present study, no such constraints for the stresses have been imposed, but it is assumed that the ratio of the interfacial shear stress to the shear strength of the plastically deformed metal is only a function of the interfacial friction conditions. Moreover, the validity of the proposed slip-line field in terms of the semi-included angle α and the friction angles η (see Fig. 7) have been discussed.

Figure 7 shows a stationary hard asperity (or a wear particle) and a softer surface moving with a velocity U. It also shows two families of slip-lines, denoted as α-lines and β-lines, along which the shear stress is equal to the shear strength of the material. A stagnant region, or dead zone, is shown by the area BJC ahead of the plowing edge. The slip-line analysis is developed on the assumption that the plane-strain condition approximates the plowing situation well. Figure 8 shows the proposed slip-line field with the corresponding velocity diagram (hodograph). The velocity

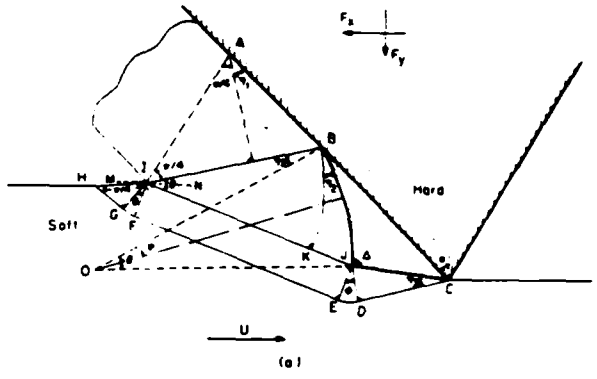

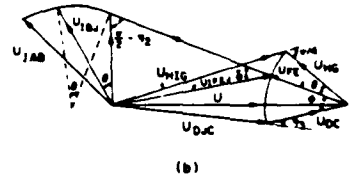

Fig. 8 (*a*) Slip-line field for plowing and (*b*) velocity diagram (hodograph)

field shown in Fig. 8(*b*) is kinematically admissible. In order for a microchip (or wear particle) to form it is assumed that a ridge HI and a dead zone BJC are formed. The material being plowed flows over the hard particle along the boundaries CJ, JB, and BA.

The slip-line field shown in Figs. 7 and 8(*a*) is composed of domains with orthogonal α- and β-shear lines. The triangular fields AIB, HIG, and JDC, and the rectangular field IFEJ are networks of straight α- and β-lines. Because the α- and β-lines have no curvature, the hydrostatic pressure remains the same throughout these fields. The centered-fans (sectors) GIF, BIK, and EJD, are networks of straight and circular orthogonal slip-lines. In these fields the hydrostatic pressure is the same along a radial line, but changes from one radial line to another. The normal and tangential tractions on boundaries

HI and *IA* are zero because *HI* and *IA* are stress-free surfaces. Thus the α- and β-lines must meet these surfaces at 45 deg.

The domain *KBJ* is a set of orthogonal α- and β-lines contained within the curved boundaries *BK* and *BJ* which are arcs of circles with centers at *I* and *O* and radii *IB* and *OB*, respectively, and a straight line *KJ*. The α-lines in *KBJ* are arcs of concentric circles with center at *I* and the β-lines are straight lines passing through *I* (Fig. 7). Thus, the hydrostatic pressure is constant along the straight β-lines, but it assumes different values on each β-line due to the circular α-lines. The details of the geometrical construction of the field KBJ are given in the Appendix.

The angles η_1, η_2, and η_3 which the α- and β-lines make with the interface ABJC depend on the interfacial shear strength, s_j, along each of these boundary segments. The angles η_j are given by

$$s_j = k\cos(2\eta_j)$$

or

$$\eta_j = \frac{1}{2}\cos^{-1}(s_j/k) \quad j = 1,2,3 \tag{1}$$

where 1, 2, and 3 represent the boundaries AB, BJ, and JC, respectively.

3.2 Geometrical Constraints on the Slip-Line Field. The proposed slip-line field assumes that material is removed in the form of microchips. In order for the chip formation process to occur, the material must first flow around I and then parallel to the rigid boundary AB. For this plastic flow to take place the angles $H\hat{I}M$, $B\hat{I}N$, and $J\hat{I}N$ must be nonzero, i.e., the following relations must be satisfied

$$H\hat{I}M = \frac{\pi}{4} - 2\theta + \alpha - \eta_1 > 0$$

or

$$\theta < \frac{1}{2}\left(\frac{\pi}{4} + \alpha - \eta_1\right) \tag{2}$$

$$B\hat{I}N = \alpha - \eta_1 > 0$$

or

$$\alpha > \eta_1 \tag{3}$$

and

$$J\hat{I}N = \theta + \eta_1 - \alpha > 0$$

or

$$\theta > \alpha - \eta_1 \tag{4}$$

Combining relations (2)–(4) the range for θ can be obtained as

$$\alpha - \eta_1 < \theta < \frac{1}{2}\left(\frac{\pi}{4} + \alpha - \eta_1\right) \tag{5}$$

and

$$\theta < \frac{\pi}{4}$$

The proposed slip-line field also assumes the formation of a dead zone BJC. For a dead zone to form, two relations must be satisfied: the sum of all the angles at point *J* must be equal to 2π and the angle $B\hat{C}J$ must be nonzero. Hence

$$2\pi = \Delta + \frac{\theta}{2} + \left(\frac{\pi}{2} - \frac{\theta}{2}\right) + \left(\frac{\pi}{2} - \eta_2\right) + \phi + \left(\frac{\pi}{2} - \eta_3\right)$$

or

$$\Delta = \frac{\pi}{2} + \eta_2 + \eta_3 - \phi \tag{6}$$

and

$$B\hat{C}J = \pi - \Delta - \theta - \eta_1 + \eta_2 = \pi - \left(\frac{\pi}{2} + \eta_2 + \eta_3 - \phi\right) - \theta - \eta_1 + \eta_2 > 0$$

or

$$\phi + \frac{\pi}{2} - \eta_1 - \eta_3 > \theta \tag{7}$$

Because the velocity along the β-line HGFEDC must be constant, the following relations should be satisfied (Fig. 8(*b*))

$$U_{HG} = U_{DC}$$

or

$$\frac{\sin\left(\frac{\pi}{4} + \alpha - \eta_1 - 2\theta\right)}{\sin\left(\frac{3\pi}{4}\right)} = \frac{\sin(\eta_1 + \eta_3 + \theta - \phi - \alpha)}{\sin\eta_3}$$

or

$$\phi = \eta_1 + \eta_3 + \theta - \alpha - \sin^{-1}\left[\sqrt{2}\sin\left(\frac{\pi}{4} + \alpha - \eta_1 - 2\theta\right)\sin\eta_3\right] \tag{8}$$

and

$$U_{EF} = U_{HG}$$

or

$$\frac{\sin(\delta + \alpha - \theta - \eta_1)}{\sin\delta} = \frac{\sin\left(\frac{\pi}{4} + \alpha - \eta_1 - 2\theta\right)}{\sin\left(\frac{3\pi}{4}\right)}$$

or

$$\delta = \eta_1 + \theta - \alpha + \tan^{-1}\left[\frac{\sqrt{2}\sin\left(\frac{\pi}{4} + \alpha - \eta_1 - 2\theta\right)\sin(\eta_1 + \theta - \alpha)}{1 - \sqrt{2}\sin\left(\frac{\pi}{4} + \alpha - \eta_1 - 2\theta\right)\cos(\eta_1 + \theta - \alpha)}\right] \tag{9}$$

The lengths *AB* and *OB* can be expressed in terms of the slip-line field angles and the length *JC* as

$$AB = JC\,\frac{\cos\left(\eta_2 + \frac{\theta}{2}\right)\sin(\eta_1 - \eta_2 + \theta + \Delta)}{\sqrt{2}\cos\left(\frac{\pi}{4} - \eta_1\right)\sin\theta\,\sin\left(\eta_1 - \eta_2 + \frac{\theta}{2}\right)} \tag{10}$$

$$OB = JC\,\frac{\cos\frac{\theta}{2}\sin(\eta_1 - \eta_2 + \theta + \Delta)}{\sin\theta\,\sin\left(\eta_1 - \eta_2 + \frac{\theta}{2}\right)} \tag{11}$$

3.3 Coefficient of Friction. If p is the hydrostatic pressure on a slip-line and Φ the angle of rotation of an α-line with the x-axis (shear angle), the equilibrium equations and the yield criterion can be combined into the following two equations known as Henky's equations [13, 14]

$$\begin{aligned} p + 2k\Phi &= \text{constant} \quad (\alpha\text{-line}) \\ p - 2k\Phi &= \text{constant} \quad (\beta\text{-line}) \end{aligned} \tag{12}$$

The pressure, p, along any slip-line can be obtained from the known boundary conditions and equations (12). The stresses at each location are then found from Mohr's circle. The hydrostatic pressure, p, along some α- and β-lines and the

normal and tangential stresses σ_n and σ_t, respectively, along the boundaries AB, BJ, and JC are given in the following.

On the stress-free surfaces HI and IA the principal stresses are,

$$\sigma_1 = 0 \quad \sigma_{II} = -k \quad \sigma_{III} = -2k$$

From Mohr's circle the normal and tangential stresses on the boundary AB are:

$$\sigma_n^{AB} = k(1+\sin 2\eta_1) \quad \sigma_t^{AB} = k\cos 2\eta_1 \tag{13}$$

Along the β-line IB and the α-line BK the hydrostatic pressures respectively are:

$$p^{IB} = k \quad p^{BK} = k(1+2\psi)$$

Then the stresses along the boundary BJ can be obtained from Mohr's circle and the pressure p^{BA} as

$$\sigma_n^{BJ} = k(1+2\psi+\sin 2\eta_2) \quad \sigma_t^{BJ} = k\cos 2\eta_2 \tag{14}$$

The hydrostatic pressure along the α-lines IG, IF, and JD, respectively, is given by

$$p^{IG} = k \quad p^{IF} = k(1+2\theta) \quad p^{JD} = k(1+2\theta+2\phi)$$

From Mohr's circle and the known pressure p^{JD}, the stresses on the boundary JC can be obtained as

$$\sigma_n^{JC} = k(1+2\theta+2\phi+\sin 2\eta_3) \quad \sigma_t^{JC} = -k\cos 2\eta_3 \tag{15}$$

The horizontal and vertical forces F_x and F_y, respectively, acting at the interface $ABJC$ can be obtained by summation along the boundary. Thus

$$\begin{aligned} F_x &= F_x^{AB} + F_x^{BJ} + F_x^{JC} \\ &= AB[\sigma_n^{AB}\cos\alpha - \sigma_t^{AB}\sin\alpha] \\ &+ OB\left[\int_0^{\theta} \{\sigma_n^{BJ}\cos(\eta_2-\eta_1+\alpha-\psi) \right. \\ &- \left. \sigma_t^{BJ}\sin(\eta_2-\eta_1+\alpha-\psi)\}d\psi\right] \\ &+ JC[\sigma_n^{JC}\cos(\pi-\Delta-\eta_1+\eta_2-\theta+\alpha) \\ &+ \sigma_t^{JC}\sin(\pi-\Delta-\eta_1+\eta_2-\theta+\alpha)] \end{aligned} \tag{16}$$

and

$$\begin{aligned} F_y &= F_y^{AB} + F_y^{BJ} + F_y^{JC} \\ &= AB[\sigma_n^{AB}\sin\alpha + \sigma_t^{AB}\cos\alpha] \\ &+ OB\left[\int_0^{\theta} \{\sigma_n^{BJ}\sin(\eta_2-\eta_1+\alpha-\psi) \right. \\ &+ \left. \sigma_t^{BJ}\cos(\eta_2-\eta_1+\alpha-\psi)\}d\psi\right] \\ &+ JC[\sigma_n^{JC}\sin(\pi-\Delta-\eta_1+\eta_2-\theta+\alpha) \\ &- \sigma_t^{JC}\cos(\pi-\Delta-\eta_1+\eta_2-\theta+\alpha)] \end{aligned} \tag{17}$$

where

$$0 \le \psi \le \theta$$

Substituting equations (10), (11), and (13)-(15) into equations (16) and (17) and integrating, the horizontal and vertical forces acting on the interface $ABJC$ can be obtained. The horizontal force, F_x, is given by

$$\begin{aligned} F_x = JCk\Bigg[&\frac{\sin(\beta+\Delta-\alpha)}{\sin\left(\beta-\alpha-\frac{\theta}{2}\right)}\Bigg[\frac{\sqrt{2}\cos\left(\eta_2+\frac{\theta}{2}\right)\sin\left(\frac{\pi}{4}+\eta_1-\alpha\right)}{\sin\theta} \\ &+ (1+\sin 2\eta_2)\cos\left(\beta-2\alpha-\frac{\theta}{2}\right) \\ &+ \frac{\theta\sin(\beta-2\alpha)}{\sin\frac{\theta}{2}} - (2-\cos 2\eta_2)\sin\left(\beta-2\alpha-\frac{\theta}{2}\right)\Bigg] \\ &- (1+2\theta+2\phi)\cos(\beta+\Delta-2\alpha) + \sin(\beta+\Delta-2\alpha-2\eta_3)\Bigg] \end{aligned} \tag{18}$$

Similarly, the vertical force F_y is given by

$$\begin{aligned} F_y = JCk\Bigg[&\frac{\sin(\beta+\Delta-\alpha)}{\sin\left(\beta-\alpha-\frac{\theta}{2}\right)}\Bigg[\frac{\sqrt{2}\cos\left(\eta_2+\frac{\theta}{2}\right)\cos\left(\frac{\pi}{4}+\eta_1-\alpha\right)}{\sin\theta} \\ &- (1+\sin 2\eta_2)\sin\left(\beta-2\alpha-\frac{\theta}{2}\right) \\ &+ \frac{\theta\cos(\beta-2\alpha)}{\sin\frac{\theta}{2}} - (2-\cos 2\eta_2)\cos\left(\beta-2\alpha-\frac{\theta}{2}\right)\Bigg] \\ &+ (1+2\theta+2\phi)\sin(\beta+\Delta-2\alpha) + \cos(\beta+\Delta-2\alpha-2\eta_3)\Bigg] \end{aligned} \tag{19}$$

where

$$\beta = \eta_1 - \eta_2 + \theta + \alpha$$

Thus, the coefficient of friction, $\mu = F_x/F_y$, due to plowing can be expressed as

$$\mu = \frac{\xi_0[\xi_1\sin\omega_1 + \xi_2\cos\omega_2 + \xi_3\sin\omega_3 - \xi_4\sin\omega_2] - \xi_5\cos\omega_4 + \sin\omega_5}{\xi_0[\xi_1\cos\omega_1 - \xi_2\sin\omega_2 + \xi_3\cos\omega_3 - \xi_4\cos\omega_2] + \xi_5\sin\omega_4 + \cos\omega_5} \tag{20}$$

where

$$\xi_0 = \frac{\sin(\beta+\Delta-\alpha)}{\sin\left(\beta-\alpha-\frac{\theta}{2}\right)} \quad \xi_1 = \frac{\sqrt{2}\cos\left(\eta_2+\frac{\theta}{2}\right)}{\sin\theta} \quad \xi_2 = 1+\sin 2\eta_2$$

$$\xi_3 = \frac{\theta}{\sin\frac{\theta}{2}} \quad \xi_4 = 2-\cos 2\eta_2 \quad \xi_5 = 1+2\theta+2\phi$$

$$\omega_1 = \frac{\pi}{4}+\eta_1-\alpha \quad \omega_2 = \beta-2\alpha-\frac{\theta}{2} \quad \omega_3 = \beta-2\alpha$$

$$\omega_4 = \beta+\Delta-2\alpha \quad \omega_5 = \beta+\Delta-2\alpha-2\eta_3$$

It is evident from equations (18) through (20) that the coefficient of friction depends on the semi-asperity angle α, the ratios s_j/k (i.e., the "friction" conditions at the interface ABJC), and the magnitude of θ. There can be an infinite number of solutions for the friction coefficient within the limits set by relations (5). The stress field in a deforming material can be uniquely defined only when the boundary conditions (stresses or velocities) of the deforming zone are completely specified. Then the actual state of stresses can be obtained from the extremum principles proposed by Hill [22] for a rigid-plastic body. In machining problems, however, some of the boundary conditions are unknown and, moreover, the boundaries themselves are undetermined. In this case, the extremum principles are no longer applicable and the machining process is not uniquely defined [23]. In the present analysis, therefore, the angle θ was varied within the

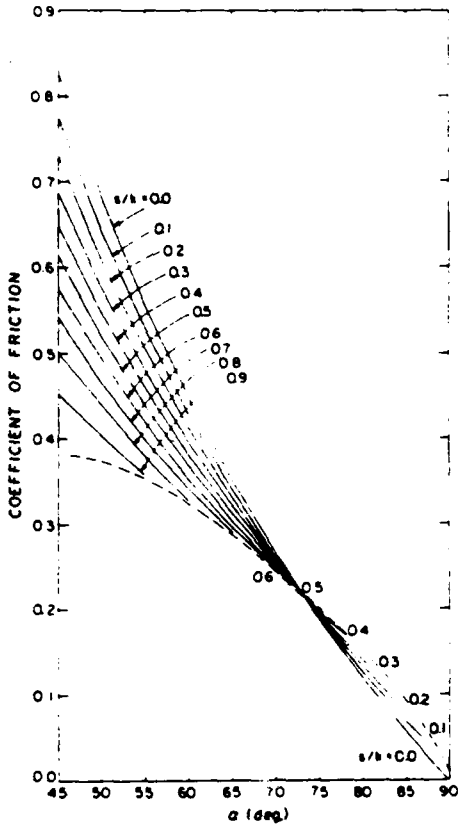

Fig. 9(a) Minimum friction values

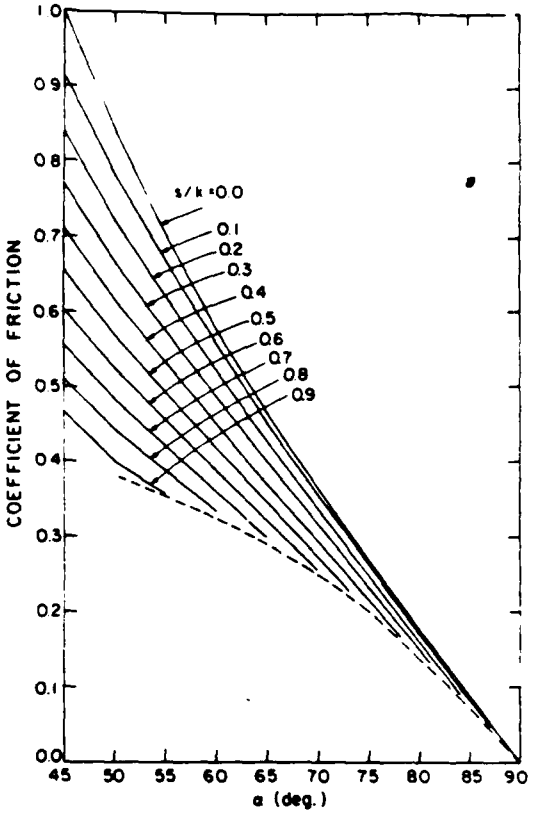

Fig. 9(b) Maximum friction values

Fig. 9 Slip-line field solutions for the coefficient of friction due to plowing as a function of the semi-asperity angle for different interfacial shear stresses

limits set by the relations (5) and the minimum and maximum magnitudes of the coefficient of friction were obtained as functions of α and s_j/k.

The minimum and maximum magnitudes of the coefficient of friction as a function of the semi-asperity angle α are plotted in Figs. 9(*a*) and 9(*b*), respectively, for the case when the same "friction" conditions prevail along the interface *ABJC*, i.e., for $\eta_1 = \eta_2 = \eta_3$. Several friction curves for different boundary "frictional" conditions s/k are shown. The coefficient of friction obtains high values when α is low (sharp asperities) and decreases rapidly to very small magnitudes for high values of α (shallow asperities). Moreover, the magnitude of s/k affects the coefficient of friction significantly only when the semi-asperity angle is sufficiently small. When α takes values in the range 45–55 deg, for example, variations of the magnitude of s/k may alter the coefficient of friction by 50 percent. Conversely, as α increases the effect of the interfacial friction on the magnitude of the coefficient of friction becomes marginal.

The coefficient of friction predicted here is correct only when the geometric constraints given by equations (5)–(9) are satisfied. The dashed-curve in Figs. 9(*a*) and 9(*b*) is a limiting curve for the assumed slip-line field. Outside this dashed-curve different slip-line fields must be sought. The friction curves corresponding to low values of the ratio s/k may be the appropriate curves for lubricated sliding conditions, or for unlubricated sliding with dissimilar (incompatible) metals where the interfacial adhesion will be weak. Furthermore, the friction curves associated with high values of s/k may be the appropriate curves for unlubricated sliding conditions with similar (or compatible) metals. In the limiting case for which $s/k = 1$, i.e., for "sticking" interfacial conditions, the α- and β-lines will meet the boundaries tangentially and at right angles. In this case the proposed slip-line field cannot exist. Nevertheless, "sticking" interfacial friction conditions are unlikely to prevail even with similar metals sliding on themselves under dry sliding conditions, due to surface contamination which reduces the interfacial shear strength and results in s/k magnitudes less than one.

In order to examine the accuracy of the theoretically predicted coefficients of friction, experimental results from our study and other investigations were compared with theoretical solutions of similar s/k magnitudes. Hisakado [11] slid conical diamond sliders on carbon steel and copper (typical cases of dissimilar pairs) and obtained values for s/k between 0.1 and 0.12. Moreover, when carbon steel was slid on itself, a case which may be interpreted as sliding between similar metals, a value of 0.4 for s/k was deduced. Tsukizoe and Sakamoto [21, 24] conducted similar experiments and reported a value for s/k equal to 0.11 for diamond conical sliders traversing on copper, aluminum and low carbon steel. However, when sintered carbide conical sliders were traversed on copper the deduced value of s/k was about 0.22. This can be interpreted as a case of sliding between materials of partial or poor compatibility. Friction data for conical diamond tools of different negative rake angles traversed on AISI 1095 steel have also been reported recently by Sin et al. [25]. Figure 10 shows the minimum and maximum friction coefficient curves for $s/k = 0.0$, 0.1, and 0.2 together with obtained experimental data. The experimental results shown in the figure

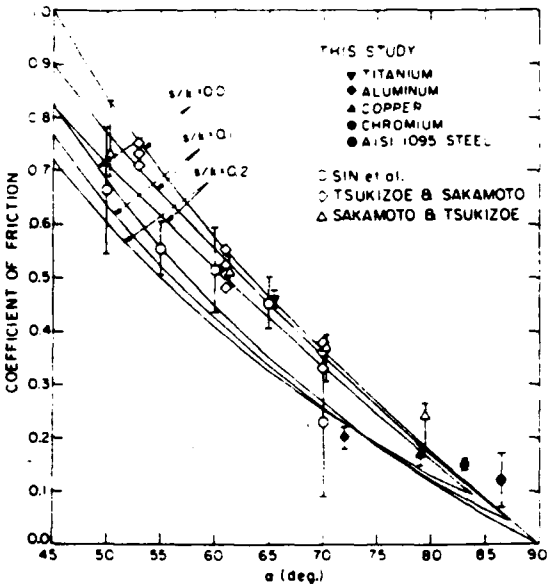

Fig. 10 Theoretical and experimental friction coefficients obtained from lubricated (filled symbols) and dry (open symbols) experiments with conical sliders [21, 24, 25]

have been obtained from lubricated experiments conducted with like metals sliding on themselves and from cutting data quoted in references [21, 24, 25]. It is evident that the agreement between theoretical and experimental friction coefficients is remarkably good. In the case of the lubricated experiments the calculation of the angle α was based on the obtained surface profiles. It was assumed that the formed grooves resulted from the plowing action of hard surface asperities (or accicular wear particles entrapped at the interface) of the same semi-included angle α. For each experiment at least four profiles were obtained at different locations of the wear track and perpendicular to the direction of sliding, and a mean value of α was calculated. The data of the lubricated experiments plotted in Fig. 10 are the mean values of several experiments obtained for different sliding distances.

Satisfactory agreement was also obtained between experimental and theoretical friction coefficients for large values of s/k. Table 2 lists data from an experimental study on machining of steel with carbide tools of different negative rake angles by Komanduri [26], and theoretical results obtained from the slip-line analysis for $s/k = 0.7$. The agreement between theory and experiment is indeed reasonably good.

A comparison between theory and experimental results obtained from lubricated experiments between like metals and unlubricated experiments between similar and dissimilar metals, when the plowing surface was significantly harder than the plastically deformed material, indicates that the accuracy of the theoretical model is remarkably good. However, the agreement between theoretical and experimental friction coefficients obtained from unlubricated experiments with like metals sliding on themselves, appears to be inadequate. This discrepancy between theory and experiment is discussed next.

3.4 Validity of the Analytical Model. It has been shown so far that when the relations (5) through (9) are satisfied, solutions for the coefficient of friction in reasonably good agreement with the experimental results can be obtained. One of the major assumptions of the analysis is that the hard asperity does not deform plastically when plowing and

Table 2 Experimental and theoretical friction coefficients

α (deg)	Coefficient of Friction		
	Experimental[a]	Theoretical ($s/k = 0.7$)	
		min	max
45	0.50	0.54	0.55
50	0.46	0.46	0.48
55	0.40	0.40	0.42
60	0.37	0.34	0.36
65	0.32	0.29	0.30

[a] Data from Reference [26].

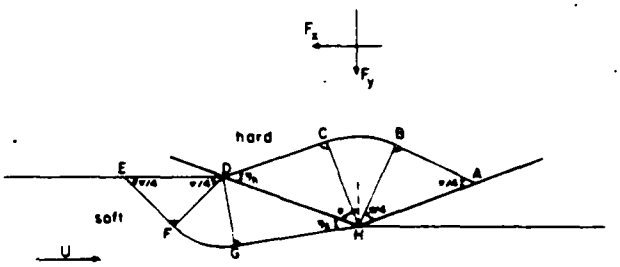

Fig. 11 Slip-line field for plastically deforming hard asperity during plowing

microcutting of the soft surface occurs. However, under certain conditions plastic deformation of the hard asperity may take place, despite the lower hardness of the opposed surface. Kayaba et al. [27, 28] have shown that when the asperity angle is less than a critical value, which is determined by the hardness ratio between the asperity and the flat surface, the hard asperity undergoes plastic deformation even though it is harder than the mating surface.

Figure 11 shows a possible slip-line field for a plastically deforming hard asperity. The figure shows a hard asperity and a soft surface which have both deformed plastically at the same time. In order for the slip-line field shown in Fig. 11 to form, the angles $B\hat{H}C$ and $G\hat{D}F$ must be nonzero. These constraints yield the following relations

$$2\alpha + \eta_h - \frac{3\pi}{4} > 0$$

or

$$\eta_h > \frac{3\pi}{4} - 2\alpha \tag{21}$$

and

$$\alpha + \eta_s - \frac{\pi}{4} > 0$$

or

$$\eta_s > \frac{\pi}{4} - \alpha \tag{22}$$

where the subscripts h and s denote "hard" and "soft," respectively. The slip-line fields *ABH* and *DFE* are fields of constant pressure equal to, k_h and k_s, respectively. Then, the pressure in *CDH* and *HDG* can be obtained from Henky's relations (i.e., equations (12)), and the normal and tangential stresses along the interface *HD* from Mohr's circle. Thus, the normal and tangential stresses on *HD* calculated from the slip-line fields of the hard and soft materials, σ_n^h, σ_t^h and σ_n^s, σ_t^s, respectively, are as follows

$$\sigma_n^h = k_h\left(1 - \frac{3\pi}{2} + 4\alpha + 2\eta_h + \sin 2\eta_h\right) \tag{23a}$$

$$\sigma_t^h = k_h \cos 2\eta_h \tag{23b}$$

and

$$\sigma_n^s = k_s\left(1 - \frac{\pi}{2} + 2\alpha + 2\eta_s + \sin 2\eta_s\right) \tag{24a}$$

$$\sigma_t^s = k_s \cos 2\eta_s \tag{24b}$$

Along the interface *HD* equilibrium must be satisfied thus, if $\sigma_t^h = \sigma_t^s = s$, from equations (23*b*) and (24*b*) it follows

$$\eta_h = \frac{1}{2}\cos^{-1}(mf) \tag{25}$$

and

$$\eta_s = \frac{1}{2}\cos^{-1} f \tag{26}$$

where $m = k_s/k_h$ is the shear strength ratio, which is equal to the hardness ratio, and $f = s/k_s$ with $0 < m < 1$ and $0 \le f < 1$. Kayaba et al. [27] used a similar analysis and by equating the normal stresses σ_n^h and σ_n^s at the interface *HD*, they obtained a relation for the critical value of α, denoted by α_c in the present work, as follows

$$\alpha_c = \frac{1}{2(2-m)}\left[m - 1 + \frac{\pi}{2}(3-m) + m\cos^{-1} f \right.$$

$$\left. - \cos^{-1}(mf) + \sqrt{1 - f^2}\,\sqrt{1 - (mf)^2} - \sqrt{1 - (mf)^2}\right] \tag{27}$$

This equation gives the value of the critical semi-asperity angle as a function of the hardness ratio m and the interfacial friction conditions f. For a given set of m and f, all the asperities with $\alpha < \alpha_c$ must deform plastically.

In the present study the above analysis has been extended further to obtain a relation for the coefficient of friction when plastic deformation of the hard asperity and the soft surface take place at the same time. Equations (23*a*) and (23*b*) can be used to calculate the vertical and tangential forces (see Fig. 11) and hence the friction coefficient from the relation $\mu = F_x/F_y$. Thus

$$\mu = \frac{\left[1 - \frac{3\pi}{2} + 4\alpha + \cos^{-1}(mf)\right]\cos\alpha + \sin[\alpha + \cos^{-1}(mf)]}{\left[1 - \frac{3\pi}{2} + 4\alpha + \cos^{-1}(mf)\right]\sin\alpha - \cos[\alpha + \cos^{-1}(mf)]} \tag{28}$$

Since $0 \le f < 1$ and $0 < m < 1$ it follows that $0 \le mf < 1$. Therefore, from relations (21), (22), (25), and (26) the following relations must be satisfied in order for the assumed slip-line model (Fig. 11) to be valid

$$\frac{\pi}{4} - \alpha < \frac{1}{2}\cos^{-1} f \le \frac{\pi}{4} \tag{29}$$

and

$$\frac{3\pi}{4} - 2\alpha < \frac{1}{2}\cos^{-1}(mf) \le \frac{\pi}{4} \tag{30}$$

In the present study α assumes values in the range $[\pi/4, \pi/2]$. For this range of values of α the relation (29) and the right hand side of relation (30) are always satisfied. The only constraint to be satisfied then is

$$\cos^{-1}(mf) > \frac{3\pi}{2} - 4\alpha \tag{31}$$

In conclusion, when $\alpha < \alpha_c$, where α_c is given by equation (27), and relation (31) is satisfied the coefficient of friction can be obtained from equation (28). Conversely, if $\alpha > \alpha_c$ the hard asperity does not deform plastically and the coefficient of friction is given by equation (20) if relations (5) through (9) are satisfied.

When the asperities are much harder than the plowed surface it may be assumed that $m << 0.1$. For the particular case that $m = 0.1$ equation (27) predicts $\alpha_c \approx 20$ deg for all values of f between 0 and 0.9. This implies that only the asperities with semi-asperity angle less than 20 deg will deform plastically. Because this value of α_c is significantly less than the values of α obtained from the dry and lubricated experiments, it is reasonable to assume that only the soft surface will undergo plastic deformation. In that case, the coefficient of friction is given by equation (20) and the agreement with the experimental results is very good (Fig. 10 and Table 2).

For lubricated sliding conditions it may be assumed that $f = 0.1$, and for m between 0 and 0.8, for example, the magnitudes of α_c predicted by equation (27) were lower than the values of α obtained from the lubricated experiments. Thus, under lubricated conditions $\alpha > \alpha_c$ and equation (20) can be used again for estimating the coefficient of friction. The agreement with the experimental results for this case is also satisfactory as shown in Fig. 10. It remains, then, to examine the disagreement between the theoretical coefficients of friction obtained from equation (20) and those obtained from the unlubricated experiments with like metals sliding on themselves.

It is reasonable to assume that in dry sliding f varies between 0.2 (contaminated surfaces) to 0.9 (clean surfaces). If this range for f is considered, equation (27) may predict values of α_c higher than the values of α obtained from the dry experiments. Thus, if relation (31) is satisfied the coefficient of friction must be obtained from equation (28). It was found that for $m = 0.8$, 0.9, and 1.0 and for f between 0.2 and 0.9, relation (31) is indeed satisfied when α assumes values equal to those obtained from the dry experiments and also that $\alpha < \alpha_c$. Thus, for unlubricated sliding the theoretical friction coefficients were obtained from equation (28). Table 3 lists the values of α obtained from the dry experiments, the corresponding experimental friction coefficients and the theoretical friction coefficients obtained from equation (28) for $m = 0.8$, 0.9, and 1.0. The table also lists the values of f for which solutions that satisfy the criterion $\alpha < \alpha_c$ and the relation (31) were obtained. The agreement between theory and experiment is reasonable. It must be mentioned, however,

Table 3 Experimental and theoretical coefficients of friction for dry sliding

Material	α (deg)	Coefficient of Friction Experimental (dry experiments)	Theoretical ($0.2 \le f \le 0.9$) $m = 0.8$	$m = 0.9$	$m = 1.0$
Pure aluminum	57 ± 15	0.73 ± 0.04	0.73 – 1.46	0.75 – 1.46[a]	0.76 – 1.40[a]
OFHC Copper	71 ± 9	0.96 ± 0.02	–	0.40 – 0.76	0.40 – 0.90
Pure Titanium	61 ± 10	0.48 ± 0.02	0.63 – 1.0[a]	0.64 – 1.36	0.65 – 1.33[a]
AISI 1095 Steel	64 ± 9	0.50 ± 0.08	0.55 – 0.73[c]	0.56 – 1.12	0.57 – 1.41
Electroplated Chromium	76 ± 6	0.58 ± 0.03	–	0.30 – 0.52[a]	0.30 – 0.67

[a]Solutions valid for $0.2 \le f \le 0.8$
[b]Solutions valid for $0.2 \le f \le 0.7$
[c]Solutions valid for $0.2 \le f \le 0.6$

that due to the large scatter of the magnitude of α, a direct comparison between theoretical friction coefficients based on the mean value of α and experimental coefficients of friction may not be appropriate. Consequently, the agreement between the predictions of equation (28) and experiments can be improved if solutions for the theoretical coefficients of friction based on the statistical distribution of α are obtained for each metal. However, this will require further analytical work based on the topography statistics. Nevertheless, since the agreement between theory and experiment given in Table 3 is acceptable, such an analysis has not been attempted in this study.

In the present analysis it was assumed that the plane-strain condition approximates the plowing situation well and that the soft material deforms plastically forming microchips without work-hardening. The good agreement between experimental and theoretical results obtained from the presented analysis ensures that the estimation of the plowing friction coefficient based on the obtained analytical expressions is appropriate.

Although the plane-strain assumption approximates plowing fairly well, a refined technique (e.g., Finite Element Analysis) may provide a more realistic solution. Adopting an appropriate Finite Element Mesh for plowing, solutions for the coefficient of friction and three-dimensional deformation fields for the material being plowed, can be obtained. Moreover, geometrical constraints similar to those of the slip-line analysis need not be imposed on the finite element analysis because the solution does not depend on an assumed flow field. This implies that solutions for the coefficient of friction can be obtained for any interfacial "friction" conditions s/k, and any magnitudes of the semi-asperity angle α. In addition, the effect of work-hardening of the subsurface can be included in a three-dimensional finite element analysis. However, an analysis like this for plowing could be expensive and may not be necessary for determining the coefficient of friction in most cases. It can be effective, however, in predicting the wear coefficient in abrasion, where the problem is a continuous chip formation and metal flow around the hard abrasive (i.e., a three-dimensional problem).

From the experimental and theoretical results of the present study it is evident that plowing indeed plays an important role in friction under both dry and lubricated sliding conditions. The magnitude of the friction force and the amount of material removal thus can be significantly reduced if plastic deformation and plowing of the sliding surfaces are made to vanish. Deposition of hard and smooth layers (such as oxides, nitrides and carbides) of sufficient thickness on the surfaces may result in only elastic deformation of the sliding surfaces. Under these conditions the friction force arises primarily from interfacial adhesion and/or shearing of the lubricant film and, thus, could be very low. Furthermore, the wear resistance of the surfaces could be increased by several orders of magnitude. Work in progress with metals covered with oxide and nitride layers shows that indeed the deformation of the surfaces is primarily elastic and that wear is practically insignificant.

4 Conclusions

The following conclusions can be drawn from the present study:

1. Experimental evidence from both dry and lubricated sliding demonstrates the significance of the plowing mechanism in friction.

2. Based on the slip-line field analysis a relationship between the coefficient of friction due to plowing and the sharpness of the asperities, the interfacial "friction" conditions and the shape of the plastic zone was obtained. The coefficients of friction predicted by this slip-line model are in good agreement with the friction coefficients obtained from lubricated and cutting experiments.

3. In the case of dry sliding between like metals, plastic deformation of the plowing asperities may take place. A slip-line model that accounts for plastic deformation of the asperity and the plowed surface at the same time was proposed. The friction coefficients predicted by this model are in fair agreement with the friction coefficients obtained from unlubricated experiments between like metals.

Acknowledgments

This work was done under the sponsorship of the Office of Naval Research, Contract N00014-82-K-0520. The personal support of Dr. A. W. Ruff and Dr. R. S. Miller is gratefully appreciated.

References

1 Suh, N. P., and Sin, H.-C., "The Genesis of Friction," *Wear*, Vol. 69, 1981, pp. 91-114.

2 Komvopoulos, K., Saka, N., and Suh, N. P., "The Mechanism of Friction in Boundary Lubrication," ASME JOURNAL OF TRIBOLOGY, Vol. 107, 1985, pp. 452-462.

3 Cocks, M., "Wear Debris in the Contact between Sliding Metals," *Journal of Applied Physics*, Vol. 29, 1958, pp. 1609-1610.

4 Cocks, M., "Interaction of Sliding Metal Surfaces," *Journal of Applied Physics*, Vol. 33, No. 7, 1962, pp. 2152-2161.

5 Cocks, M., "Frictional Interaction of Indium Surfaces," *Journal of Applied Physics*, Vol. 36, 1965, pp. 649-650.

6 Cocks, M., "Role of Displaced Metal in the Sliding of Flat Metal Surfaces," *Journal of Applied Physics*, Vol. 35, No. 6, 1964, pp. 1807-1814

7 Cocks, M., "Shearing of Junctions Between Metal Surfaces," *Wear*, Vol. 9, 1966, pp. 320-328.

8 Antler, M., "Processes of Metal Transfer and Wear," *Wear*, Vol. 7, 1964, pp. 181-203.

9 Bowden, F. P., Moore, A. J. W., and Tabor, D., "The Ploughing and Adhesion of Sliding Metals," *Journal of Applied Physics*, Vol. 14, 1943, pp. 80-91

10 Goddard, J., and Wilman, H., "A Theory of Friction and Wear during the Abrasion of Metals," *Wear*, Vol. 5, 1962, pp. 114-135.

11 Hisakado, T., "On the Mechanism of Contact between Solid Surfaces," *Bulletin of the JSME*, Vol. 13, No. 55, 1970, pp. 129-139.

12 Suh, N. P., Sin, H.-C., and Saka, N., "Fundamental Aspects of Abrasive Wear," *Fundamentals of Tribology*, Eds. Suh, N. P., and Saka, N., The MIT Press, Cambridge, MA, 1980, pp. 493-518.

13 Hill, R., *The Mathematical Theory of Plasticity*, Oxford University Press, London, 1967, pp. 128-160.

14 Kachanov, L. M., *Fundamentals of the Theory of Plasticity*, MIR publishers, Moscow, 1974, pp. 148-184.

15 Lee, E. H., "The Theoretical Analysis of Metal-Forming Problems in Plane Strain," ASME *Journal of Applied Mechanics*, Vol. 19, 1952, pp. 97-103.

16 Green, A. P., "The Plastic Yielding of Metal Junctions due to Combined Shear and Pressure," *Journal of the Mechanics and Physics of Solids*, Vol. 2, 1954, pp. 197-211.

17 Challen, J. M., and Oxley, P. L. B., "An Explanation of the Different Regimes of Friction and Wear Using Asperity Deformation Models," *Wear*, Vol. 53, 1979, pp. 229-243.

18 Rowe, G. W., and Wetton, A. G., "Theoretical Considerations in the Grinding of Metals," *Journal of the Institute of Metals*, Vol. 97, 1969, pp. 193-200.

19 Lee, E. H., and Shaffer, B. W., "The Theory of Plasticity Applied to a Problem of Machining," ASME *Journal of Applied Mechanics*, Vol. 18, 1951, pp. 405-413.

20 Abebe, M., and Appl, F. C., "A Slip-Line Solution for Negative Rake Angle Cutting," *Proc. Ninth N. Amer. Manuf. Res. Conf.*, SME, Dearborn, MI, 1981, pp. 341-348.

21 Sakamoto, T., and Tsukizoe, T., "Friction and Prow Formation in a Scratch Process of Copper by a Diamond Cone," *Wear*, Vol. 44, 1977, pp. 393-403.

22 Hill, R., "On the State of Stress in a Plastic-Rigid Body at the Yield Point," *Philosophical Magazine*, Vol. 42, 1951, pp. 868-875.

23 Dewhurst, P., "Is the Machining Process Uniquely Defined?" *Annals of the CIRP*, Vol. 27, 1978, pp. 1-4.

24 Tsukizoe, T., and Sakamoto, T., "Friction in Scratching without Metal Transfer," *Bulletin of the JSME*, Vol. 18, No. 115, 1975, pp. 65-72.

25 Sin, H., Saka, N., and Suh, N. P., "Abrasive Wear Mechanisms and the Grit Size Effect," *Wear*, Vol. 55, 1979, pp. 163-190.

26 Komanduri, R., "Some Aspects of Machining with Negative Rake Tools Simulating Grinding," *Int. J. Mach. Tool Des. Res.*, Vol. 11, 1971, pp. 223-233.

27 Kayaba, T., Kato, K., and Hokkirigawa, K., "Theoretical Analysis of the

Plastic Yielding of a Hard Asperity Sliding on a Soft Flat Surface," *Wear*, Vol. 87, 1983, pp. 151-161.

28 Kayaba, T., Hokkirigawa, K., and Kato, K., "Experimental Analysis of the Yield Criterion for a Hard Asperity Sliding on a Soft Flat Surface," *Wear*, Vol. 96, 1984, pp. 255-265.

APPENDIX

Geometrical Construction of the Domain KBJ

The construction of the field *KBJ* is shown in Fig. 12. From the geometry shown in this figure, it is found that $I\hat{J}B = (\pi/2) - \eta_2 - (\theta/2)$ and, hence, the circle (Q) which passes from *I* and *B* is geometrically determined. Thus, the intersection between the circle (Q) and the line which passes from I and makes an angle θ with *IB* defines point *J*. Consequently, the bisector of BJ intersects circle (Q) at O. The boundary *BJ* of the slip-line field can be obtained by drawing a circle (S) with center at O and radius OB.

Two characteristic slip-lines in field KBJ are shown in Fig. 12. Line TP is a β-line and the curve *PR*, which is an arc of a circle centered at *I* with radius *IP*, is an α-line. The angle, ω, that the α-lines meet the boundary *BJ* is not constant. It assumes a value equal to η_2 at *B* and *J* and a slightly higher value between. This implies that the interfacial shear stress, s, which is related to the interfacial angle, ω, through the following relation

$$s = k\cos(2\omega)$$

is not constant along the boundary *BJ*. In order to simplify the calculations it is reasonable to assume that $\omega = \eta_2$.

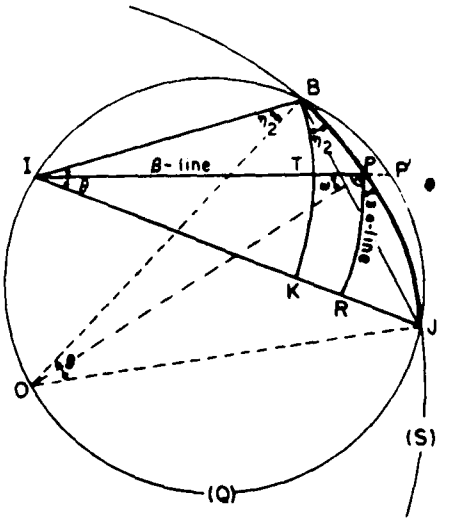

Fig. 12 Geometrical construction of field KBJ

This assumption is fairly correct because the arc *BJ* of circle (S) is very close to that of circle (Q), i.e., the distance PP' is very small so that the approximation $I\hat{P}O \simeq I\hat{B}O$ or $\omega \simeq \eta_2$ is valid. Thus, equation (1) can be used for calculating the shear stress on the boundary *BJ*.

DISCUSSION

F. E. Kennedy, Jr.[1]

The authors should be congratulated for producing a quite complete plasticity analysis of plowing phenomena in sliding contacts. Their model agrees very well with experimental friction coefficients obtained in a variety of tests with conical sliders under both lubricated and unlubricated conditions. Those results point out quite clearly the importance of plastic deformation in plowing and the major contribution of plowing to friction in many sliding contacts involving hard asperities. The application of the model to the authors' dry sliding experiments involving like materials prompts several questions, however. In particular, I hope that the authors might clarify the following points:

1. How were the semi-asperity angles used in Table 3 determined for the cases of like materials in dry sliding? Were the across-the-groove surface profiles of the disk specimens (Figure 1) used, and if so, would those across-the-groove angles be indicative of the angles of plowing asperities on the pin specimens measured in the sliding direction? Was there any evidence from the microscopic observation of the pin surfaces (eg. Figures 2-6) that asperities with α as small as 60° were actually present on the pins?

2. Could third-body particles (wear debris) be responsible for much of the plowing? Either loose debris or debris accumulation on the leading edge of the pins (as a prow) could have attack angles as large as those used in calculations for Table 3. Such debris could easily be work hardened to a hardness greater than that of the material being plowed.

3. It appears that the authors assumed that all plowing asperities, including both the rigid asperity of Figure 7 and the deforming hard asperity of Figure 11, were conical in shape. Would the resulting plastic flow around the cone really be approximated by a plane strain condition?

[1] Thayer School of Engineering, Dartmouth College, Hanover, N.H. 03755.

K. Kato[2]

Several analytical results to estimate the friction force and wear type with slip-line field theory were proposed in the past, some of which are listed by the authors.

The authors should be congratulated in trying to give a more precise analysis for the plowing process. The agreement between the calculated and experimental values of the coefficient of friction seems very good. But the discusser would like to suggest some points to be checked for better understanding:

(1) The question of the wear type: Although the authors' analysis is for the plowing process which should not generate wear debris, Figs. 7 and 8 imply the formation of microchips. Were any microchips of wear debris observed in the sliding tests and, if so, how large were they on the average?

(2) Observations by other researchers: What would be the experimental evidence for the existence of dead zone in their studies?

(3) The question of the quantitative differences between authors' and other researchers' calculated values. Every theoretical model has its own assumptions. In order to know its reliability and usefulness, quantitative comparisons between theoretical values by different methods are necessary. How large would the quantitative differences be between calculated values of authors and Challen et al. [A1] for example?

The discusser obtained good agreement between experimental values and theoretical values calculated with the theory of Challen et al. [A2].

Additional References

A1 Challen, J. M., and Oxley, "An Explanation of the Different Regimes of Friction and Wear Using Asperity Deformation Models," *Wear*, Vol. 53, 1979, pp. 229-243.

A2 Kato, K., and Hokkirigawa, K., "Abrasive Wear Diagram," *Proceedings of Eurotrib 85 Congres International de Tribologie*, Lyon, France, Sept. 9-12, 1985.

[2] Tohoku University, Sendai, Japan; Currently at NASA Lewis Research Center, Cleveland, Ohio.

Authors' Closure

We wish to express our appreciation to Professors Kennedy and Kato for their generous comments on the paper and for the critical questions. We hope that our response will help clarify the points raised by the discussers.

Reply to Professor F. E. Kennedy

The angles in Table 3 were determined from the surface profiles obtained perpendicular to the sliding direction. We have assumed that groove formation resulted from the microcutting action of the entrapped wear particles and/or hard asperities, and that the angle α is the same in directions perpendicular and parallel to the sliding direction. It is possible that some of the wear debris adhered initially to the surfaces and agglomerated to form wedges (prows), such as those reported in references [3] through [8], before it became loose eventually. The micrographs of the worn surfaces have indicated, however, that in most cases long plowing grooves formed parallel to the sliding direction. This experimental evidence suggests that plowing takes place primarily due to the wear debris entrapped at the interface. Because microscopic observation of the interface during sliding is not possible, and the orientation of the wear particles trapped at the interface cannot be determined, it was decided to use the values of α from the transverse surface profiles. Different kinds of experiments, such as with wedges of known cutting angles α or with abrasive papers where the slopes of the abrasive grits can be measured, are necessary. Nevertheless, a comparison of the theoretical values of the coefficient of friction with experimental values obtained from cutting experiments with conical tools of known angles α has shown that the aggreement was very good (see Fig. 10 and Table 2).

With respect to the question about the plane strain assumption for the plastic flow, plane strain conditions can be assumed to prevail when the width of cut is much larger than the depth of cut. The plane strain condition is an appropriate assumption when the rigid asperity (or wear particle) has the shape of a wedge. The flow is then confined to planes normal to the edge of the wedge and the problem can be analyzed fairly accurately with two-dimensional slip-line fields such as those shown in Figs. 7 and 11. Moreover, the plane strain condition is a reasonable approximation even when the wear debris and the asperities are idealized with spheres or cones, for example, provided that the depth of penetration is significantly less than the width of the formed groove. This is typically the case in metal sliding where the penetration depth to groove width ratio is much less than one. In the present study the depth-to-width ratio assumed values less than 0.3 (for lubricated sliding it was below 0.2) and thus the plane strain assumption for the plastic flow seems reasonable. Because the theoretical friction coefficients obtained from the slip-line analysis were in good agreement with the experimental friction results the plane-strain assumption, we think, is justified.

Reply to Professor K. Kato

The term plowing has been reserved for the plastic flow of a soft surface when a loaded rigid asperity slides over it. From the wear point of view, the plastically deforming material flows upwards and sideways of the microcutting edge resulting in the formation of wear debris (microchips) and ridges. Under certain conditions, e.g., for very soft metals such as indium and lead, the amount of wear debris produced is small and the deformed material is displaced along the sides of the groove. This type of wear, where very small amount of material is removed, has been referred to in the past as plowing. Alternatively, when the amount of wear debris is significant the material is removed as in metal grinding, i.e., in discontinuous microchips. Under these conditions the type of wear is microcutting.

From the friction point of view, however, plowing is referred to as the friction mechanism responsible for the formation of grooves due to the entrapped wear particles or hard asperities. Consequently, the plowing friction mechanism should not be confused with the particular type of wear. Numerous studies in the past have shown that wear debris and microchips are generated when plowing friction conditions prevail at the interface. This was also found to be the case in the present study. Wear debris formation was observed in all experiments. Because the focus of this study was on friction, systematic characterization of the debris was not attempted. However, wear particles in the range 1-10 μm were observed and the calculated wear coefficients were in the range 10^{-4} to 10^{-2}.

Furthermore, the analysis based on the slip-line model of Figs. 7 and 8 does not depend on the formation of wear debris and microchips. The friction coefficient is determined only from the deformation field defined by the boundaries HI, IA, ABJC, and HGFEDC, and thus it is appropriate for any plowing conditions, independent of the kind of wear.

It is difficult to identify the existence of a dead zone during sliding because observation at the interface when plowing occurs is not possible. The existence of a dead zone, however, has been observed in numerous plowing experiments in the past with cutting tools and in metal grinding. Because plowing in metal sliding is essentially similar to metal grinding [18], but on a smaller scale, it is expected that a dead zone will also form in front of the plowing wear particles and asperities during sliding.

As regards to the quantitative agreement between the theoretical friction values, our approach to the problem was to consider primarily all the qualitative aspects in plowing friction. The proposed models are in agreement with the experimental evidence obtained for plowing conditions. In addition, the remarkably good agreement between theoretical and experimental friction values of our work and other studies, indicates that the theoretical models are also quantitatively correct. The qualitative differences between our model and those most commonly used in the past are apparent from the details given in the paper. Because most of these models are in poor qualitative agreement with the experimental evidence, any correlation between friction values calculated from those models and experimental results must be fortuitous.

In particular, the qualitative limitations of the models proposed by Challen and Oxley [17] have been addressed in the introduction. Hence, a quantitative comparison between our model and those of reference [17] is unrealistic. In reference [A2], however, a comparison between experimental values and theoretical values obtained from [17] was attempted. Although an artificial correction factor was introduced to bridge the gap between the theoretical and experimental friction values of that study, the agreement is poor. In fact, it was found that the experimental friction coefficient values were higher than the theoretical friction coefficients by 30 to 70 percent.

The Significance of Oxide Layers in Boundary Lubrication

K. Komvopoulos
Mem. ASME

N. Saka

N. P. Suh

Department of Mechanical Engineering,
Massachusetts Institute of Technology,
Cambridge, Mass. 02139

Analytical and experimental studies were conducted on oxidized and nonoxidized pure aluminum, OFHC copper, and electroplated chromium to investigate the role of surface oxide layers in boundary lubrication. The effects of the thickness of the oxide layers, the elastic moduli of the oxide and the metal, and the normal surface traction have been addressed. In addition, several possible failure mechanisms of both thin and thick oxide films have been proposed. The experimental results have shown that low coefficients of friction, about 0.1 or less, and especially low wear can be obtained in boundary-lubricated sliding if the metal surfaces are protected from plastic deformation by sufficiently thick oxide layers. Scanning electron microscopy has shown that when the oxide layers are not ruptured, the wear of the surfaces is negligibly small. In this case, the oxide-oxide contacts deform primarily elastically and the predominant friction mechanism is the shear of the lubricant film. Based on this evidence, a theoretical model for friction was proposed and the agreement between theoretical and experimental coefficients of friction was reasonably good. Disruption of the oxide layers during sliding, however, was found to result in plastic deformation and plowing of the surfaces.

1 Introduction

Since the early 1950s much attention was devoted to the effect of oxide films on the friction and wear of sliding surfaces. Low friction and mild wear of unlubricated metallic surfaces were attributed to the presence of thin oxide films which prevented the formation of intermetallic welds [1–4]. The formation of the protective oxide films during sliding was studied by the electrical contact resistance measurements [5–7], and the high contact resistance was assumed to indicate shearing within an oxide layer which resulted in low friction [6, 7]. Rabinowicz [4] has proposed that low friction can be obtained only when the oxide films are sufficiently thick, about 10 nm. Also, the wear of oxide-covered metal surfaces in dry sliding was investigated by Quinn et al. [8–10] and an analytical model for oxidational wear was proposed.

By contrast, the tribological behavior of oxidized metallic surfaces under lubricated sliding conditions has received only modest attention. Bowden and Young [11] have observed that lubrication of clean surfaces with long-chain fatty acids did not result in low friction typical of boundary-lubricated surfaces, but the presence of water vapor and oxygen was found to be effective. They interpreted that a strongly anchored tenacious soap film, a few molecules thick, was formed due to a complex chemical reaction between the fatty acid molecules and a thin oxide surface layer. Tingle [12] has offered similar interpretations for boundary-lubricated metal surfaces with fatty acids in solutions. Lubricated experiments with copper-beryllium alloys have shown that for a given load the degree of intimate plastic contact was greater for softer alloys [13]. Accordingly, it was suggested that the increase or decrease in the coefficient of friction with subsurface hardness was due to the breakdown of the oxide layer due to incompatible strains at the oxide-metal interface, as was also proposed by Whitehead [1] and Wilson [6, 7] for dry sliding. Experiments of Hirst and Lancaster [14] with different metals and lubricants have shown that the rate of oxidation influenced remarkably the effectiveness of the oxide films in reducing friction and wear. It was observed that oxide layers which formed slowly at room temperature yielded lower coefficients of friction as opposed to oxides formed at high temperatures.

The significance of dissolved oxygen in lubricated sliding was studied by numerous investigators. For example, steel rollers lubricated with plain mineral oil showed that the surfaces with high oxygen concentration suffered minimum wear [15]. Experimental results have also been reported for iron-chromium [16, 17] and iron-silicon [18] alloys sliding in oxygen of controlled partial pressure. Low friction was obtained when the sliding interface was completely covered by oxide mixtures and oxidized metallic debris. Begelinger and deGee [19] have observed that a drastic decrease in friction and wear occurred when the oxygen concentration in the lubricant was increased. They postulated that oxidation of the asperity contacts prevented the formation of metal-to-metal contacts wherever the lubricant layer was penetrated by the surface irregularities. Similarly, in a recent study in boundary lubrication [20] it has been shown that an optimum value for the amount of oxygen in the lubricant exists for which minimum wear occurs. When this value was exceeded a transition to a regime of high wear resulted, apparently due to the rupture of an appreciably thick oxide.

Blouet and Courtel [21] slid pure aluminum on tool steels submerged in different lubricants and discovered that the coefficient of friction and the wear rate decreased significantly when the thickness of the aluminum oxide reached a critical

Contributed by the Tribology Division for publication in the JOURNAL OF TRIBOLOGY. Manuscript received by the Tribology Division, August 15, 1985.

value of 70 nm. Experimental work on aluminum alloys slid against steels in lubricants has also shown that aluminum oxide had a marked effect on both friction and wear [22, 23], independent of oxide thickness and subsurface alloy. This is in complete disagreement with previous studies where the oxide thickness and the subsurface hardness were stated as important parameters for the effectiveness of the oxide film [1, 4, 6, 7]. It was also found that removal of the magnesium oxide, which was considered to be a solid lubricant, with an ammonium salt solution produced higher friction coefficients. However, this was not found to be the case in a different study with similar aluminum alloys without lubricants, where it was reported that the coefficient of friction was not affected by the magnesium oxide layer [24].

In the past, the friction of oxidized surfaces in lubricated sliding was explained on the basis of the conventional model for boundary lubrication [25]. It was argued that friction was low because of the reduced interfacial shear strength of the oxide-covered asperity junctions. This friction model, however, does not account for some important parameters, such as the thickness of the oxide film and the elastic moduli of the oxide layer and the metal substrate, which have been stated as important in other studies. Moreover, recent work in boundary lubrication has addressed the limitations of the conventional boundary lubrication model and has shown that the predominant steady-state friction mechanism is plowing [26]. From the wear point of view, it was also shown that the primary wear mechanism of boundary-lubricated metal surfaces is an abrasive-type mechanism [27]. These studies in boundary lubrication have indicated that the prevailing friction and wear mechanisms can be minimized if plastic deformation at the sliding interface can be made to vanish.

The aim of this study, therefore, is to investigate whether oxide films can minimize plastic deformation and thus friction and wear. In particular, this paper addresses the prevailing friction mechanisms of oxide-covered metal surfaces in boundary lubrication, and presents experimental results based on which an analytical model for friction, when the oxide film is not ruptured, is obtained. In addition, several possible failure mechanisms for thin and thick oxide films are proposed.

2 Experimental Procedures

2.1 Materials. Pure aluminum, OFHC copper and chromium (125 μm thick electroplated on AISI 1095 steel) were chosen for this investigation. The primary reasons for this choice are the availability of sufficient information on the oxidation kinetics of these metals, and the marked differences in the mechanical properties (e.g., elastic modulus and hardness) of the three metals and their oxides. The aluminum and copper specimens were annealed for an hour at 673 K and 873 K, respectively, in an argon atmosphere before oxidation. Table 1 lists the experimental materials and their properties.

Table 1 Properties of Experimental Materials

Property	Material: Aluminum	Copper	Chromium
Hardness before annealing (MPa)	294 ± 52	1,363 ± 53	6,590 ± 284
Hardness after annealing (MPa)	186 ± 16	510 ± 21	–
Oxide hardness (MPa)	19,613[a]	1,716[a]	15,690[b]
Oxide-metal hardness ratio for:			
a. Metal hardness before annealing	66.71	1.26	2.38
b. Metal hardness after annealing	105.44	3.36	–
Density (g/cm^3)	2.70	8.96	7.19
Molar volume (cm^3)	9.99	7.09	7.23
Oxide density (g/cm^3)	3.97	6.30	5.21
Oxide molar volume (cm^3)	25.68	12.62	29.17
Oxide-metal molar volume ratio	2.57	1.78	4.03

[a]Reference [4]
[b]Estimated

2.2 Oxidation of the Specimens. After polishing the pin and the disk specimens to obtain a mirror finish, they were cleaned with soap and warm water, rinsed with methanol and acetone, dried in air, and then oxidized in a furnace. The oxidation temperatures were so selected that oxide layers of a wide range of thicknesses could be obtained. After an hour of oxidation at a given temperature, the specimens were furnace cooled to room temperature to minimize cracking of the oxide layers due to thermal stresses. The temperature of oxidation was maintained to within 4°C. Table 2 lists the temperatures of oxidation for each metal, the corresponding calculated oxide

Nomenclature

A = preexponential factor
C = constant
E, E_1, E_2 = elastic moduli
E' = effective modulus
F = tangential force
L = normal force
M_{me}, M_{ox} = molecular weights
Q = activation energy
R = radius of pin, radius of cylindrical asperity, or gas constant
T = temperature
V_{me}, V_{ox} = molar volumes
a = half contact width
a_0 = half contact width of Hertzian contact
h_{min}, h_c = minimum and central lubricant film-thicknesses
k = ellipticity parameter
m, n = constants
p = pressure
p_a = actual pressure at center of contact
p_0 = maximum pressure in Hertzian contact
r = distance from centerline
s = lubricant shear strength
t = time
v = velocity
Φ = function of oxygen partial pressure
ψ = function of temperature
α = contact area ratio (a_0/a)
β = pressure ratio (p_a/p_0)
γ = viscosity-pressure coefficient
δ = stoichiometry ratio
η_0 = viscosity at ambient pressure
λ = lubricant thickness to surface roughness ratio
μ = coefficient of friction or traction ratio
ν, ν_1, ν_2 = Poisson's ratios
ξ = oxide layer thickness
ρ_{me}, ρ_{ox} = densities

Subscripts

l = layer
me = metal
ox = oxide
s = substrate

Table 2 Oxide film thickness and surface roughness for an hour of oxidation in air

Metal	Oxidation temperature (K)	Calculated Oxide thickness (nm)	Centerline average roughness (μm)
Aluminum	373	4.2	0.05
	473	7.5	0.137
	573	11.0	0.146
	673	15.6	0.152
	773	68.5	0.15
Copper	408	7.0	0.1
	433	9.0	0.1
	445	10.0	0.53
	513	12.5	0.11
	555	30.7	0.3
	673	208.0	0.28
Chromium	773	28.2	0.05
	973	126.6	0.1
	1173	926.3	1.22

thicknesses and the measured centerline average surface roughnesses. The details of calculations are given in the Appendix (equations (A4)-(A9)).

2.3 Lubricant. In order to avoid complications from the formation of boundary films, which may result from chemical reactions between the lubricant and the surfaces during sliding, a relatively inert additive-free mineral oil was used. The oil was primarily a mixture of naphthenic hydrocarbons. Table 3 lists some properties of the mineral oil.

Table 3 Properties of the lubricant

Viscosity at 310 K	74 cSt
Viscosity at 372 K	11 cSt
Density at 298 K	0.886 g/cm^3
Flash point	455 K
Surface tension at 298 K	26.9 dyn/cm

2.4 Experiments. A pin-on-disk tester was used to conduct the experiments. The experimental apparatus has been described in detail in a previous publication [26]. The normal load was 2 N, but tests were also conducted with loads in the range 0.02-1 N. The angular speed was 4.5 rad/s and the linear speed was between 0.6 and 3.5 cm/s. All tests were conducted in laboratory air at room temperature.

Before each experiment the oxidized specimens were rinsed gently with methanol and acetone, dried in air and then tested on the pin-on-disk tester. The tested specimens were cleaned again after the experiment with warm water and acetone and stored in a container with Ca_2SO_4 at room temperature. Depending on the experimental scatter at least three tests were conducted in each case. All tested specimens were observed in an optical microscope. Some of the specimens were cleaned with acetone in an ultrasonic cleaner for a few minutes and then were observed in a scanning electron microscope. A surface profilometer was used for obtaining the centerline average surface roughnesses of the oxidized and worn surfaces. The diamond stylus of the profilometer had a tip radius of 2.5 μm and the stylus force was 0.1 g. The scanning speed was about 1.5 mm/s.

3 Experimental Results

3.1 Aluminum. As Fig. 1 shows, the coefficient of friction of the nonoxidized aluminum was initially about 0.45 and then it decreased rapidly to a steady value of 0.2. The initial coefficients of friction of the oxidized aluminum surfaces, however, were significantly lower, in the range 0.1 to 0.25 (except in the case of the aluminum oxidized at 773 K for which it was high, about 0.4), and the steady-state values were only marginally lower, between 0.15 and 0.2. Roughness measurements of the oxidized surfaces have shown that the surface roughness increased with the temperature of oxidation (Table

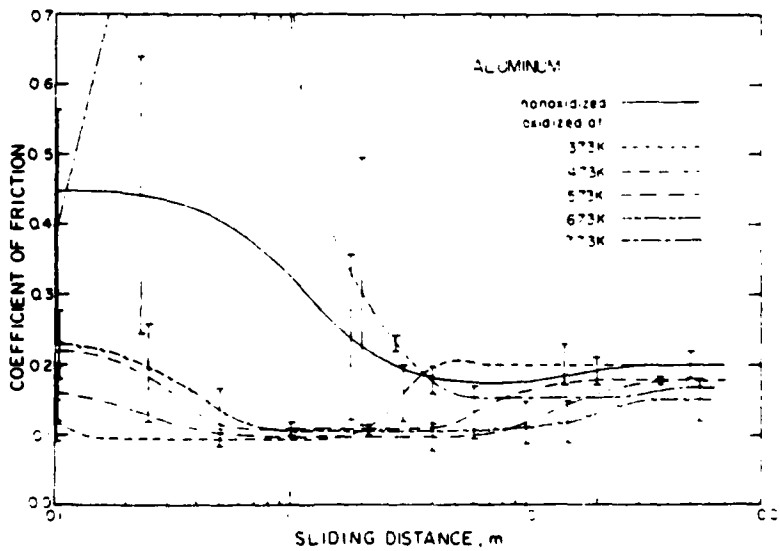

Fig. 1 Coefficient of friction versus sliding distance for nonoxidized and oxidized aluminum surfaces slid on themselves (lubricated experiments, normal load = 2 N)

2). The increase of the initial coefficient of friction with the oxidation temperature may be attributed, therefore, to the initial surface roughness. The friction curves of the aluminum oxidized at 373, 473, 573, and 673 K show a transition from a low friction to a relatively high friction regime. By contrast, the friction curve for the specimens oxidized at 773 K shows that initially the friction coefficient assumed very high values (the maximum was about 0.96) and eventually a steady-state value of 0.17.

Representative micrographs of the worn disk and pin surfaces, which were oxidized at 673 K, are shown in Fig. 2. Although a few narrow plowing grooves have formed on the surfaces plastic deformation did not occur at every location, in contrast with the nonoxidized surfaces. Figure 3 shows the worn surfaces of aluminum specimens oxidized at 673 K after the transition. It is evident that the surfaces have undergone severe plastic deformation and that the interfacial contact was primarily intermetallic. In the case of the specimens oxidized at other temperatures similar observations before and after the transition were made. However, for the aluminum oxidized at 773 K the topography of the worn surfaces was similar to those of Fig. 3, even for extremely short sliding distances.

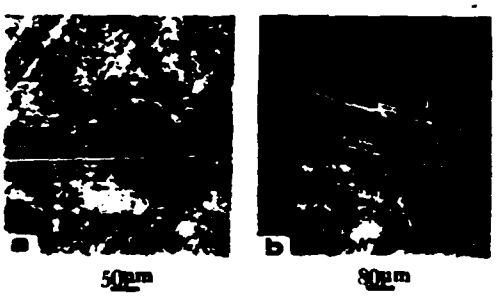

Fig. 2 Wear tracks of aluminum surfaces oxidized at 673 K: (a) disk and (b) pin (normal load = 2 N, distance slid = 17 m)

3.2 Copper. The coefficients of friction of the nonoxidized and oxidized copper are shown in Fig. 4. For the nonoxidized copper the initial coefficient of friction was 0.18 and the steady-state value was 0.17. The initial coefficient of friction of the oxidized copper assumed values between 0.12 and 0.2 depending on the roughness of the oxide layer. Surface profilometry of the oxidized copper surfaces demonstrated that the roughness increased due to oxidation (see Table 2). For example, the highest initial coefficient of friction was about 0.2 and was obtained with copper specimens oxidized at 445 K, the temperature for which the roughest oxide was formed. Marginally lower steady-state coefficients of friction, between 0.09 and 0.15, were found for the oxidized copper.

Scanning electron micrographs have shown that surface plowing occurred at the initiation of sliding. More and relatively large grooves were formed on the nonoxidized copper surfaces and on the copper with thin oxide layers. Examination of the plowed surfaces with a profilometer indicated that the depth of the grooves was larger than the thickness of the

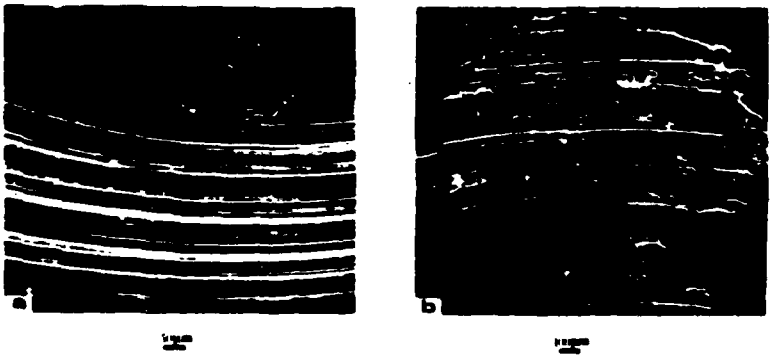

Fig. 3 Wear tracks of aluminum surfaces oxidized at 673 K: (a) disk and (b) pin (normal load = 2 N, distance slid = 29.5 m)

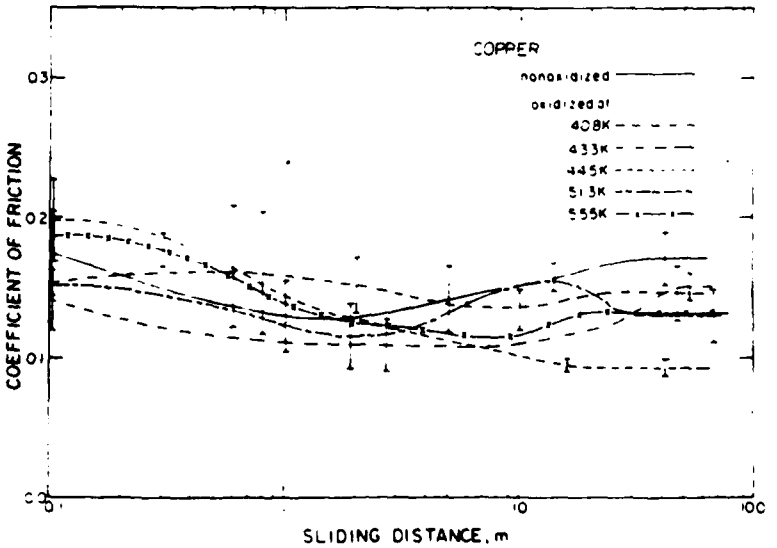

Fig. 4 Coefficient of friction versus sliding distance for nonoxidized and oxidized copper surfaces slid on themselves (lubricated experiments, normal load = 2 N)

oxide layer. However, in the case of the thick oxide layers (e.g., 31 and 208 nm thick) many grooves with depths less than the oxide thickness were also found. It appears, therefore, that plastic deformation and complete rupture of the oxide layer occurred at the initiation of sliding only in the case of the thin oxide films.

Figure 5 shows numerous plowing grooves on both surfaces. Rupture of ridges formed due to plowing, and wear debris formation is also noticeable in Figs. 5(*a*) and 5(*c*). Typical micrographs of worn surfaces oxidized at 555 K are shown in Fig. 6. It is evident, by comparing the surfaces shown in Figs. 5(*a*) and 6(*a*), that fewer plowing marks have been formed on the disk surface of Fig. 6(*a*), possibly due to the protection against plowing provided by the thicker oxide. However, many plowing grooves have been formed on the pin surface (Fig. 6(*b*)). This may be attributed to the continuous contact of the pin during sliding, in contrast to the disk surface where contact with the pin occurs at any location only once in each revolution. Thus, plastic deformation and removal of the protective oxide layer may have occurred initially on the pin surface and much later on the disk. Figure 6(*a*) is an example of

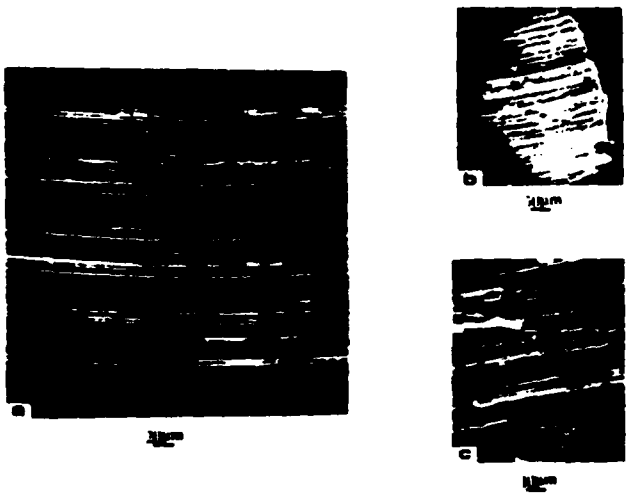

Fig. 5 Wear tracks of copper surfaces oxidized at 408 K: (*a*) disk, (*b*) pin, and (*c*) higher magnification of pin surface (normal load = 2 N, distance slid = 23 m)

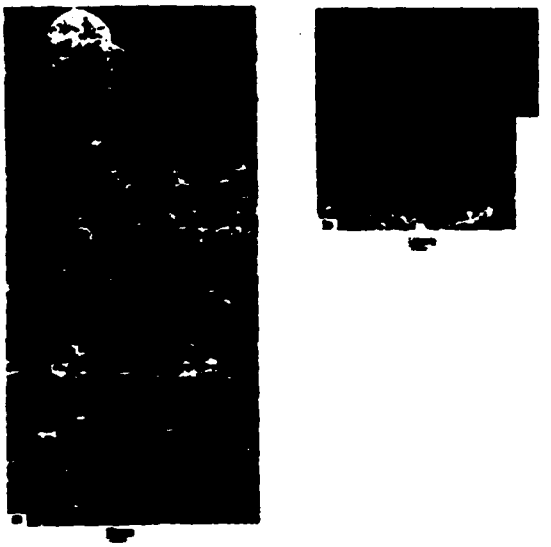

Fig. 6 Wear tracks of copper surfaces oxidized at 555 K: (*a*) disk and (*b*) pin (normal load = 2 N, distance slid = 29 m)

the partially removed oxide film. The figure also shows oxide islands on the sliding interface which have survived rupture and locations where the oxide has been removed. Similar observations were made on copper oxidized at 673 K.

3.3 **Chromium.** Figure 7 shows the friction coefficients of the nonoxidized and oxidized chromium. The nonoxidized chromium produced an initial coefficient of friction of 0.2 and after 0.5 m of sliding it attained a maximum of 0.35. A steady-state value of 0.15 was reached after 5 m of sliding. The friction curves of the oxidized chromium are substantially different at the very beginning of sliding. However, the steady-state values of the oxidized chromium were very close to the steady-state friction coefficient of the nonoxidized chromium, about 0.15. The most interesting result was that the coefficients of friction increased with the oxide thickness; the coefficient of friction of the thinner oxide formed at 773 K was markedly lower than the friction coefficient of the nonoxidized chromium until a steady-state was reached. Then it re-

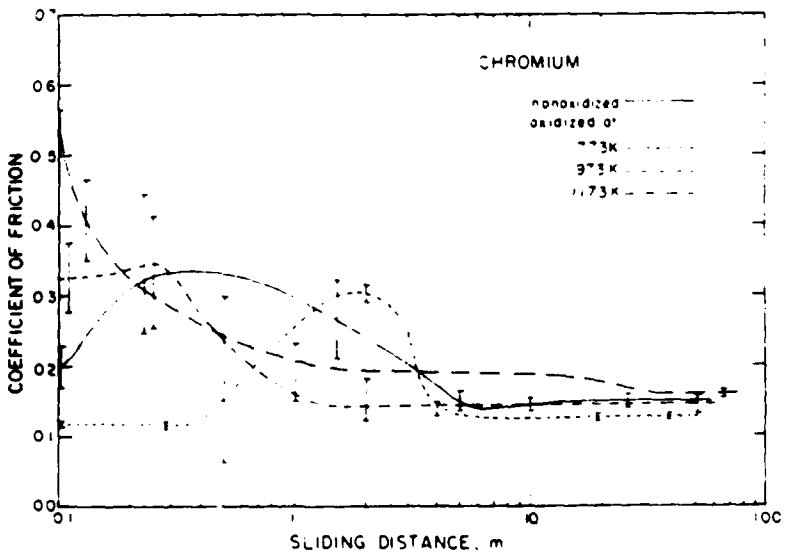

Fig. 7 Coefficient of friction versus sliding distance for nonoxidized and oxidized chromium surfaces slid on themselves (lubricated experiments, normal load = 2 N)

mained constant and was slightly lower than the steady-state coefficient of friction of the nonoxidized chromium, i.e., about 0.13.

Scanning electron microscopy and surface profilometry indicated that the surface roughness increased with the oxide thickness (Table 2). The differences in the initial coefficient of friction can be associated, therefore, with variations of the surface roughness as a function of the oxide film thickness. All oxidized surfaces were green, but those oxidized at 773 K retained the initial mirror finish. The oxide film produced after oxidation especially at 1173 K, was quite darker and duller than the other two cases.

As in the case of aluminum, the thinner chromium oxide showed a transition from low to high friction and wear. Micrographs of the low friction-wear regime obtained for different sliding distances illustrated that initially, when the coefficient of friction was about 0.12, the surfaces did not show any evidence of plastic deformation. However, after relatively short distances of sliding a maximum value of 0.31 was reached and many plowing marks formed on the surfaces, eventhough the coefficient of friction reduced eventually to a low steady-state value equal to 0.13. Figures 8 and 9 show characteristic micrographs of chromium oxidized at 773 K obtained from the low and high friction regimes, respectively. Figure 8 shows no evidence of plowing on any of the surfaces. (The cracks on the surfaces were observed on all the chromium surfaces after oxidation.) The micrographs have been taken before the maximum coefficient of friction was reached (i.e., before the transition from low to high friction). By contrast, Fig. 9 shows that plastic deformation and groove formation took place on both surfaces. The micrographs have been obtained after the maximum (about 0.35) coefficient of friction was reached and after a steady-state value of 0.14 was attained. The surface topography of the oxide layers formed at 973 and 1173 K was similar to that of Fig. 9 even for extremely short sliding distances. It was also found that the surfaces of the chromium pins which were oxidized at 973 and 1173 K suffered severe plowing and rupture of the oxide film almost within the first revolution. Plastic deformation and plowing of the disk surfaces, however, was noticeably less than that of the pin surfaces.

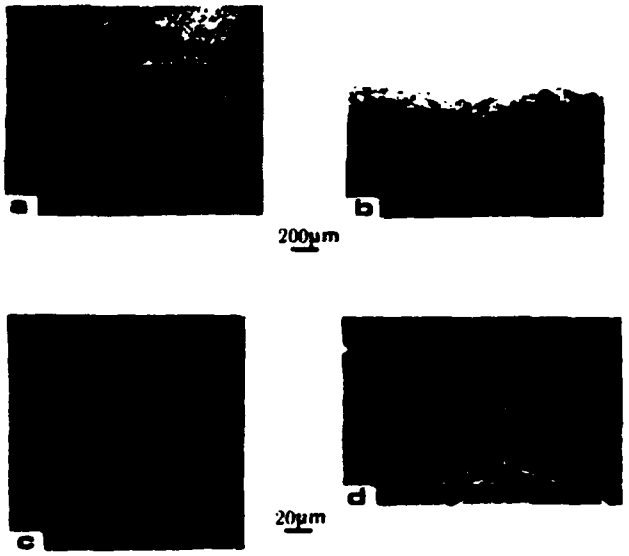

Fig. 8 Wear tracks of chromium surfaces oxidized at 773 K: (a) disk, (b) pin, (c) and (d) higher magnification of disk and pin surfaces, respectively (normal load = 2 N, after 20 revolutions of sliding)

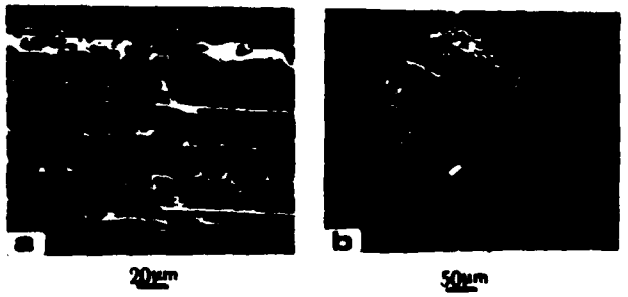

Fig. 9 Wear tracks of chromium surfaces oxidized at 773 K: (a) disk and (b) pin (normal load = 2 N, distance slid = 28.3 m)

3.4 Experiments With Light Loads. To investigate the significance of the normal load on the friction and wear behavior, experiments with loads in the range 0.02 to 1 N were also conducted. One of the striking findings was that for a certain material, oxide thickness and load combination, plastic deformation of the sliding pairs was negligibly small. In addition, the magnitudes of the initial coefficients of friction with loads less than or equal to 1 N were noticeably lower than those obtained with 2 N. However, the steady-state values were only marginally lower than those obtained with the 2 N normal load.

Figure 10 shows the initial coefficients of friction for the load range 0.02 to 2 N. The figure shows a general trend for lower friction up to 1 N, and higher friction at 2 N. The reduction of the initial friction coefficient is more significant for oxidized aluminum than for oxidized copper and chromium. This discrepancy may be due to the removal of the oxide film from the copper and chromium surfaces, especially for the relatively heavy loads. It is also worth noting that the initial coefficients of friction of the nonoxidized surfaces are, in general, lower than those of the oxidized surfaces perhaps due to the rougher surfaces of the oxide layers. This appears to be more significant in the case of very light loads (less than 0.5 N). A possible reason for this discrepancy may be the instantaneous flattening (i.e., deformation) of the oxide undulations due to the heavy loads, in contrast to the case of the light loads.

Figure 11 shows the steady-state values of the coefficient of friction versus load for both nonoxidized and oxidized surfaces. The results are scattered and, thus, cannot be consid-

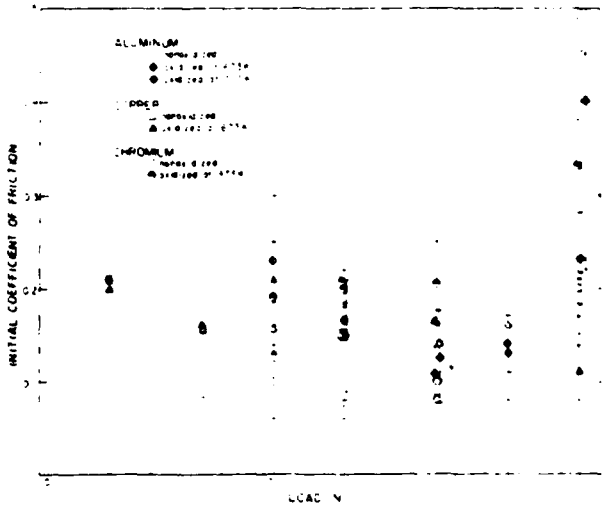

Fig. 10 Initial coefficients of friction versus load for nonoxidized and oxidized aluminum, copper, and chromium surfaces slid on themselves (lubricated experiments)

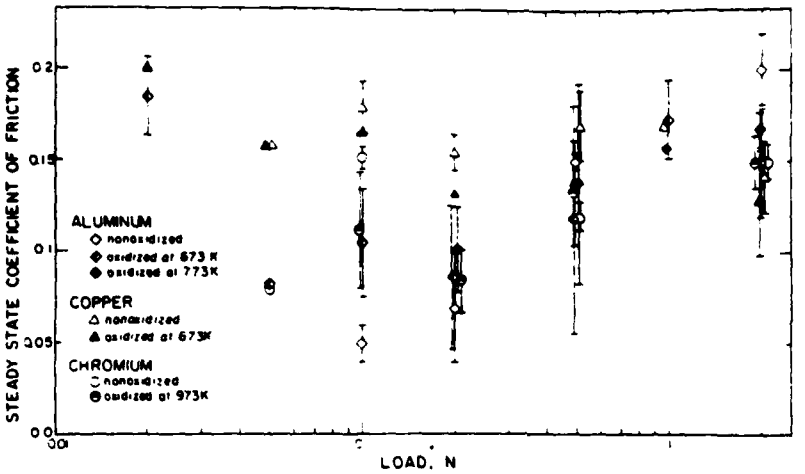

Fig. 11 Steady-state coefficients of friction versus load for nonoxidized and oxidized aluminum, copper, and chromium surfaces slid on themselves (lubricated experiments)

Fig. 12 Wear tracks of copper surfaces oxidized at 673 K: (a) disk and (b) pin (normal load = 0.05 N, distance slid = 55 m)

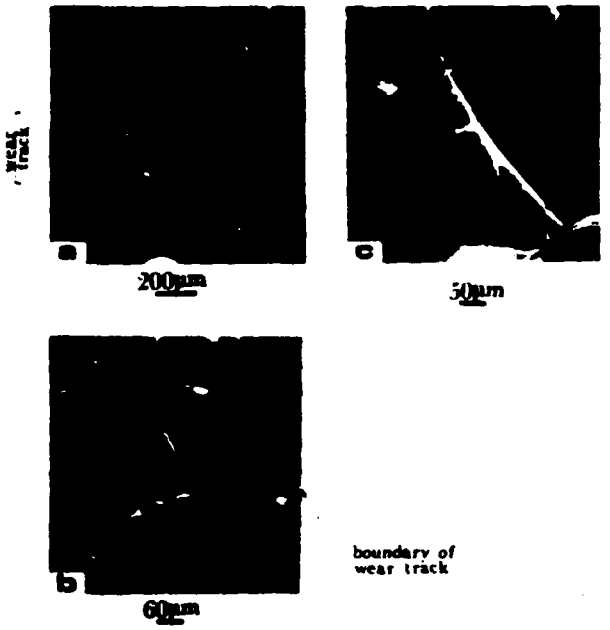

Fig. 13 Wear tracks of chromium surfaces oxidized at 973 K: (a) disk, (b) higher magnification of disk surface, and (c) pin (normal load = 0.2 N, distance slid = 68 m)

ered conclusive due to almost complete rupture of the oxide layers when the steady-state friction was attained. The somewhat lower steady-state friction values obtained for light loads may be attributed to less plowing of the surfaces as opposed to the steady-state friction values for heavy loads (e.g., for 2 N) where severe plowing occurred. Indeed, surface micrographs of the worn surfaces showed fewer and significantly smaller grooves on the surfaces for sliding with light loads.

Figure 12 supports the validity of the above remarks. The micrographs of this figure were obtained after sliding copper oxidized at 673 K on itself for 55 m with a load of 0.05 N. Two plowing grooves can be seen on the disk surface (Fig. 12(*a*)). However, despite the relatively large distance of sliding the rest of the surface is still covered with the oxide layer. More, and relatively smaller grooves have formed on the pin surface as shown in Fig. 12(*b*), due to the continuous contact of the pin surface which resulted in severe plastic deformation and, thus, removal of the oxide film. Nevertheless, the number and size of the plowing grooves, as well as the width of the wear tracks are significantly smaller than those obtained from the experiments with 2 N.

The most promising experimental results were found in the case of chromium. It was found that under light loads low friction coefficients, about 0.1 or less, and practically no wear occurred. This was found to be the case even for the thick oxides for which high friction and wear were found for 2 N. The oxidized surfaces appeared to have deformed only elastically in contrast to the nonoxidized surfaces where plastic deformation (plowing) occurred even for very light loads. The topography of the surfaces after large sliding distances was not altered at all and micrographs similar to that of Fig. 8 were obtained. Figure 13, for example, shows the surfaces of chromium oxidized at 973 K and slid for 68 m under a load of 0.2 N. Neither the disk nor the pin surface shows any evidence of plastic deformation. Figure 13(*b*), which is a higher magnification of Fig. 13(*a*), shows that only burnishing has taken place wherever contact was established. The worn surfaces of the same materials but under a load of 2 N were similar with those of Fig. 9 even for very short sliding distances. It appears, therefore, that under the 0.2 N load the deformation at the contact interface was primarily elastic.

4 Analysis and Discussion

It has been proposed in the past that low friction and mild wear can be obtained when the oxides are hard and easily shearable [1], with thicknesses larger than a critical value [1, 4]. But easily shearable oxides are soft and thus they cannot resist penetration during sliding. The experimental work of

this investigation has demonstrated on the contrary that oxide films of any thickness may be effective depending on the normal and tangential surface tractions. It has also been argued that the relative hardness of the oxide to the metal substrate controls the deformation at the oxide-metal interface and thus the disruption of the protective oxide layer [6, 7, 13]. However, when the oxide is not ruptured during sliding, the oxide-oxide contacts deform primarily elastically and the interfacial stresses and strains depend on the elastic properties (e.g., modulus of elasticity) of the oxide and the metal subsurface, and the thickness of the oxide layer.

It is evident, therefore, that the friction and wear mechanisms associated with oxidized metallic surfaces in lubricated sliding must be analyzed in terms of the appropriate parameters when the deformation mode of the interfacial contacts is elastic or plastic.

4.1 Friction Coefficient When The Deformation Mode Is Elastic. It is evident from Figs. 8 and 13 that when the oxide is not removed, plastic deformation and wear of the sliding surfaces are virtually insignificant. Under these conditions, the deformation of the sliding contacts is elastic. The experimental friction coefficients for this case were in the range 0.1 to 0.2, which are typical of boundary-lubricated surfaces. Moreover, the lubrication regime can also be defined in terms of the ratio of the lubricant film thickness to the combined surface roughness, λ. For the pin-on-disk geometry the minimum and central film thicknesses, h_{min} and h_c, can be obtained as [28]

$$h_{min} = 3.63RU^{0.68}G^{0.49}W^{-0.073}(1-e^{-0.68k}) \quad (1)$$

$$h_c = 2.69RU^{0.67}G^{0.53}W^{-0.067}(1-0.61e^{-0.73k}) \quad (2)$$

where,

$$U=\frac{\eta_0 v}{E'R} \quad G=\gamma E' \quad W=\frac{L}{E'R^2}$$

and R is the radius of the pin, η_0 is the viscosity at ambient pressure, v is the sliding velocity, γ is the viscosity-pressure coefficient, L is the normal load, E' is the effective modulus of elasticity ($=E/(1-\nu^2)$), and k is the ellipticity parameter which is equal to 1.0339 for a sphere on flat type of contact [28].

Because the micrographs and surface profiles of the nonoxidized surfaces have shown plowing and plastic deformation in all cases, only the lubrication regime of the oxidized metal surfaces needs to be identified. The most likely case for elastohydrodynamic film lubrication corresponds to the experiments conducted with the lightest load (0.02 N) and highest sliding speed (3.5 cm/s). For these values of L and v, and for $E = 4.14 \times 10^{11}$ N/m^2 and $\nu = 0.25$ (which are typical values for oxides), and $R = 3.175$ mm (radius of pin), the following values of h_{min} and h_c were calculated from equations (1) and (2)

$$h_{min} \simeq 0.0196\ \mu m \quad h_c \simeq 0.0346\ \mu m$$

On the assumption that the roughness values of the pin surfaces are the same as the roughness values of the disk surfaces (Table 2), the estimated film-thickness values for h_{min} and h_c are significantly smaller (in most cases by an order of magnitude or more) than the combined surface roughness. For example, the largest value that the ratio λ can assume is 0.49 and is obtained for the roughness value 0.05 μm (i.e., combined surface roughness of 0.071 μm) and film thickness of 0.0346 μm. It can be concluded, therefore, that $\lambda < 1$ and that sliding of the elastically deformed oxidized surfaces occurred in the boundary lubrication regime.

The elastic boundary-lubricated sliding contact can be idealized as shown in Fig. 14 and expressions for the coefficient of friction or, more appropriately, the traction ratio can be obtained from a Hertzian-type analysis. The figure shows an elastic layer of uniform thickness, ξ, and elastic properties E_l and ν_l, rigidly adhered to an elastic half-space with elastic-properties E_s and ν_s. The elastic medium is loaded by an asperity, which is assumed to be rigid and cylindrical. From the Hertzian solution for homogeneous and isotropic media, the normal pressure at the asperity contact can be expressed as

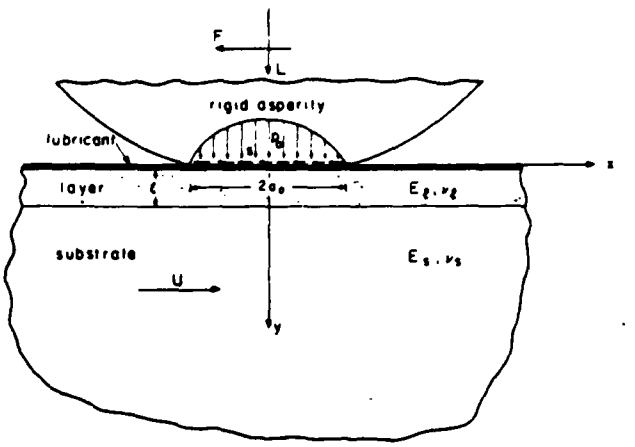

Fig. 14 Model of contact between a stationary rigid cylindrical asperity and a sliding elastic layered medium

$$p(r) = p_0\left[1-\left(\frac{r}{a_0}\right)^2\right]^{1/2} \quad (3)$$

where p_0 is the maximum pressure along the centerline of the contact (i.e., at $r = 0$), r is the distance from the centerline and a_0 is the half width of the contact given by

$$a_0 = 2\left[\frac{LR(1-\nu^2)}{\pi E}\right]^{1/2} \quad (4)$$

where L is the normal load per unit length (normal to the xy-plane), R is the radius of the cylindrical asperity, and E and ν, are the elastic modulus and Poisson's ratio of the half-space.

In the case of layered media, however, the stresses and strains deviate from the Hertzian solution, depending on the ratio of the elastic moduli of the layer and the substrate, and the ratio of the contact width to the layer thickness [29-32]. For moderate values of the ratio of the elastic moduli Gupta and Walowit [31], for instance, have proposed that the pressure at the contact of a cylindrical indenter and a layered medium can be approximated fairly accurately as a weighted sum of elliptic and parabolic functions, i.e.,

$$p = \frac{p_0}{1-\frac{8}{3\pi}}\left[\left(\alpha-\frac{8}{3\pi}\beta\right)\left\{1-\left(\frac{r}{a}\right)^2\right\}^{1/2} + (\beta-\alpha)\left\{1-\left(\frac{r}{a}\right)^2\right\}\right] \quad (5)$$

where $\alpha = a_0/a$, $\beta = p_a/p_0$, and a and p_a are the actual half contact width and actual normal pressure at $r = 0$, respectively. It is reasonable to assume moreover that the above solution is also valid when small tangential tractions, typical of boundary lubricated surfaces, are present at the contact interface.

The friction force will then arise primarily from shearing of the lubricant film. Thus, if s is the shear strength of the lubricant film, the friction force per unit length, F, will be

$$F = 2\int_0^a s\,dr = 2as \quad (6)$$

The normal load per unit length, L, can be expressed as

$$L = 2\int_0^a p(r)\,dr \quad (7)$$

Substituting the expression for the pressure $p(r)$ from equation (5) in equation (7) the normal load L per unit length can be written as

$$L=\frac{2ap_0}{1-\frac{8}{3\pi}}\int_0^a\left[\left(\alpha-\frac{8}{3\pi}\beta\right)\left\{1-\left(\frac{r}{a}\right)^2\right\}^{1/2}+(\beta-\alpha)\left\{1-\left(\frac{r}{a}\right)^2\right\}\right]d\left(\frac{r}{a}\right) \tag{8}$$

and after integration of equation (8) the normal load L is given by

$$L=\frac{\pi}{2}a\left(\frac{\alpha}{\beta}\right)p_e \tag{9}$$

where $p_e=\beta p_0$.

Then, the coefficient of friction, $\mu=F/L$, can be obtained by dividing equation (6) with equation (9) as

$$\mu=\frac{4}{\pi}\left(\frac{s}{p_e}\right)\left(\frac{\beta}{\alpha}\right) \tag{10}$$

Equation (10) indicates that the coefficient of friction is a function of the ratio s/p_e and the ratio β/α which accounts for the deviation from the Hertzian solution. The parameters α and β, however, depend on the ratio of the layer thickness to the half contact width, ξ/a, and the elastic properties, E_1, ν_1, and E_2, ν_2, of the layer and substrate respectively [31].

Figure 15 shows several friction curves as a function of the dimensionless ratio ξ/a and for different values of s/p_e and E_1/E_2. The curves were obtained from equation (10) and the parameters α and β from reference [31] for the assumed values of the ratios ξ/a and E_1/E_2 and for $\nu_1=\nu_2=0.25$. The figure shows that the coefficient of friction is almost constant when $\xi/a<0.05$ and when $\xi/a>2$. The friction coefficient decreases gradually as the ratio ξ/a assumes values in the range 0.05 to 2. When the layer is very thick (i.e., when $\xi/a\gg 1$) or very thin (i.e., when $\xi/a\ll 0.1$) the coefficient of friction attains the assymptotic value, $(4/\pi)(s/p_e)$, which corresponds to the Hertzian solution ($\alpha=\beta=1$). The effect of the elastic moduli of the layer and substrate is pronounced especially when $0.1<\xi/a<1$. In this regime the coefficient of friction decreases as the ratio E_1/E_2 increases. In general, the elastic moduli of oxides are several times higher than the moduli of metals. Hence, the curves obtained for $E_1/E_2=1$, 2, 4 and 8 are appropriate for oxide layers and metallic substrates.

Moreover, the parameter which primarily controls the magnitude of the coefficient of friction is the ratio s/p_e. Lower s/p_e ratios can reduce the coefficient of friction to 0.05, or even less. This suggests that extremely low friction coefficients could be obtained in boundary lubrication if the contact pressure can be increased significantly, but without surface plastic deformation. Figure 10, for example, shows that the coefficient of friction of the oxide-covered metal surfaces assumes relatively lower values when the load, and hence the contact pressure, was increased. However, in the case of heavy loads (2 N) the coefficient of friction was high due to plastic deformation of the surfaces. This is evident from the micrographs of the surfaces slid under 2 N.

The effect of the lubricant shear strength, s, on the coefficient of friction is equally important. It has been reported that at low pressures the lubricant shear strength is approximately constant but at high pressures it increases with the pressure in a roughly proportional manner [33, 34]. Rabinowicz has argued that the ratio s/p, where p is the hydrostatic pressure, obtains a value of about 0.1 when p is low and about 0.05 when p is high [34]. In view of the proposed range for the values that the ratio s/p may obtain, the friction curves for $s/p_e=0.05$, 0.1, and 0.2 are also shown in Fig. 15. (Because of the difficulties associated with integration, it was assumed that s/p_e is of the same order of magnitude as the mean value of s/p.)

A comparison between theoretical coefficients of friction, as given by equation (10), and experimental friction data is also shown in Fig. 15. The experimental friction coefficients have been obtained from oxidized aluminum, copper, and chromium surfaces at the onset of sliding with light loads (below 1 N) i.e., when the contact can be assumed to be elastic. The ratio of the oxide thickness to half contact width was based on the calculated thickness of the oxides (see Table 2) and by assuming that the half contact width is 1 μm, which is reasonable for the size of the asperity contacts. It is evident that the experimental data are fairly well-bounded between the theoretical friction curves of $s/p_e=0.1$ and 0.2, and the overall agreement between theoretical and experimental coefficients of friction is reasonably good. It may be concluded, therefore, that when the oxide layers do not deform plastically or fracture, the contact is primarily elastic and the predominant friction mechanism is the shear of the lubricant film.

It must be also emphasized that the above analysis does not depend on the type of the oxides formed, but only on the elastic properties of the oxide and the metal below, the ratio of the oxide thickness to the asperity half contact width, the lubricant shear strength and the pressure at the center of the contact interface, provided, of course, that the deformation is elastic.

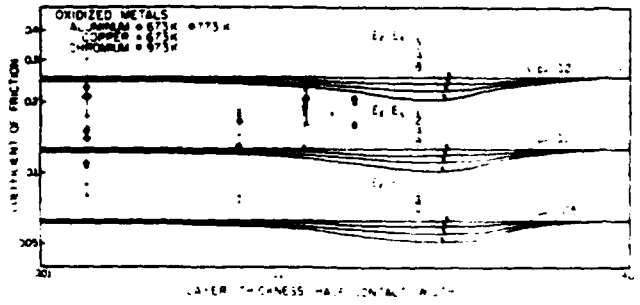

Fig. 15 Theoretical friction coefficient curves versus ratio of oxide layer thickness to asperity half contact width, and experimental friction coefficients of oxidized aluminum, copper, and chromium

4.2 The Friction Mechanism When The Deformation Mode Is Plastic. The experimental results show that the oxidized metal surfaces may deform plastically either at the onset of sliding or after sliding for a certain distance. Figures 3, 5, 6, and 9 show plowing and severe plastic deformation of the surfaces and partial or complete disruption of the oxide layer.

Removal of the oxide layer can be due to different failure mechanisms. The oxide can be removed due to debonding between the oxide and the metal. This may take place if the shear stress at the oxide-metal interface is higher than the shear strength of the interface. In this case, local debonding between the layer and the substrate will initiate plastic deformation and consequent disruption of the oxide film. This mechanism occurs when the oxide is very thin, because the shear stress does not decay sufficiently within the oxide and thus it is high at the oxide-metal interface. However, debonding can also occur

when the oxide is very thick and the interfacial pores (cavities) promote crack growth.

The oxide layer can also be disrupted due to plastic deformation in the substrate. Because the oxides in general are harder than the metal below, plastic deformation of the substrate can occur even if the oxide layer deforms elastically. This failure mechanism is more pronounced when the oxide is thin, because of the high stresses produced in the metal substrate.

It is also essential to emphasize some microstructural aspects of the oxide, especially the porosity and microcracks. The coverage of the oxide on the metal substrate depends on the oxide-metal volume ratio, known as the Pilling-Bedworth ratio [35], which represents the oxide volume divided by the volume of the metal that has been replaced by the oxide. (This assumption is valid only if the formation of the oxide takes place primarily through an inward migration of oxygen through the oxide.) Hence, if the ratio is less than one, the oxide will not cover the entire metal surface and, thus, a discontinuous oxide will form. Alternatively, if the ratio is greater than one a continuous oxide forms. The condition for the formation of a continuous oxide can be written as

$$\frac{V_{ox}}{V_{me}} > 1$$

or

$$\frac{1}{\delta}\left(\frac{\rho_{me}}{\rho_{ox}}\right)\left(\frac{M_{ox}}{M_{me}}\right) > 1 \qquad (11)$$

where V_{ox}, M_{ox}, and ρ_{ox} are the volume, the molecular weight, and the density of the oxide respectively, and V_{me}, M_{me}, and ρ_{me} are the same parameters of the metal. The parameter δ is a stoichiometric ratio. If it is assumed that the oxides formed are Al_2O_3, CuO, and Cr_2O_3 (as quoted in much of the literature), then the oxide-metal volume ratios are 1.28, 1.78, and 2.02, respectively; δ is equal to 1 in the case of CuO and equal to 2 for the case of Al_2O_3 and Cr_2O_3. Because the ratios are greater than one, the criterion set by the relation (11) is satisfied. This suggests that oxidation of aluminum, copper, and chromium results in the formation of continuous oxide layers.

Although the condition set by the relation (11) is necessary for a continuous oxide to form, it is subject to some limitations. For example, if the ratio assumes values larger than two or higher, the volume of the oxide is larger than the volume of the oxidized metal. Under these conditions high stresses may arise within the oxide. Kofstad [36] has reported that when a critical thickness has been attained fracture of the oxide due to the internal stresses may occur, resulting in a cracked and porous oxide microstructure. This was found to be the case in the present study with copper and chromium oxidized at 673 and 1173 K, respectively (i.e., for the relatively thicker oxides of the two metals). Moreover, micrographs of the oxidized surfaces have shown cracking of the oxide layers in the case of chromium, i.e., when the Pilling-Bedworth ratio assumed the highest value, 2.02. Indeed Figs. 8, 9, and 13 show cracks on the surfaces of oxidized chromium.

It is also well known that solids with internal cracks and cavities delaminate when normal and tangential tractions are applied at the interface during sliding. The primary fracture process of the thick oxides can be associated, therefore, with crack propagation in the porous oxide structure. The thicker oxides will contain more and larger pores than the thinner oxides and, thus, the cracks will propagate faster and from deeper locations, and finally will link up easily to produce large oxide flakes. The high friction and severe surface damage obtained with the thick oxide layers in the present experimental work can be attributed to the delamination of the pre-cracked and porous oxides. Moreover, instantaneous penetration of the thick oxides may also occur before the onset of sliding, due to the low resistance against penetration of the porous oxides. However, the experimental results of the present investigation show that under certain conditions even a cracked oxide may not be ruptured. This was indeed found to be the case with oxidized chromium surfaces slid under light loads (0.2 N). The coefficient of friction in these experiments was about 0.1 and the wear of the surfaces was extremely low (see Fig. 13, for example), perhaps because the low surface tractions were insufficient to cause delamination or penetration of the oxide.

The failure mechanisms of thin and thick oxide layers discussed above are schematically shown in Fig. 16. The figure shows failure due to: interfacial debonding, plastic deformation of the substrate, penetration of the layer and substrate plastic deformation, and delamination of a porous and cracked oxide layer. These failure mechanisms may occur concomitantly or separately, depending on the situation. In addition, one mechanism may initiate another one as sliding advances.

The micrographs of the worn surfaces have shown clearly that plowing and plastic deformation of the surfaces occurred when the protective oxide layer was removed. Under these

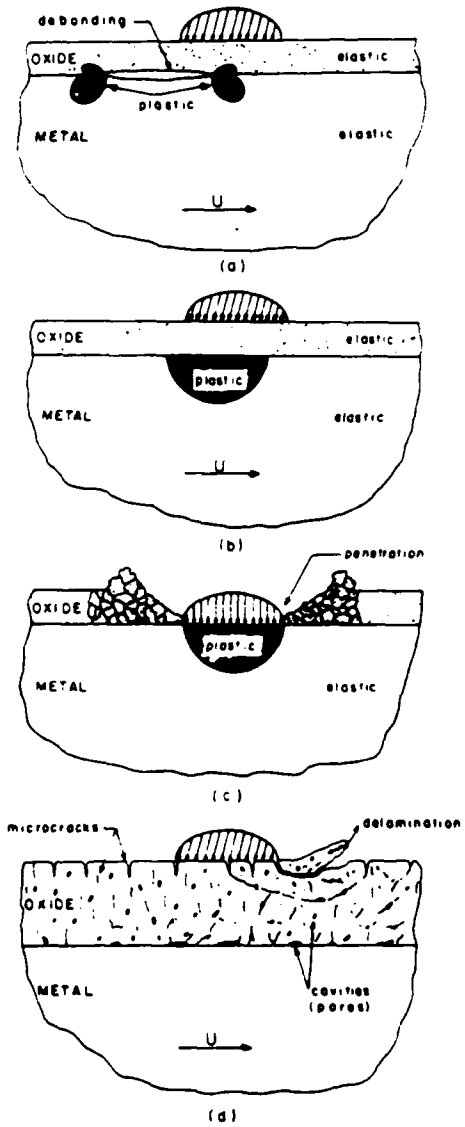

Fig. 16 Mechanisms of oxide failure due to: (a) interfacial debonding, (b) plastic deformation of the substrate, (c) penetration of oxide layer and subsurface plastic deformation, and (d) delaminatik n of porous and precracked oxide layer

conditions, the significance of the oxide and metallic debris produced is important in friction. Then the friction force arises primarily due to plowing and microcutting of the surfaces by the entrapped debris and the predominant steady-state wear mechanism is an abrasive type mechanism [26, 27]. The experimental friction coefficients, when the protective oxide layer was removed, were found to be in good agreement with the friction values obtained from the analytical models quoted in reference [26] and the surface topography statistics.

5 Conclusions

From the experimental and analytical work the following conclusions can be drawn regarding the role of oxide layers in boundary lubrication:

1. Under certain conditions, low friction and virtually insignificant wear may result in the boundary-lubricated sliding of oxide-covered surfaces.
2. When the surfaces do not undergo plastic deformation, the primary friction mechanism is the shear of the lubricant film. The proposed analytical model for these sliding conditions indicates that the coefficient of friction depends on the lubricant shear strength, the pressure at the center of contact, the ratio of the elastic moduli of the oxide layer and the metal substrate, and the ratio of the oxide thickness to the asperity half contact width. The theoretical model yields coefficients of friction in fair agreement with the experimental friction data.
3. In general, the oxide-oxide contacts deform elastically when the normal surface traction is low and the oxide layers are compact and sufficiently thick. Conversely, when the oxides are thick and porous they are ruptured easily resulting, thus, in plastic deformation of the sliding surfaces.
4. Disruption of the surface oxide layer generally results in higher friction and severe wear. The oxide and metallic wear debris produced is entrapped at the interface and plowing and microcutting of the surfaces occurs. Under these conditions, the friction force arises predominantly from plowing and the wear is controlled primarily by an abrasive-type wear mechanism.

Acknowledgments

This work was sponsored by the Office of Naval Research under Contract N00014-82-K-0520. The personal support of Dr. A. W. Ruff and Dr. R. S. Miller is gratefully acknowledged.

References

1 Whitehead, J. R., "Surface Deformation and Friction of Metals at Light Loads," *Proc. Roy. Soc. (London)*, Series A, Vol. 201, 1950, pp. 109–124.
2 Lancaster, J. K., "The Formation of Surface Films at the Transition Between Mild and Severe Metallic Wear," *Proc. Roy. Soc. (London)*, Series A, Vol. 273, 1963, pp. 466–483.
3 Peterson, M. B., Florek, J. J., and Lee, R. E., "Sliding Characteristics of Metals at High Temperatures," *Trans. ASLE*, Vol. 3, 1960, pp. 101–109.
4 Rabinowicz, E., "Lubrication of Metal Surfaces by Oxide Films," *Trans. ASLE*, Vol. 10, 1967, pp. 400–407.
5 Cocks, M., "Surface Oxide Films in Intermetallic Contacts," *Nature*, Vol. 170, 1952, pp. 203–204.
6 Wilson, R. W., "Influence of Oxide Films on Metallic Friction," *Proc. Roy. Soc. (London)*, Series A, Vol. 212, 1952, pp. 450–452.
7 Wilson, R. W., "The Contact Resistance and Mechanical Properties of Surface Films on Metals," *Proc. Phys. Soc.*, Series B, Vol. 68, 1955, pp. 625–641.
8 Quinn, T. F. J., "The Effect of "Hot-Spot" Temperatures on the Unlubricated Wear of Steel," *Trans. ASLE*, Vol. 10, 1967, pp. 158–168.
9 Quinn, T. F. J., and Sullivan, J. L., "A Review of Oxidational Wear," *Proc. Int. Conf. on Wear of Materials*, St. Louis, Mo., April 25–28, 1977, Eds. Glaeser, W. A., Ludema, K. C., and Rhee, S. K., ASME, New York, 1977, pp. 110–115.
10 Quinn, T. F. J., Sullivan, J. L., and Rowson, D. M., "New Developments in the Oxidational Theory of the Mild Wear of Metals," *Proc. Int. Conf. on Wear of Materials*, Dearborn, Mich., April 16–18, 1979, Eds. Ludema, K. C., Glaeser, W. A., and Rhee, S. K., ASME, New York, 1979, pp. 1–11.
11 Bowden, F. P., and Young, J. E., "Friction of Clean Metals and the Influence of Adsorbed Films," *Proc. Roy. Soc. (London)*, Series A, Vol. 208, 1951, pp. 311–325.
12 Tingle, E. D., "Influence of Water on the Lubrication of Metals," *Nature*, Vol. 160, 1947, p. 710.
13 Moore, A. J. W., and Tegart, W. J. McG., "Relation Between Friction and Hardness," *Proc. Roy. Soc. (London)*, Series A, Vol. 212, 1952, pp. 452–458.
14 Hirst, W., and Lancaster, J. K., "The Influence of Oxide and Lubricant Films on the Friction and Surface Damage of Metals," *Proc. Roy. Soc. (London)*, Series A, Vol. 223, 1954, pp. 324–338.
15 Bjerk, R. O., "Oxygen – An "Extreme-Pressure Agent"," *Trans. ASLE*, Vol. 16, No. 2, 1973, pp. 97–106.
16 Barnes, D. J., Wilson, J. E., Stott, F. H., and Wood, G. C., "The Influence of Oxide Films on the Friction and Wear of Fe-5% Cr Alloy in Controlled Environments," *Wear*, Vol. 45, No. 2, 1977, pp. 161–176.
17 Wilson, J. E., Stott, F. H., and Wood, G. C., "The Development of Wear – Protective Oxides and Their Influence on Sliding Friction," *Proc. Roy. Soc. (London)*, Series A, Vol. 369, 1980, pp. 557–574.
18 Lee, R. Y., and Eliezer, Z., "On The Critical Thickness of Protective Films at Sliding Interfaces," *Wear*, Vol. 95, 1984, pp. 165–175.
19 Begelinger, A., and deGee, A. W. J., "On the Mechanism of Lubricant Film Failure in Sliding Concentrated Steel Contacts," ASME JOURNAL OF LUBRICATION TECHNOLOGY, Vol. 98, No. 4, 1976, pp. 575–579.
20 Nakayama, K., and Okamoto, J., "Effect of Dissolved Oxygen on Friction and Wear of Copper Under Boundary Lubrication," *Trans. ASLE*, Vol. 23, No. 1, 1980, pp. 53–60.
21 Blouet, J., and Courtel, R., "Phases of Wear of the Aluminum/Steel Couple in Lubricated Friction," *Wear*, Vol. 34, 1975, pp. 109–125.
22 Overfelt, R. A., Wert, J. J., and Hunt, W. H., "The Influence of Thermal Oxide Characteristics on the Friction Behavior of Aluminum Auto Body Sheet Alloys," *Trans. ASLE*, Vol. 24, No. 2, 1981, pp. 175–185.
23 Edwards, W. T., Bhargava, V., Wert, J. J., Wefers, K., and Hunt, W. H., "The Influence of Surface Oxide Characteristics on the Friction Behavior of Aluminum and Aluminum Alloys," *Proc. Int. Conf. on Wear of Materials*, San Francisco, California, March 30–April 1, 1981, Eds. Rhee, S. K., Ruff, A. W., and Ludema, K. C., ASME, New York, 1981, pp. 23–30.
24 Sargent, L. B., "The Influence of Aluminum Oxides on the Transfer of Some Aluminum Alloys to Steel in Sliding Contact," *Lubr. Eng.*, Vol. 38, No. 10, 1981, pp. 615–621.
25 Bowden, F. P., and Tabor, D., *The Friction and Lubrication of Solids*, Clarendon Press, Oxford, 1958, pp. 219–227.
26 Komvopoulos, K., Saka, N., and Suh, N. P., "The Mechanism of Friction in Boundary Lubrication," ASME JOURNAL OF TRIBOLOGY, Vol. 107, 1985, pp. 452–462.
27 Komvopoulos, K., Suh, N. P., and Saka, N., "Wear of Boundary-Lubricated Metal Surfaces," *Wear*, Vol. 107, 1986, pp. 107–132.
28 Hamrock, B. J., and Dowson, D., *Ball Bearing Lubrication The Elastohydrodynamics of Elliptical Contacts*, A Wiley-Interscience Publication, John Wiley, New York, 1981, pp. 207 and 212.
29 Chen, W. T., and Engel, P. A., "Impact and Contact Stress Analysis in Multilayer Media," *Int. J. Solids Structures*, Vol. 8, 1972, pp. 1257–1281.
30 Pao, Y. C., Wu, T.-S., and Chiu, Y. P., "Bounds on the Maximum Contact Stress of an Indented Elastic Layer," ASME *Journal of Applied Mechanics*, Vol. 38, 1971, pp. 608–614.
31 Gupta, P. K., and Walowit, J. A., "Contact Stresses Between an Elastic Cylinder and a Layered Elastic Solid," ASME JOURNAL OF LUBRICATION TECHNOLOGY, Vol. 96, 1974, pp. 250–257.
32 Chiu, Y. P., and Hartnett, M. J., "A Numerical Solution for Layered Solid Contact Problems With Application to Bearings," ASME JOURNAL OF LUBRICATION TECHNOLOGY, Vol. 105, 1983, pp. 585–590.
33 Briscoe, B. J., Scruton, B., and Willis, F. R., "The Shear Strength of Thin Lubricant Films," *Proc. Roy. Soc. (London)*, Series A., Vol. 333, 1973, pp. 99–114.
34 Rabinowicz, E., "Friction-Especially Low Friction," *Fundamentals of Tribology*, Eds. Suh, N. P., and Saka, N., The MIT Press, Cambridge, MA, 1980, pp. 351–364.
35 Pilling, N. B., and Bedworth, R. E., "The Oxidation of Metals at High Temperatures," *J. Inst. Metals*, Vol. 29, 1923, pp. 529–591.
36 Kofstad, P., *High-Temperature Oxidation of Metals*, John Wiley, New York, 1966, pp. 228–233.

APPENDIX

Thickness of the Oxide Films

The oxidation rate $d\xi/dt$ of metals can be expressed approximately in terms of the oxygen partial pressure, p_{O_2}, and the temperature of oxidation, T, as follows [A1]

$$\frac{d\xi}{dt} = \frac{1}{\xi^m} \Phi(p_{O_2}) \cdot \psi(T) \qquad \text{(A1)}$$

where ξ is the oxide thickness, and Φ and ψ are functions of

the oxygen partial pressure and the temperature of oxidation, respectively. From the literature [A1] the following expressions for the above functions can be quoted

$$\Phi(p_{O_2}) \sim [p_{O_2}]^{1/n} \quad 2 < n < 8$$
$$\psi(T) \sim \exp(-Q/RT) \tag{A2}$$

where Q is the activation energy and R is the gas constant. Substitution of equations (A2) into equation (A1) and integration gives the following relationship for the oxide film thickness

$$\xi^{m+1} = A \cdot \exp(-Q/RT) \cdot t \tag{A3}$$

where $A = C(m+1)[p_{O_2}]^{1/n}$ and C is a constant.

(*a*) ***Aluminum.*** In the present study, the experimental results reported in references [35, A2–A7] were used for the calculation of the oxide film thickness for an hour of oxidation. Thus, the following relationships for the oxide thickness, in the corresponding temperature range, are obtained

$$\ln\xi = -1{,}035\left(\frac{1}{T}\right) + 6.5 \qquad \text{for } T < 573 \text{ K} \tag{A4}$$

$$\ln\xi = -7{,}688\left(\frac{1}{T}\right) + 16.5 \qquad \text{for } 573 < T < 873 \text{ K} \tag{A5}$$

Using equation (A5) and assuming a parabolic law for the oxidation rate the following equation, which has the same form as equation (A3) for $m = 1$, is obtained,

$$\xi^2 = 5.67 \times 10^8 \exp(-30{,}500/\text{RT}) \cdot t \qquad \text{for } 573 < T < 873 \text{ K}$$

where $t = 3{,}600$ *s* and ξ is in *nm*. The obtained magnitude of the activation energy, 30,500 cal/mol, is in fair agreement with the reported results [A3–A5].

(*b*) *Copper.* Based on the experimental results of references [35, A8–A10] the following two relationships for low and high temperature oxidation (for an hour of heating) are obtained

$$\ln\xi = -1{,}742\left(\frac{1}{T}\right) + 8.5 \qquad \text{for } T < 473 \text{ K} \tag{A6}$$

$$\ln\xi = -6{,}058\left(\frac{1}{T}\right) + 16.6 \qquad \text{for } 473 < T < 1173 \text{ K} \tag{A7}$$

Again, assuming a parabolic law (i.e., equation (A3) for $m = 1$) equation (A7) gives

$$\xi^2 = 7.9 \times 10^8 \exp(-24{,}000/\text{RT}) \cdot t \qquad \text{for } 473 < T < 1173 \text{ K}$$

where the oxide thickness, ξ, is in *nm* and the time, t, is equal to 3,600 s. The obtained activation energy, 24,000 cal/mol, is in close agreement with the reported values for copper for a similar temperature range [A11].

(*c*) *Chromium.* The experimental results of Phalnikar et al. [A12] for oxidation in air were used in the present study for calculating the oxide thickness. For an hour of oxidation the following equations are obtained

$$\ln\xi = -5{,}641\left(\frac{1}{T}\right) + 12.9 \qquad \text{for } 773 < T < 1073 \text{ K} \tag{A8}$$

$$\ln\xi = -13{,}003\left(\frac{1}{T}\right) + 20.2 \qquad \text{for } 1073 < T < 1273 \text{ K} \tag{A9}$$

Assuming a parabolic-type of oxidation law for equations (A8) and (A9) the following relations are obtained

$$\xi^2 = 4.84 \times 10^5 \exp(-22{,}400/RT) \cdot t \qquad \text{for } 773 < T < 1073 \text{ K}$$

$$\xi^2 = 1.0 \times 10^{12} \exp(-51{,}500/RT) \cdot t \qquad \text{for } 1073 < T < 1273 \text{ K}$$

where the oxide thickness, ξ, is in *nm* and the time, t, is equal to 3,600 s.

The magnitudes of the activation energies are in fair agreement with those reported by Gulbransen and Andrew [A13]; the discrepancy may be attributed in part to the effect of the oxygen partial pressure which was different in each study. Nevertheless, the disagreement is not large and both investigations suggest that a parabolic oxidation rate law is essentially obeyed between 773 K and 1373 K.

References of Appendix

A1 Kubaschewski, O., and Hopkins, B. E., *Oxidation of Metals and Alloys*, Butterworths, London, 1962, pp. 35–53.

A2 Reference [A1], p. 38.

A3 Smeltzer, W. W., "Oxidation of Aluminum in the Temperature Range 400°–600°C," *J. Electrochem. Soc.*, Vol. 103, 1956, pp. 209–214.

A4 Smeltzer, W. W., "Principles Applicable to the Oxidation and Corrosion of Metals and Alloys," *Corrosion*, Vol. 11, 1955, pp. 366–374.

A5 Gulbransen, E. A., and Wysong, W. S., "Thin Oxide Films On Aluminum," *J. Phys. and Colloid Chem.*, Vol. 51, 1947, pp. 1087–1103.

A6 Gulbransen, E. A., "The Kinetics of Oxide Film Formation on Metals and Alloys," *Trans. Electrochem. Soc.*, Vol. 91, 1947, pp. 573–604.

A7 Aylmore, D. W., Gregg, S. J., and Jepson, W. B., "The Oxidation of Aluminium in Dry Oxygen in the Temperature Range 400–650°C," *J. Inst. Metals*, Vol. 88, 1960, pp. 205–208.

A8 Rhodin, T. N., "Low Temperature Oxidation of Copper. I. Physical Mechanism," *J. Am. Chem. Soc.*, Vol. 72, 1950, pp. 5102–5106.

A9 Valensi, G., "Theoretical and Experimental Investigations on the Simultaneous Formation of Several Layers During Oxidation," *Proc. Int. Conf. on Surface Reactions*, Pittsburgh, PA, 1948, p. 156.

A10 Vernon, W. H. J., "The Formation of Protective Oxide Films on Copper and Brass by Exposure to Air at Various Temperatures," *J. Chem. Soc.*, Vol. 128, 1926, pp. 2273–2282.

A11 Tylecote, R. F., "Review of Published Information on the Oxidation and Scaling of Copper and Copper-Base Alloys," *J. Inst. Metals*, Vol. 78, 1950, pp. 259–300.

A12 Phalnikar, C. A., Evans, E. B., and Baldwin, W. M., "High Temperature Scaling of Cobalt-Chromium Alloys," *J. Electrochem. Soc.*, Vol. 103, 1956, pp. 429–438.

A13 Gulbransen, E. A., and Andrew, K. F., "Kinetics of the Oxidation of Chromium," *J. Electrochem. Soc.*, Vol. 104, 1957, pp. 334–338.

The Role of Hard Layers in Lubricated and Dry Sliding

K. Komvopoulos[1]
Mem. ASME

N. Saka

N. P. Suh

Department of Mechanical Engineering,
Massachusetts Institute of Technology,
Cambridge, MA 02139

Lubricated and dry experiments on titanium and steel surfaces with and without TiN sputtered coatings of various thicknesses have been conducted. The significance of the layer thickness, interfacial "friction", magnitudes of normal and tangential surface tractions, and the mechanical properties of the layer and of the substrate (e.g., elastic modulus and hardness) are critically examined. The conditions under which the deformation mode at the solid-solid contacts is elastic or plastic are addressed in light of the experimental evidence and a finite element analysis. It is shown that surfaces with very low friction, especially for unlubricated sliding, and practically zero wear rates can be obtained in both lubricated and dry sliding by coating the surfaces with sufficiently thick TiN layers. Removal of the protective TiN layer resulted in plowing, severe damage, and delamination.

1 Introduction

It is well established now that friction and surface damage can be minimized if plastic deformation of the material at the contact interface is prevented. Hard and sufficiently thick coatings, which can withstand high stresses without plastic deformation or fracture, are more effective in reducing friction and wear than soft layers. For instance, unlubricated experiments with nickel and copper electroplated with chromium, cobalt, rhenium, and rhodium demonstrated that the wear coefficients were lower by one to three orders of magnitude than the wear coefficients of the unplated surfaces [1]. Furthermore, chemically and physically vapor-deposited hard coatings, such as nitrides, carbides, and oxides, on metallic and ceramic substrates have significantly improved the tribological properties of various machine elements and cutting tools [2-7]. High wear-resistance coatings have also been produced by such nonconventional techniques as laser processing; a laser beam is used to melt a mixture of metallic compounds and bind them onto the substrate [8].

A literature survey has indicated that a variety of techniques can be successfully employed to produce surfaces with low friction and minimal wear in sliding. In particular, the beneficial effects of ion implantation on the tribological properties of sliding surfaces have been observed in several studies [9-11]. Ion implantation of pure iron and commercially pure titanium, for example, has significantly reduced the coefficient of friction and especially the surface damage [11]. The high wear resistance of the implanted surfaces was attributed to the hardened layer which lowered the friction force by minimizing plowing; the low friction, in turn, reduced the subsurface delamination and wear. Also, the friction values of the ion implanted titanium were markedly lower than those reported for lubricated titanium [12]. In comparison with other surface hardening processes, ion implantation has several advantages. It is carried out at relatively low temperatures and it does not affect even the highest surface finish. Moreover, there is no interface, as with a coating, to suffer debonding. The thickness of the ion implanted layers, however, is limited to 200 nm approximately and thus this process is appropriate only for sliding under light loads.

By contrast, high wear-resistance coatings with good adherence to various substrates and without coating-thickness limitations can be obtained by deposition processes such as sputtering, ion plating and reactive evaporation. Indeed, aluminum alloys and steel surfaces subjected to rolling and sliding contacts, and cutting tool inserts experienced extremely low wear when coated with a 5 μm thick TiN layer by magnetron reactive sputtering [13, 14]. Similarly, radio-frequency sputter deposition of 4-5 μm thick TiN on high speed steel cutting tools increased the tool life by a factor of 2 to 4 [5]. Also, ion-plated high speed drills with 1.5 μm TiN produced low friction at the chip-tool interface and minimal wear [6]. Dry and lubricated experiments with aluminum, titanium and stainless steel surfaces coated with 4-8 μm thick TiC and TiN by a reactive evaporation process showed that the coefficient of friction and the surface damage were noticeably lower than the uncoated surfaces [15]. In fact, friction coefficients of 0.1 or less were reported for some of the dry tests depending on the base material and the deposited layer.

Although most of the past investigations have provided useful information about the significance of hard layers on the tribological properties of various materials, the role of such critical parameters as the layer thickness, surface tractions and the mechanical properties of the layer in relation to those of the substrate, have not been explained adequately. In fact, in most cases the coating thickness for a certain application was selected empirically through a trial and error procedure. The purpose of this study, therefore, is to address these important issues in light of the experimental evidence and the analytical results. Moreover, recent studies have indicated that even in boundary lubrication the prevailing friction and wear mechanisms are due to plowing and plastic deformation of the

[1] Present address: Department of Mechanical and Industrial Engineering, University of Illinois at Urbana-Champaign, Urbana, IL 61801

Contributed by the Tribology Division for publication in the JOURNAL OF TRIBOLOGY. Manuscript received by the Tribology Division, June 30, 1986

material near the interface [16, 17]. Hence, another aim of this work is to show that surfaces with very low friction and virtually zero wear can be obtained under certain conditions in both lubricated and dry sliding.

2 Experimental Procedures

2.1 Materials and Lubricant. Pure titanium (99.7 percent) and AISI 1095 steel were chosen for this investigation. The primary reason for this choice was the significance of the friction and wear properties of these metals in many sliding applications. A mineral oil, which was rich in naphthenic hydrocarbons, was used in the lubricated experiments. The density of the mineral oil at 298 K was 0.886 g/cm^3 and the kinematic viscosity at 310 and 372 K was 74 and 11 cSt, respectively.

2.2 Sample Preparation. The disk and pin samples were obtained from pure titanium, and AISI 1095 steel rods. The disks were 2.54 cm in diameter, and the pins were 0.635 cm with hemispherically shaped tips of the same diameter. After cutting and machining, the titanium disks were polished with 240 and 600 grit SiC abrasive paper in water. Then the disks and the pins were polished with 0.3 μm α-alumina, cleaned with warm water and soap, and further polished with 0.05 μm γ-alumina to a very smooth surface finish. The steel disk and pin specimens were first polished with 120, 240, and 500 grit abrasive cloth and oil. The samples were then cleaned and polished with 600 grit SiC abrasive paper in water. Finally, the steel samples were polished with 0.3 μm α-alumina and 0.05 μm γ-alumina to obtain a smooth surface finish. Examination of the polished titanium and steel specimens with an optical microscope did not show any embedded SiC or Al_2O_3 particles on the surfaces. After polishing with alumina the samples were cleaned with soap and warm water, rinsed with methanol, dried in air, and stored in a desiccator with Ca_2SO_4 at room temperature. Before each experiment the samples were again rinsed with isopropyl alcohol and dried in air.

The hardnesses of the polished titanium and steel specimens were found to be 3,030 MPa (309 kg/mm^2) and 3,501 MPa (357 kg/mm^2), respectively.

2.3 Coating Procedures. Reactive Sputtered Deposition was used to coat TiN on the specimens. The polished and cleaned titanium and steel specimens were loaded on a flat surface, 15.24 cm in diameter, inside a vacuum system. A high purity titanium target (99.99 percent) of the same diameter was centered above the flat surface and parallel to the surfaces to be coated. The distance between the specimens and the target was 4.5 cm and the specimens were placed within a circle 7.6 cm in diameter.

The chamber was initially evacuated to a pressure of 6.6×10^{-7} Torr and a high purity argon gas (99.995 percent) was admitted at a flow rate of 56.5 cm^3/min. The pressure in the chamber was 10×10^{-3} Torr for the deposition of the thicker TiN coatings and 16×10^{-3} Torr for the others. To obtain good adhesion between the substrate and TiN films the substrates were lightly sputter etched with argon to remove any surface contaminants and particularly any native oxides. The specimens were sputtered for 30 s at 50 W, and the titanium target for 20 min at 500 W. The titanium target was then sputtered for 1 min with argon at 500 W to produce a thin titanium layer, 10-20 nm, on the specimens. The flat surface was tilted by 120 degrees and a mixture of nitrogen and argon (26% N_2 and 74% Ar) at 10×10^{-3} Torr was admitted into the system at a flow rate of 8.6 cm^3/min. The power was then increased to 900 W and the system was left to attain a steady state for about 10 min. Then, the flat surface was brought back to the initial position (i.e., parallel to the target), the power was raised to 950 W (5.2 W/cm^2) and deposition of TiN on the surfaces was initiated. During deposition a voltage of 240 V (bias voltage) was applied to the specimens for cleaning the deposited TiN from N_2 which was not combined with Ti to synthesize TiN. The bias voltage applied to the target was 2,750 V.

After deposition for 15 min, the flat surface was tilted again by 120 degrees and the system was cooled down for 15 min. Then the specimens were brought again below the target and deposition was continued for 15 min before cooling again until the necessary time for deposition was completed. The temperature of the specimens during deposition was less than 473 K. This temperature rise was due to the applied voltage (240 V) and the bombardment of the surfaces with TiN and primarily with free electrons from the titanium target. After coating, the samples were tilted again by 120 degrees, the power and the bias voltage were turned off and the mixture of N_2 and Ar gas was pumped out. Then dry N_2 was admitted into the system, the pressure was equalized to that of the atmosphere and the system was left to cool down for 15-20 min before removing the specimens.

The thicknesses of the TiN films after deposition times of 75, 7.5, and 0.75 min were estimated to be 1, 0.1, and 0.01 μm, respectively. Nevertheless, the actual film thickness was measured with a profilometer as follows. A piece of smooth glass was loaded on the flat surface together with the specimens to be coated. A small piece of Si was placed on the glass surface to prevent deposition of TiN on the area underneath. After coating, the Si piece was removed and the film thickness was measured by obtaining profiles perpendicular to the perimeter of the uncoated glass surface. The measured thicknesses for deposition for 75, 7.5, and 0.75 min were 0.8, 0.2, and 0.02 μm, respectively. The coatings produced were golden yellow in color. Microhardness measurements with a Knoop indenter (load 0.245 N (25 g)) of titanium and steel coated with 0.8 μm TiN yielded a mean value of 20,594 MPa (2,100 kg/mm^2).

2.4 Experimental Details. A pin-on-disk tester was used to conduct the experiments. The disk was mounted on a plate which was rotated at 4.5 rad/s and the pin was held stationary in a holder. The holder was attached to a rigid arm via a flexible ring on which four strain gages were mounted. The tangential (friction) force was measured continuously by the strain gages and a recorder which was balanced and calibrated before each test. Other details of the experimental apparatus are given in reference [16].

The normal load was in the range 0.02 to 2 N, and the sliding distance was between 0.02 and 100 m. The sliding speed was kept low, between 0.87 and 3.53 cm/s, to avoid hydrodynamic effects due to high speeds. All experiments were conducted at room temperature (294 to 298 K) with identical metal pairs and relative humidity 26 to 58 percent.

The wear tracks of the tested samples were observed in a Scanning Electron Microscope (SEM). Characteristic micrographs for each material combination were obtained. An Energy Dispersive X-ray Analyzer (EDAX) was also used to check whether the AISI 1095 steel substrate was exposed during the tests with 0.8 μm thick TiN coatings.

3 Experimental Results

3.1 Friction. The friction coefficients of lubricated titanium surfaces, with and without TiN coatings, slid on themselves are shown in Fig. 1. Figure 1(*a*) shows the friction curves of titanium substrates coated with 0.8 μm thick TiN layers. The coefficient of friction assumed a value of 0.09 with the initiation of sliding and then it remained constant. The friction coefficient was the same even for sliding distances of 150 to 200 m. Almost identical friction values were obtained for normal loads of 0.2 and 2 N.

Figure 1(*b*) shows the friction data of lubricated titanium

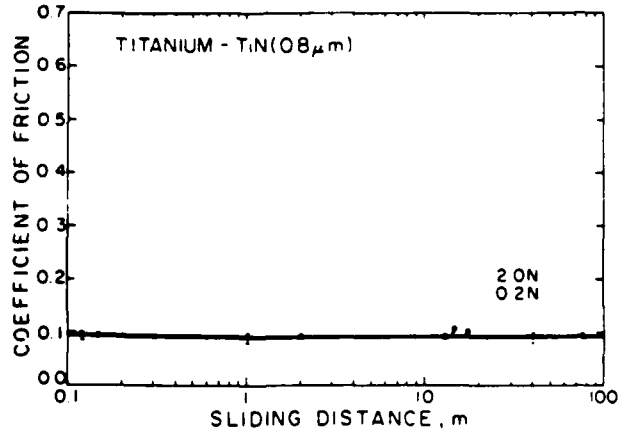

Fig. 1(a)

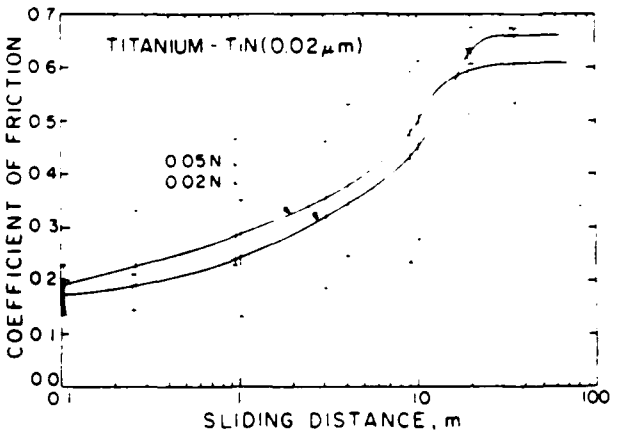

Fig. 1(c)

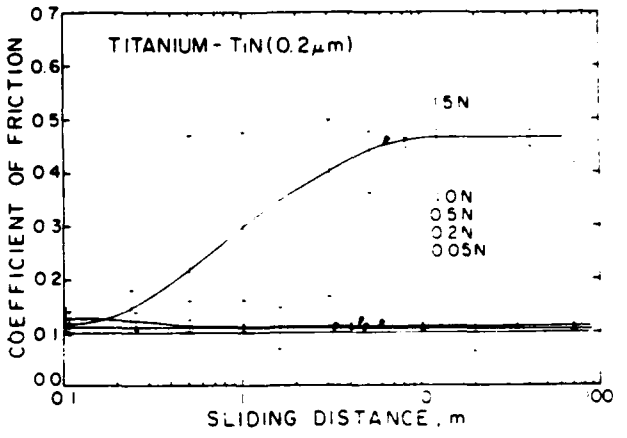

Fig. 1(b)

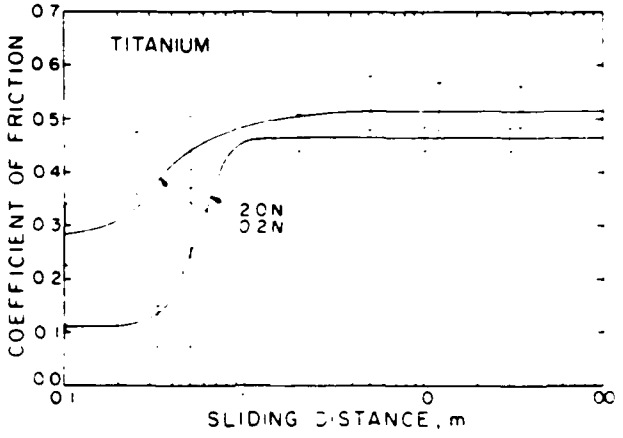

Fig. 1(d)

Fig. 1 Friction coefficient versus sliding distance for titanium coated with: (a) 0.8 μm, (b) 0.2 μm, and (c) 0.02 μm TiN layers; and (d) for uncoated titanium. (Lubricated experiments with identical surfaces.)

with 0.2 μm TiN coatings. The figure shows several friction curves for different loads. A comparison between Figs. 1(*a*) and 1(*b*) indicates that for loads less than or equal to 1 N, the friction values corresponding to the 0.2 μm TiN coatings are only slightly higher than those of the 0.8 μm TiN coatings. However, for relatively heavier loads (e.g., 1.5 N) the coefficient of friction of 0.2 μm TiN increased from an initial value of 0.11 to a steady-state value of 0.46. This marked increase in friction did not occur, however, when the TiN layer was 0.8 μm thick even for 2 N (Fig. 1(*a*)).

Friction coefficient data for titanium with 0.02 μm thick TiN layers are presented in Fig. 1(*c*). An increase of the coefficient of friction from an initial value of about 0.2 to a value in the range 0.55 to 0.65 is evident, even for lighter loads (0.02 and 0.05 N). Much higher friction coefficients resulted when titanium surfaces were slid on themselves. In this case, however, in contrast to the 0.02 μm TiN coated surfaces, the transition from low to high friction was very abrupt. Figure 1(*d*) shows that large friction values, 0.45 to 0.55, have resulted from sliding lubricated titanium on itself for short distances, less than 1 m. These steady-state high friction values for lubricated titanium are similar to those reported in the literature [12].

In order to investigate friction and wear of TiN-coated titanium surfaces in dry sliding, unlubricated experiments with 0.8 μm thick TiN coatings deposited on titanium were conducted. The friction coefficient curves for 0.2 and 2 N normal loads are plotted in Fig. 2. Friction curves from unlubricated titanium for the same loads are also shown for comparison. Low friction coefficients, between 0.1 and 0.2, were initially

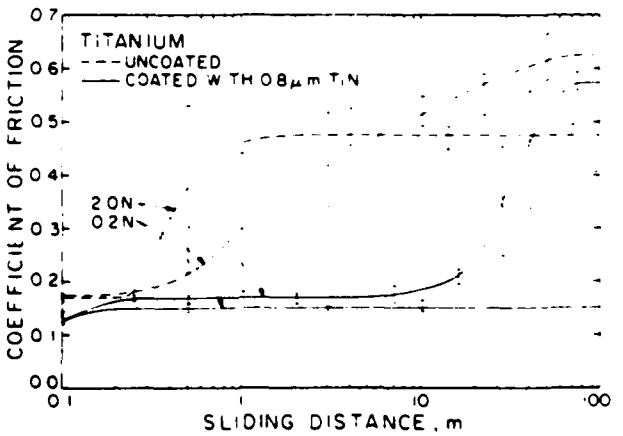

Fig. 2 Friction coefficient versus sliding distance for uncoated and 0.8 μm TiN-coated titanium. (Unlubricated experiments with identical surfaces.)

produced for both coated and uncoated titanium surfaces. But as sliding continued, the coefficient of friction of the uncoated titanium increased rapidly to values larger than 0.45 when a steady-state value was assumed. The transition from low to high friction was abrupt when the load was 2 N and gradual when it was 0.2 N. It is interesting to note, moreover, that lower friction for significant sliding distances was produced with 0.8 μm thick TiN layers. The friction data for a load of 2 N in Fig. 2 show that friction coefficients about 0.16 were obtained for sliding distances less than 15 m. Thereafter the

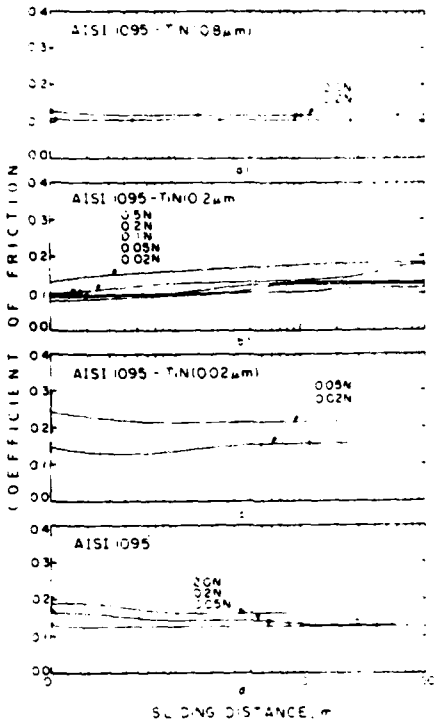

Fig. 3 Friction coefficient versus sliding distance for AISI 1095 steel coated with: (a) 0.8 μm, (b) 0.2 μm, and (c) 0.02 μm TiN layers; and (d) for uncoated AISI 1095 steel. (Lubricated experiments with identical surfaces.)

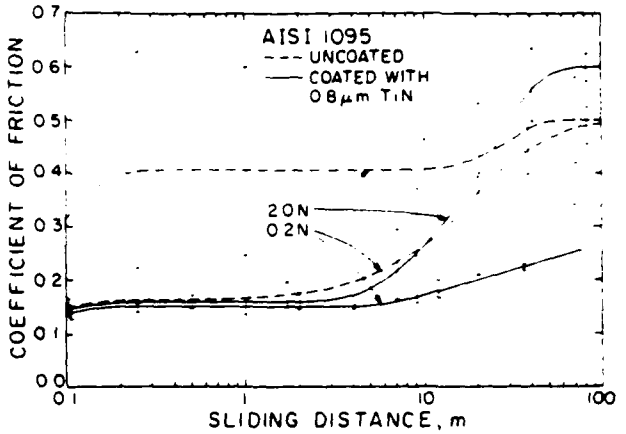

Fig. 4 Friction coefficient versus sliding distance for uncoated and 0.8 μm TiN-coated AISI 1095 steel. (Unlubricated experiments with identical surfaces.)

friction coefficient increased gradually and assumed eventually a steady-state value equal to 0.57. Furthermore, the bottom curve of Fig. 2 demonstrates that a constant friction coefficient of 0.15 may result even for large sliding distances when the load is 0.2 N.

Figures 1 and 2 demonstrate that the friction force between titanium surfaces can be maintained low, when the surfaces are coated with sufficiently thick TiN layers. The experimental data show that the unlubricated friction values are higher by a factor of two than the corresponding lubricated values, but they are very low for unlubricated sliding between similar surfaces. In addition, the results have shown that lubrication affects the transition from low to high friction significantly (e.g., friction curves for 2 N in Figs. 1(*a*) and 2 for coated titanium). Hence, when the sliding interface is lubricated the loads for which low friction is obtained are higher than the corresponding loads for unlubricated interfaces.

Friction data of lubricated AISI 1095 steel, with and without TiN coatings, are shown in Fig. 3. Friction curves of steel substrates with 0.8 μm TiN layers are plotted in Fig. 3(*a*). The values that the coefficient of friction assumes are in the range 0.1 to 0.12, i.e., slightly higher than those of Fig. 1(*a*). But, the friction curves for 0.2 and 2 N are very close.

The coefficient of friction of steel surfaces coated with 0.2 and 0.02 μm thick TiN are shown in Figs. 3(*b*) and 3(*c*), respectively. A comparison of Figs. 3(*a*), 3(*b*), and 3(*c*) indicates that the friction force increases when the thickness of the TiN layer is decreased. For example, the coefficients of friction of the 0.2 and 0.02 μm TiN coatings were in the range 0.09 to 0.19 and 0.13 to 0.29, respectively, i.e., higher than the values obtained with the 0.8 μm TiN coatings. Nevertheless, a transition from low to markedly high friction, such as that shown in Figs. 1(*b*) and 1(*c*) for instance, was not observed for the TiN coated steel. In fact, a gradual increase of friction with the distance slid has taken place (e.g., Fig. 3(*b*)). The primary reason for this discrepancy between titanium and steel substrates coated with identical TiN layers may be attributed to the lower steady-state friction of the lubricated AISI 1095 steel surfaces as opposed to the higher steady-state friction of lubricated titanium (Fig. 1(*d*)). Indeed, Fig. 3(*d*) shows that the coefficient of friction of lubricated AISI 1095 steel assumed initially a value between 0.12 and 0.2, and a steady-state value of 0.12, for loads equal to 0.05, 0.2, and 2 N. These values of the coefficient of friction are significantly lower than the steady-state friction coefficient of lubricated titanium.

As with titanium, unlubricated experiments on steel with 0.8 μm TiN have been conducted and the friction coefficients are shown in Fig. 4, together with the curves of uncoated steel surfaces. It is evident that a transition from a relatively low to a high friction regime resulted in this case. The initial friction coefficient of the coated steel surfaces was about 0.15. However, as sliding continued, it assumed higher values eventually. In particular, when the load was 2 N, the coefficient of friction increased after sliding for about 4 m to a steady-state value of 0.6. For the 0.2 N load, the transition from low to high friction was initiated after 7 m of sliding, but the increase was gradual and the friction values produced were quite lower than those obtained with a load of 2 N after the transition, for the range of sliding distances examined. The friction curves of the uncoated steel surfaces (Fig. 4) indicate that initially low friction, about 0.16, resulted when the load was 0.2 N, but after 2 m of sliding it increased to a steady-state value of 0.5. When the load was 2 N, however, high friction resulted with the onset of sliding (higher than 0.3) and the steady-state value was 0.5. The experimental results of Figs. 2 and 4 clearly indicate that when titanium and steel surfaces are coated with 0.8 μm thick TiN layers remarkably low (especially for unlubricated sliding between similar surfaces) friction coefficients, about 0.15, may be obtained.

3.2 Wear. The tested specimens were observed in a scanning electron microscope and several characteristic micrographs of the surfaces were obtained. It was found that unlike the uncoated surfaces the TiN-coated surfaces for which low friction was maintained did not deform plastically. The surfaces coated with 0.8 μm TiN did not show any evidence of plastic deformation even for normal loads of 2 N when lubricated. Examination of these surfaces at high magnifications did not reveal any change in the initial surface topography even after sliding for 150 to 200 m. The tested surfaces were found to be smooth and shiny just as the coated surfaces. However, plowing and severe plastic deformation of the sliding interfaces, like the uncoated surfaces, occurred when the coefficient of friction was high.

Characteristic micrographs of the steel surfaces coated with 0.8 μm TiN from lubricated experiments are shown in Fig. 5.

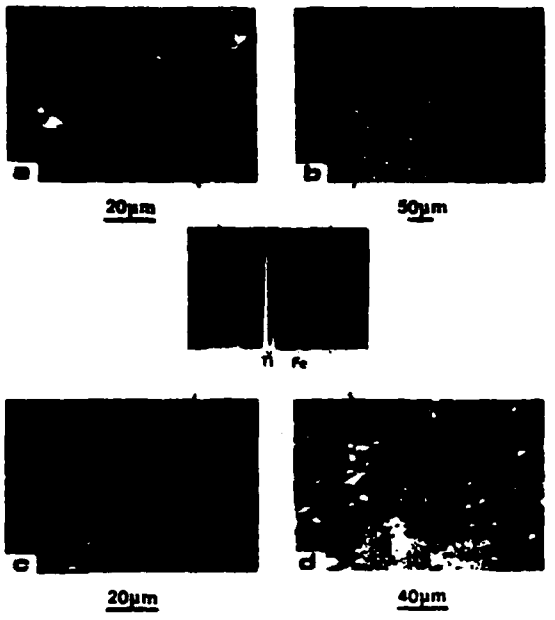

Fig. 5 Wear tracks of lubricated AISI 1095 steel coated with 0.8 μm TIN: (a) disk and (b) pin (load = 0.2 N); (c) disk and (d) pin (load = 2 N).

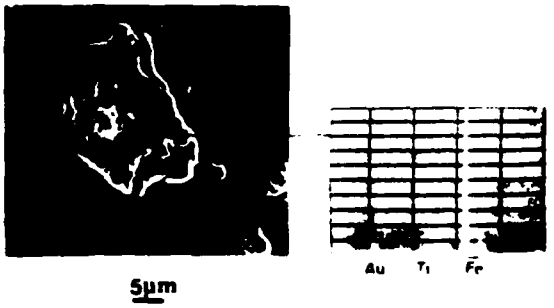

Fig. 6 Patch, rich in iron, on AISI 1095 steel coated with 0.8 μm TIN. (The surface was coated with a thin gold layer, about 0.01 μm, before observation for better resolution.)

Energy Dispersive X-ray Analysis of the surfaces did not show any exposure of the steel substrate. The micrographs indicate that the disk and pin surfaces deformed primarily elastically. Similar observations were made for titanium substrates. Micrographs of the 0.8 μm TiN-coated titanium and steel surfaces obtained before sliding showed identical surface topographies with those in Fig. 5. Examination of the TiN-coated titanium and steel surfaces showed that the 0.8 μm TiN layers were discontinuous. Small patches, rich in iron, where TiN was not successfully deposited were identified on the coated steel surfaces (Fig. 6). These patches may have resulted from material deformation due to the thermal stresses produced during deposition. The bright marks on the surfaces shown in Fig. 5 are patches similar to those of Fig. 6. Nevertheless, the friction coefficients were low and the wear rates were virtually zero.

Insignificant wear rates were also obtained after sliding titanium and steel substrates with 0.02 μm TiN coatings on themselves with loads less than 1 N. Figure 7 shows some characteristic surface topographies obtained from lubricated experiments with titanium coated with 0.2 μm TiN. When the load was 0.02 N the wear of the surfaces was practically insignificant (Figs. 7(*a*) and 7(*b*)). For heavier loads, 0.5 N, the disk surface was slightly polished (burnished), as shown in Fig. 7(*c*), and the pin surface was slightly deformed (Figs. 7(*d*) and 7(*e*)). However, when the load was larger than 1 N, plowing and severe surface damage of both surfaces occurred.

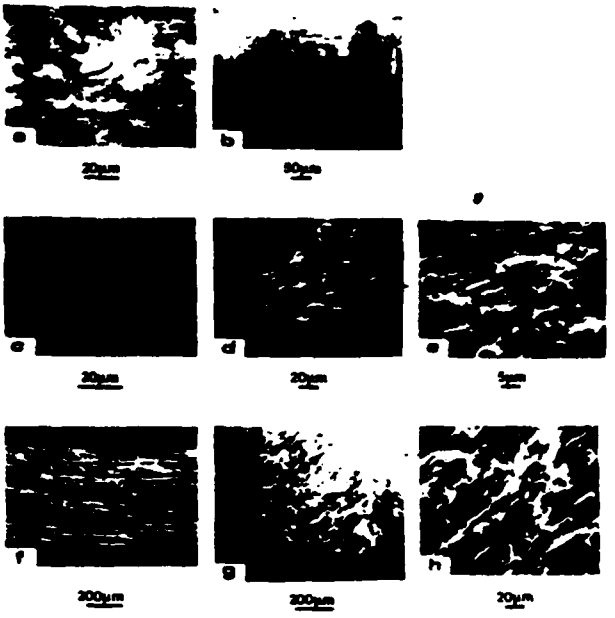

Fig. 7 Wear tracks of lubricated titanium coated with 0.2 μm TiN: (a) disk and (b) pin (load = 0.02 N, distance slid = 45.4 m); (c) disk, (d) pin and (e) higher magnification of a location on the pin surface (load = 0.5 N, distance slid = 88 m); (f) disk, (g) pin and (h) higher magnification of a location on the pin surface (load = 1.2 N, distance slid = 15.7 m).

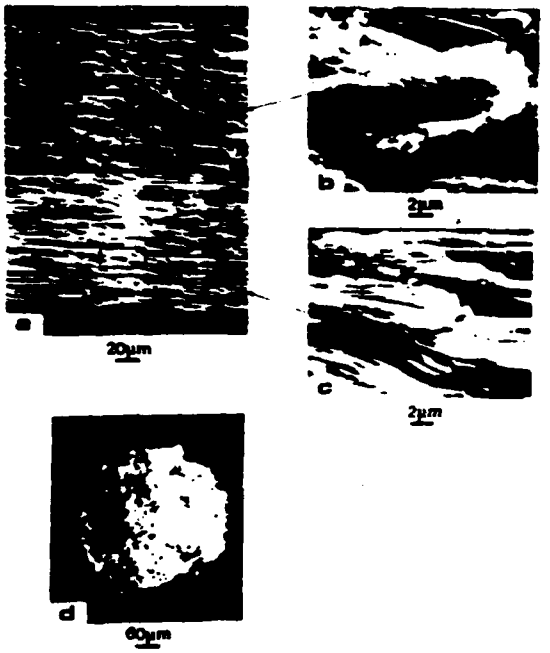

Fig. 8 Wear tracks of lubricated titanium coated with 0.02 μm TiN: (a) disk, (b) and (c) wear sheets on the disk surface, and (d) pin (load = 0.05 N, distance slid = 37.8 m).

Figure 7 (bottom row), for example, shows that plowing and extensive plastic deformation of the surfaces resulted when the load was 1.2 N, although the distance slid was significantly less than the former cases (Figs. 7(*a*) through 7(*e*)). Relatively large wear sheets were found on the wear tracks of the disk and pin surfaces. Figure 7(*h*), for example, shows some typical wear sheets on the pin surface. It is evident that in this case the protective TiN layer was ruptured resulting in high wear rates similar to the uncoated titanium surfaces. Furthermore, the friction coefficient was about 0.46 which is typical for

lubricated titanium surfaces slid on themselves (see Fig. 1(*d*)). Similar observations were made for steel coated with 0.2 μm TiN when the load was increased.

Surface damage and plowing occurred when the thickness of the TiN coating was 0.02 μm, even for light loads (0.02 N). In fact, it was found that plowing grooves were formed on the surfaces at the onset of sliding, probably due to rapid rupture and removal of the thin TiN layer. The micrographs were similar to those obtained from lubricated titanium and steel surfaces slid on themselves. Delamination wear sheets were observed on titanium coated with 0.02 μm TiN even for loads of 0.02 N. Figure 8 shows the disk and pin surfaces of titanium with 0.02 μm TiN coating after sliding for 37.8 m with a load of 0.05 N. Both surfaces have been severely damaged and material lift off (wear sheets) can be observed especially on the disk surface (Figs. 8(*b*) and 8(*c*)). Figure 9 shows the wear tracks of steel disk and pin surfaces coated with 0.02 μm TiN after 45 m of sliding with 0.05 N. Plowing grooves have formed on both surfaces. The micrographs have indicated that when the substrate material was titanium, plowing and plastic deformation were more severe than when the substrate material was steel. This may be attributed to the significantly higher friction coefficient of lubricated titanium which resulted in high tangential surface tractions and thus high wear rates.

Micrographs of titanium and steel surfaces, with and without 0.8 μm TiN coatings, from unlubricated experiments were also obtained. When the load was 0.2 N the surface topography of the TiN-coated titanium surfaces remained smooth and shiny as it was before sliding. When the substrate was of steel, however, burnishing and very fine grooves were observed, especially for large sliding distances. Again, the wear rate in both cases was negligible. Similar observations were made for loads of 2 N for short sliding distances (i.e., when the coefficient of friction was below 0.2). For sliding distances larger than 10 m, however, severe plowing and damage of the surfaces occurred, as with the uncoated surfaces for which plastic deformation was observed with the initiation of sliding even for 0.02 N. Figure 10 shows the wear tracks of titanium surfaces coated with 0.8 μm TiN after the transition of the coefficient of friction from low to high values. It is clear that the surfaces have deformed plastically and large delamination wear sheets have formed on the surfaces (Figs. 10(*b*) and 10(*d*)). The micrographs obtained from TiN-coated steel surfaces when the friction coefficient was high showed extensive plowing of both surfaces. A comparison of the wear tracks of the TiN-coated and uncoated surfaces showed similar surface topographies when the coefficient of friction was high. It may be concluded, therefore, that rupture of the protective TiN layer, especially when the load was 2 N, after sliding for a certain distance resulted in high wear rates similar to those of the uncoated surfaces.

Fig. 9 Wear tracks of lubricated AISI 1085 steel coated with 0.02 μm TiN: (*a*) disk and (*b*) pin (load = 0.05 N, distance slid = 45 m).

4 Analysis and Discussion

The experimental results of this study demonstrate that low friction (especially in dry sliding) and practically zero wear can be obtained when metallic surfaces are coated with sufficiently thick TiN layers. The micrographs of the tested surfaces have shown that the deformation at the sliding contacts is primarily elastic when the TiN layers were not ruptured. In addition, the layer thickness, surface tractions (both normal and tangential) and interfacial "friction" conditions (i.e., lubricated or dry interfaces), were found to affect the efficacy of the TiN-coated surfaces in reducing friction and minimizing surface damage. The experimental evidence has indicated that the same surface topography and low friction coefficients can be obtained even for large sliding distances, provided that plastic deformation or fracture of the coated surfaces is prevented. The state of stresses generated at the solid-solid contacts then is of especial interest.

Analytical solutions for infinite half-space media subjected to normal and tangential surface tractions are well known [18, 19]. The stress field within an isotropic and homogeneous infinite half-space due to a sliding line contact was obtained long ago by Smith and Liu [20], and for a circular sliding contact with hemispherically distributed normal and tangential trac-

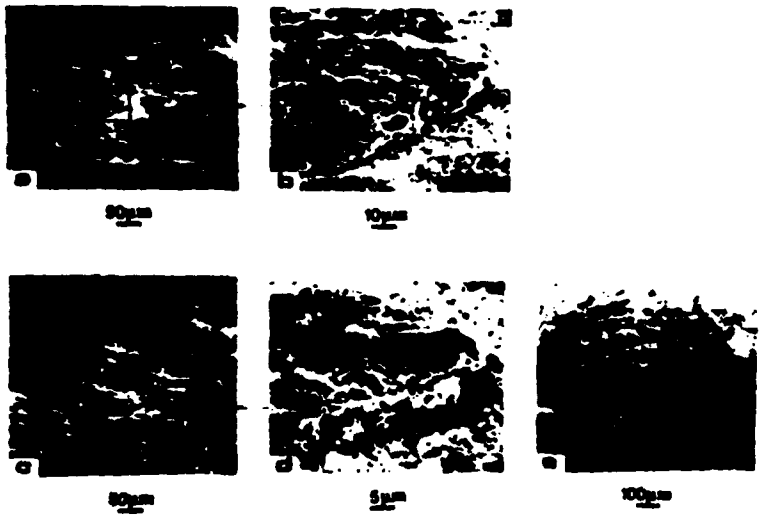

Fig. 10 Wear tracks of unlubricated titanium coated with 0.8 μm TiN: (*a*) disk and (*b*) delamination wear sheet on the disk surface (load = 2 N, distance slid = 67.2 m); (*c*) disk, (*d*) delamination wear sheet on disk, and (*e*) pin (load = 2 N, distance slid = 29 m).

tions by Hamilton and Goodman [21, 22]. The problem of an elliptical contact with elliptically distributed tractions was analyzed by Sackfield and Hills [23, 24], and recently Bryant and Keer [25] have extended the work of Hamilton and Goodman for the general case of an elliptical contact with sticking within the contact region. The literature of contact mechanics between non-conforming surfaces is recently reviewed by Johnson [26]. The main conclusion of these studies is that the maximum value of the von Mises stress moves toward the surface as the friction coefficient is increased.

In the case of thin elastic layers on half-space substrates, the derivation of analytical expressions leads to serious difficulties. The problem of a thin layer on a rigid substrate has been analyzed by Hannah [27], but only the numerical results for the contact pressure were obtained. General solutions to the contact problem of semi-infinite and layered media were derived by Sneddon [28] in terms of Fourier Integral Transforms. However, solution of these integrals requires elaborate numerical computations. Nevertheless, numerical results for a thin layer rigidly adhered to an elastic substrate subjected to surface tractions have shown a rapid decay of the stresses within the layer, when the ratio of the elastic moduli of the layer and the substrate is larger than one and the layer is sufficiently thick [29, 30]. Furthermore, approximate numerical solutions obtained by Gupta and Walowit [31] to the contact problem of a layered elastic solid indented by an elastic cylinder have demonstrated that under certain conditions the solution is non-Hertzian. The complex analytical expressions for the stress field within layered solids, and the tedious numerical computations for solution, call for different type of analyses. Numerical techniques, such as finite element methods, are therefore more appropriate.

4.1 The Finite Element Model. Under the usual plane-strain assumption, sliding at the solid-solid contact can be simulated by a rigid circular cylinder pressed against and traversed on an infinite half-space. Figure 11 shows the finite element mesh of the elastic half-space. The mesh is refined at the center where contact with the rigid cylinder at point O is established initially. The finite element mesh consists of 326 quadrilateral 8-node isoparametric elements and 30 interface elements which are used to detect contact between a nodal point on $\gamma\gamma'$ and the rigid surface. Thus, the solution does not depend on the assumed distribution of the surface tractions or the displacements at the contact, unlike most of the previous finite element analyses. Moreover, the present analysis accounts for interfacial friction; a "friction coefficient" value is assigned to the in erface elements which, in turn, is used for the calculation of the shear tractions at the interface by multiplying the contact normal stress at each node with the preassigned friction value.

The layered half-space is modeled by assuming different elastic properties to the elements of the top rows of the finite element mesh. The rigid cylinder was modeled with a circle, initially tangent to the half space at O, with 28.1 μm radius. The total number of nodes was 1148 and the smallest dimensions of the mesh in the x- and y-directions are of 1 and 0.5 μm, respectively. A 3×3 integration scheme was used for the 8-node elements.

Sliding was simulated by imposing 0.5 μm incremental upward displacements to the nodes of boundary BC followed by 0.5 μm incremental horizontal displacements to the nodes of boundary AB. In order to compare the stresses developed by the same surface tractions within the half-space and layered media, the mesh of the layered surface was moved upwards until the maximum contact pressure assumed a value similar to that obtained for the half-space, but for 0.5 μm vertical displacements. For the vertical displacement of the mesh, only the center node of boundary BC was constrained against lateral displacement. The rest of the nodes on BC were allowed to move along the x-direction to account for the Poisson's effect. The analysis is based on the general purpose finite element code ABAQUS. Numerical results are presented for the area below the contact (detail $\alpha\beta\beta'\alpha'$ in Fig. 11). For simplicity, a Poisson's ratio of 0.3 was assumed in all cases.

4.2 Analytical Results. The Mises equivalent stress contours of a penetrated elastic half-space with interfacial "friction" coefficients $\mu = 0$, 0.1 and 0.5 and ratio of penetration depth to radius of rigid cylinder $d/R = 0.0178$ are shown in Figs. 12(*a*)–12(*c*). Moreover, Fig. 12(*d*) shows the Mises stress contours of a penetrated elastic layered surface with $\mu = 0.1$, $d/R = 0.0089$, elastic modulus ratio of layer to substrate $E_l/E_s = 4$, and ratio of layer thickness to cylinder radius $h/R = 0.142$. The elastic modulus ratio value of 4 is appropriate for hard layers such as TiN and metallic substrates. The interface between the layer and the substrate is represented by the horizontal line in Fig. 12(*d*). Because of symmetry, the stress contours within half of the region $\alpha\beta\beta'\alpha'$ are shown in Fig. 12. In order to compare the stresses below the contact due to penetration by a rigid cylinder loaded with the same load, the above values of d/R were assumed so that the resultant normal force was approximately the same in all cases.

Figure 12(*a*) shows that for a frictionless interface yielding

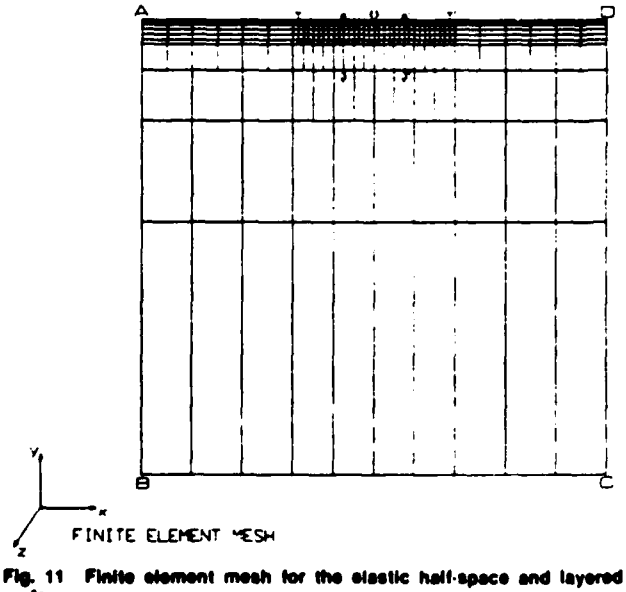

Fig. 11 Finite element mesh for the elastic half-space and layered surfaces

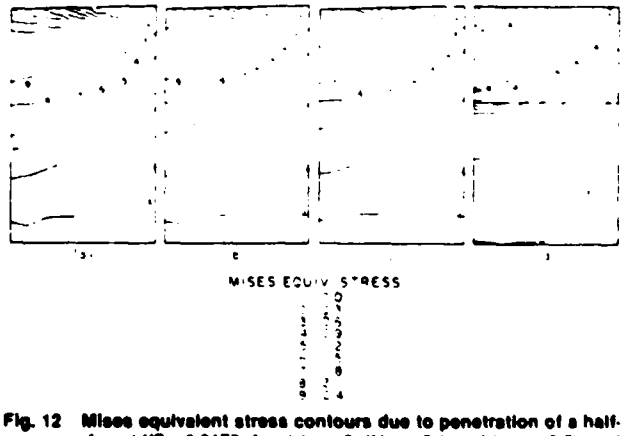

Fig. 12 Mises equivalent stress contours due to penetration of a half-space surface ($d/R = 0.0178$, for: (*a*) $\mu = 0$, (*b*) $\mu = 0.1$ and (*c*) $\mu = 0.5$), and (*d*) penetration of a layered surface ($d/R = 0.0089$, $\mu = 0.1$, $E_l/E_s = 4$ and $h/R = 0.142$). (Stresses are in GPa.)

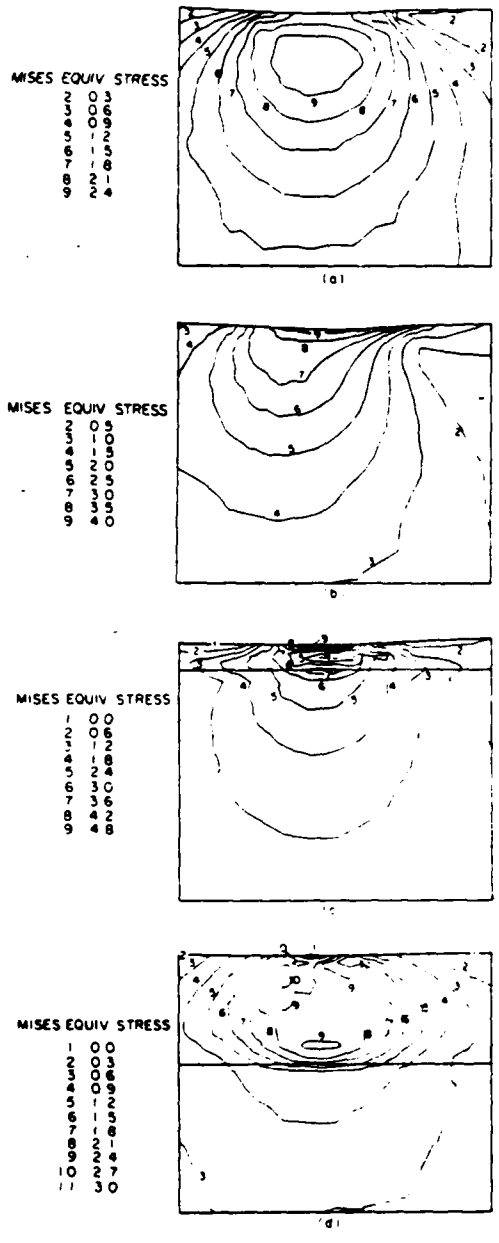

Fig. 13 Mises equivalent stress contours after penetration and sliding of a half-space surface ($d/R = 0.0178$, for: (a) $\mu = 0.1$ and (b) $\mu = 0.5$), and penetration and sliding of a layered surface ($\mu = 0.1$, $E_f/E_s = 4$, for: (c) $d/R = 0.0142$, $h/R = 0.0356$ and (d) $d/R = 0.0089$, $h/R = 0.142$). (Stresses are in GPa.)

will initiate below the surface where the Mises equivalent stress assumes a maximum. Yielding will still initiate below the surface when the interfacial friction is low (Fig. 12(*b*)). However, in this case Mises stresses with higher magnitudes than the frictionless case have arisen near at the interface. The maximum value of the Mises stress occurs closer to the surface as the friction at the interface is further increased (Fig. 12(*c*)). Under these frictional conditions yielding may initiate at the contact interface. Figure 12(*d*), however, indicates that yielding can be made to vanish when a hard layer is rigidly adhered to the substrate. In this case, the Mises equivalent stress assumes the highest value in the layer which has a yield strength significantly higher than the substrate and thus, it can deform elastically. Furthermore, a comparison of Figs. 12(*b*) and 12(*d*) clearly shows that the surface hard layer has resulted in lower stresses in the substrate. In the particular case of TiN layers deposited on titanium and steel, the yield strength of the layer is about an order of magnitude higher than the yield strength of the substrate. Thus, the deformation mode will be elastic provided that the thickness of the layer is sufficient for the stresses to decrease to such magnitudes that yielding in the substrate will vanish.

Under sliding conditions the stresses below the contact increase due to the generated tangential surface tractions, especially when the interfacial friction is high. Figure 13 shows the Mises equivalent stress contours produced from penetration and then sliding of the rigid surface over a half-space with and without a hard layer. The analysis has shown that in all cases the stresses assumed a steady-state after a 0.5 μm horizontal displacement of the nodes on AB. Figure 13(*a*) shows that when $\mu = 0.1$ the Mises stress contours are almost identical with those obtained after penetration (Fig. 12(*b*)). This implies that the elastic stress field does not change noticeably when the coefficient of friction is 0.1 or less, in accord with previous analytical studies. Nevertheless, as Fig. 13(*b*) shows, when $\mu = 0.5$ the stresses are by a factor of 2 approximately higher than the stresses obtained for $\mu = 0.1$. Moreover, the locus of the Mises stress with the highest value has reached the surface. Consequently, when $\mu = 0.5$ yielding should initiate at the surface near the center of contact.

Figures 13(*c*) and 13(*d*) show the Mises stress contours in a layered surface for the case that $\mu = 0.1$ and $E_f/E_s = 4$. The ratio d/R was set equal to 0.0142 and 0.0089 in Figs. 13(*c*) and 13(*d*), respectively, in order for the resultant normal force to be the same with that of the solutions in Figs. 13(*a*) and 13(*b*). Again, the horizontal lines intersecting the stress contours represent the layer-substrate interface. The solutions of Figs. 13(*c*) and 13(*d*) represent cases of relatively thin ($h/R = 0.0356$) and thick ($h/R = 0.142$) hard layers deposited on the same substrate and loaded with similar loads.

It is evident from Fig. 13(*c*) that high stresses have developed in the layer near the contact surface. However, a comparison with Fig. 13(*a*) clearly shows that the Mises stress at and below the interface of the layer and the substrate assumed similar values in both cases, apparently because of the insufficient layer-thickness. Accordingly, the disruption of the 0.02 and 0.2 μm thick TiN layers can be attributed to plastic deformation of the metal substrate near the interface, where the criterion of yielding will be satisfied. By contrast, when the layer is sufficiently thick, Fig. 13(*d*), the stresses can be markedly reduced within the hard layer and thus, yielding in the substrate can be prevented. Under these conditions, both the layer and the substrate will deform elastically. In view of the results of Fig. 13(*d*), the experimental evidence according to which the topography of the 0.8 μm TiN-coated surfaces was the same as before the initiation of sliding can be explained. That is, the 0.8 μm thickness of the TiN layers was sufficient, for the applied surface tractions, to reduce the stresses in the substrate and, consequently, to eliminate yielding at and below the layer-substrate interface.

Figures 12 and 13 demonstrate the significance of the layer thickness, the magnitude of the surface tractions (normal and tangential) and the interfacial friction on the stresses below the contact interface. Moreover, the experimental work has shown that the TiN layers minimized the plowing component of friction resulting, thus, in coefficients of friction in the range 0.1 to 0.15 for both lubricated and dry sliding. The hard layer in this particular case, therefore, not only reduces the stresses in the substrate but it also lowers the magnitude of the frictional tractions. A comparison of the stress fields in Figs. 12(*c*), 12(*d*), 13(*b*) and 13(*d*) clearly shows how significant this could be for the magnitude of the stresses experienced by the substrate. Thus, the interfacial friction (i.e., the magnitude of the interfacial shear stress which may be related to the composition of the materials and the lubricant) plays a significant role on the magnitude of the stresses produced below the

sliding contacts and, thus, it has a marked effect on the tribological properties of the surfaces.

It should be made clear, however, that the primary purpose of the presented finite element analysis is to investigate the initiation of yielding below the contact interface in relation to some critical parameters such as the layer thickness, the coefficient of friction between the half-space surface and the rigid surface, the magnitude of the surface tractions and the mechanical properties of the layer and the substrate. An elastic-plastic analysis of a semi-infinite surface with and without a hard layer will be presented in a forthcoming paper.

In summary, the experimental and analytical work of this study has shown that coating the surfaces with sufficiently thick hard layers may result in elastic deformation at the solid-solid contacts. Under these conditions, low friction and virtually zero wear can be obtained in both lubricated and dry sliding.

5 Conclusions

In light of the experimental and analytical results of this work the following conclusions regarding the role of hard layers in lubricated and dry sliding can be drawn:

(1) Hard layers, such as TiN, can reduce the coefficient of friction of both lubricated and unlubricated surfaces by minimizing plowing and plastic deformation.

(2) The wear rates of the coated surfaces were virtually zero when the hard layer was not deformed plastically.

(3) The finite element analysis and the experimental evidence have verified that the deformation mode at the asperity contacts depends on the layer thickness, the interfacial friction, the magnitude of the surface tractions, and the mechanical properties (such as the modulus of elasticity and hardness) of the hard layer in relation to those of the substrate.

(4) Rupture and removal of the protective hard layer was found to result in high friction, severe damage, and delamination of the sliding surfaces.

Acknowledgments

The work presented in this paper was sponsored by the Office of Naval Research under Contract N00014-82-K-0520. The personal support and encouragement of Dr. A. W. Ruff and Dr. R. S. Miller are appreciated.

References

1 Georges, J. M., and Rabinowicz, E., "The Effect of Film Thickness on the Wear of Hard Electrodeposits," *Wear*, Vol. 14, 1969, pp. 171-180.

2 Hintermann, H. E., "Adhesion, Friction and Wear of Thin Hard Coatings," *Wear*, Vol. 100, 1984, pp. 381-397.

3 Spalvins, T., "Coatings for Wear and Lubrication," *Thin Solid Films*, Vol. 53, 1978, pp. 285-300.

4 Schintlmeister, W., Wallgram, W., Kanz, J., and Gigl, K., "Cutting Tool Materials Coated by Chemical Vapour Deposition," *Wear*, Vol. 100, 1984, pp. 153-169.

5 Su, K.-Y., and Cook, N. H., "Enhancement of High Speed Steel Tool Life by Titanium Nitride Sputter Coating," *Proc. Fifth N. Am. Metalworking Res. Conf.*, University of Massachusetts, Amherst, MA, May 23-25, 1977, SME, pp. 297-302.

6 Henderer, W. E., "Performance of Titanium Nitride Coated High-Speed Steel Drills," *Proc. Eleventh N. Am. Manuf. Res. Conf.*, University of Wisconsin-Madison, Madison, WI, May 24-26, 1983, SME, pp. 337-341.

7 Young, C. T., Becker, P. C., and Rhee, S. K., "Performance Evaluation of TiN and TiC/TiN Coated Drills," *Proc. Int. Conf. on Wear of Materials*, Reston, VA, April 11-14, 1983, ed. Ludema, K. C., ASME, New York, 1983, pp. 235-242.

8 Belmondo, A., and Castagna, M., "Wear-Resistant Coatings by Laser Processing," *Thin Solid Films*, Vol. 64, 1979, pp. 249-256.

9 Dearnaley, G., "Applications of Ion Implantation in Metals," *Thin Solid Films*, Vol. 107, 1983, pp. 315-326.

10 Smidt, F. A., et al., "The Use of Ion Implantation for Materials Processing," NRL Memorandum Report No. 5716, Naval Research Laboratory, Washington, D.C., March 6, 1986.

11 Shepard, S. R., and Suh, N. P., "The Effects of Ion Implantation on Friction and Wear of Metals," ASME JOURNAL OF LUBRICATION TECHNOLOGY, Vol 104, 1982, pp. 29-38.

12 Rabinowicz, E., "Boundary Lubrication of Titanium," *Proc. Fifth World Petr. Congr.*, Vol. 6, Sect. VI-Paper 21, 1958, pp. 319-332.

13 Bair, S., Ramalingam, S., and Winer, W. O., "Tribological Experience with Hard Coats on Soft Metallic Substrates," *Wear*, Vol. 60, 1980, pp. 413-419.

14 Ramalingam, S., and Winer, W. O., "Reactively Sputtered TiN Coatings for Tribological Applications," *Thin Solid Films*, Vol. 73, 1980, pp. 267-274.

15 Jamal, T., Nimmagadda, R., and Bunshah, R. F., "Friction and Adhesive Wear of Titanium Carbide and Titanium Nitride Overlay Coatings," *Thin Solid Films*, Vol. 73, 1980, pp. 245-254.

16 Komvopoulos, K., Saka, N., and Suh, N. P., "The Mechanism of Friction in Boundary Lubrication," ASME JOURNAL OF TRIBOLOGY, Vol. 107, 1985, pp. 452-462.

17 Komvopoulos, K., Suh, N. P., and Saka, N., "Wear of Boundary-Lubricated Metal Surfaces," *Wear*, Vol. 107, 1986, pp. 107-132.

18 Timoshenko, S. P., and Goodier, J. N., *Theory of Elasticity*, Third edition, McGraw-Hill, New York, 1970, pp. 398-420.

19 Mindlin, R. D., "Compliance of Elastic Bodies in Contact," ASME *Journal of Applied Mechanics*, Vol. 16, 1949, pp. 259-268.

20 Smith, J. O., and Liu, C. K., "Stresses Due to Tangential and Normal Loads on an Elastic Solid With Application to Some Contact Stress Problems," ASME *Journal of Applied Mechanics*, Vol. 75, 1953, pp. 157-166.

21 Hamilton, G. M., and Goodman, L. E., "The Stress Field Created by a Circular Sliding Contact," ASME *Journal of Applied Mechanics*, Vol. 33, 1966, pp. 371-376.

22 Hamilton, G. M., "Explicit Equations for the Stresses Beneath a Sliding Spherical Contact," *Proc. Instn. Mech. Engrs.*, Vol. 197C, 1983, pp. 53-59.

23 Sackfield, A., and Hills, D. A., "Some Useful Results in the Classical Hertz Contact Problem," *Journal of Strain Analysis*, Vol. 18, 1983, pp. 101-105.

24 Sackfield, A., and Hills, D. A., "Some Useful Results in the Tangentially Loaded Hertzian Contact Problem," *ibid*, pp. 107-110.

25 Bryant, M. D., and Keer, L. M., "Rough Contact Between Elastically and Geometrically Identical Curved Bodies," ASME *Journal of Applied Mechanics*, Vol. 49, 1982, pp. 345-352.

26 Johnson, K. L., "One Hundred Years of Hertz Contact," *Proc. Instn. Mech. Engrs.*, Vol. 196, 1982, pp. 363-378.

27 Hannah, M., "Contact Stress and Deformation in a Thin Elastic Layer," *Quart. Journ. Mech. and Appl. Math.*, Vol. IV, 1951, pp. 94-105.

28 Sneddon, I. N., *Fourier Transforms*, McGraw-Hill, 1951, pp. 395-415.

29 Barovich, D., Kingsley, S. C., and Ku, T. C., "Stresses on a Thin Strip or Slab with Different Elastic Properties from that of the Substrate Due to Elliptically Distributed Load," *Int. J. Engng. Sci.*, Vol. 2, 1964, pp. 253-268.

30 Ku, T. C., Kingsley, S. C., and Ramsey, J. H., "Stresses in a Thin Slab with Different Elastic Properties from that of the Substrate Due to Distributed Normal and Shearing Forces on the Surface of the Slab," *Int. J. Engng. Sci.*, Vol. 3, 1965, pp. 93-107.

31 Gupta, P. K., and Walowit, J. A., "Contact Stresses Between an Elastic Cylinder and a Layered Elastic Solid," ASME JOURNAL OF LUBRICATION TECHNOLOGY, Vol. 96, 1974, pp. 250-257.

Wear, *107* (1986) 107 - 132

WEAR OF BOUNDARY-LUBRICATED METAL SURFACES

KYRIAKOS KOMVOPOULOS, NAM P. SUH* and NANNAJI SAKA

Department of Mechanical Engineering, Massachusetts Institute of Technology, Cambridge, MA 02139 (U.S.A.)

(Received August 1, 1985; accepted August 20, 1985)

Summary

In the past, the friction and wear of boundary-lubricated metallic surfaces were attributed to adhesion and shearing of lubricants. However, examination of the friction and wear of pure metals lubricated with mineral oil indicates that while the friction coefficient was typical of the values obtained in boundary-lubricated sliding, the predominant wear mechanism was an abrasive-type mechanism. Scanning electron microscopy and surface profilometry revealed many ploughing grooves on the surfaces. These results indicate that the ploughing mechanism may be the predominant factor in controlling friction and wear of boundary-lubricated surfaces. On the basis of slip line field analysis and surface topography statistics an approximate expression for the wear coefficient was derived. It was found that the wear coefficient depends on the sharpness of the surface asperities (or the entrapped wear debris), the interfacial "friction" and the extent of the plastically deformed zone below the surface.

1. Introduction

Wear in boundary lubrication attracted the attention of many investigators in the past and numerous reviews of lubricated wear appeared in the literature [1 - 4]. Most of the investigations, however, focused on the reduction of friction and wear, and little effort was devoted to identify the primary wear mechanism or mechanisms by which boundary-lubricated surfaces wear. Consequently, although many of the published results provide valuable information about the friction and wear of specific materials, a consistent theory for boundary-lubricated wear has not been developed yet.

One of the earliest empirical relations for wear in boundary lubrication was obtained by Burwell and Strang [5] who slid high carbon steel on hardened steel in purified hexadecane. The experimental results of their study showed that the amount of wear was proportional to the distance slid and the normal load, and was independent of the apparent area of contact.

*Present address National Science Foundation, Washington, DC, U.S.A.

0043-1648/86/$3.50

However, for normal pressures larger than one-third of the hardness of the softer material wear increased rapidly.

Rabinowicz [6, 7] has proposed that adhesive wear prevails even in boundary lubrication. Surface asperities were assumed to penetrate through the lubricant film during sliding, forming junctions similar to those formed during unlubricated sliding and resulting in wear particle formation [8]. On the basis of an asperity junction model for wear, Rabinowicz has shown that the ratio of the lubricated wear rate to the unlubricated wear rate is equal to $\bar{\alpha}^{3/2}$, where $\bar{\alpha}$ is a non-dimensional parameter defined by Bowden *et al.* [9] and Bowden and Tabor [10] as $\bar{\alpha} = A_m/A$, with A_m and A representing the metal–metal contact area and the real area of contact respectively.

Rowe [11] suggested that wear particles in boundary lubrication are formed at the metal–metal contacts by an adhesion process similar to that proposed by Archard for dry sliding wear [8], and the actual normal load acting through the metallic contacts was assumed to be equal to $\bar{\alpha}L$, where L is the total normal load. Rowe proposed that the heat of adsorption is the most critical parameter that controls the magnitude of $\bar{\alpha}$. He assumed that

$$\bar{\alpha} \approx \frac{D_m \tau_0}{U} \exp\left(-\frac{E}{RT}\right)$$

where D_m is the diameter of the adsorbed molecule, U is the sliding velocity, τ_0 is the frequency of vibration of the adsorbed molecule, E is the heat of adsorption, R is the molar gas constant and T is the absolute temperature of the surface film. However, this assumption is unrealistic because it assumes that $\bar{\alpha}$ and hence the coefficient of friction, which is a function of $\bar{\alpha}$ [10], depend on the sliding velocity. This argument is in complete disagreement with the experimental evidence according to which the coefficient of friction of boundary-lubricated surfaces is independent of the sliding velocity.

In recent years some important objections to the adhesive wear mechanism and its contribution to wear in boundary lubrication have been raised. It has been suggested that for typical boundary-lubricated conditions weak adhesion between the asperity junctions is expected and, therefore, adhesion cannot be the prevailing wear mechanism [12]. Indeed, recent work on boundary lubrication demonstrated that ploughing of the sliding surfaces occurred at the onset of sliding and that adhesion had a secondary effect [13]. Furthermore, experiments conducted on steels of different microstructures indicated that the hardness alone cannot be used as a measure of wear and that the microstructure has also a significant effect on the wear resistance [14]. In a recent investigation Jahanmir [15] observed that in boundary lubrication wear particles, ranging in size from 1 to 15 μm, are formed primarily by surface deformation, ploughing and delamination of the subsurface. However, under boundary-lubricated conditions, when the surface tractions are too small, crack propagation cannot occur. In this case, as Suh [16] has argued, the wear process due to delamination of the subsurface will be extremely slow and the wear rate will be controlled by the rate of crack

nucleation. Thus a wear particle will form only when a large number of cracks have already been nucleated so that they can link up easily even though the friction coefficient between boundary-lubricated surfaces is low.

Heilman *et al.* [17] studied the formation of wear debris under unlubricated and lubricated conditions and observed that delamination of the base material did not occur. It was found, however, that transfer layers began to develop very early, which finally delaminated to generate wear particles. They proposed that liquid lubricants can reduce wear by dispersing and separating small wear particles before they can accumulate to form transfer layers which may later delaminate forming large wear debris. Under boundary-lubricated conditions, however, the lubricant film is only a few molecules thick and thus dispersion of the wear debris is clearly impossible.

In general, under boundary-lubricated conditions the coefficient of friction assumes values between 0.1 and 0.2 and the wear coefficient is in the range 10^{-6} - 10^{-3}. The conventional approach taken for lubricated sliding is that the friction force arises predominantly from adhesion between the asperity contacts and shearing of the lubricant film. However, the formation of surface ploughing grooves cannot be explained on the basis of these theoretical models. Moreover, a functional relation between the wear coefficient and some important parameters, such as the "interfacial" friction conditions and the sharpness of the surface asperities and wear debris, was not obtained. It was assumed instead that wear occurs in a manner similar to that in dry sliding and on the basis of that assumption empirical relations for the wear coefficient in lubricated sliding were derived.

The purpose of this study therefore is to investigate the primary wear mechanism under boundary-lubricated conditions and to explain it in the light of the experimental results. On the basis of the experimental evidence for the predominant wear mechanism a slip line field analysis is performed and an expression for the wear coefficient is derived.

2. Experimental procedures

2.1. Materials and lubricant

Three metals were used in this investigation: aluminum (99.999% pure), oxygen-free high conductivity (OFHC) copper (99.999% pure) and chromium 125 μm thick electroplated on AISI 1095 steel. The choice of the materials was on the basis of their large range in hardness. Table 1 shows the experimental materials, their hardnesses before and after annealing and the annealing temperatures. In order to avoid complications associated with additive-laden lubricants, a relatively inert additive-free mineral oil was used in the experiments. The density of the mineral oil at 298 K is 0.89 g cm^{-3} and the flash point temperature is 457 K. The viscosity at 310 K is 74 cSt and at 372 K it is 11 cSt.

TABLE 1

Experimental materials

Material	*Hardness* (MPa)		*Temperature of annealing* (K)
	Before annealing	*After annealing in Ar for 1 h*	
Al (99.999% pure)	294 ± 52	186 ± 16	673
OFHC Cu (99.999% pure)	1363 ± 53	510 ± 21	873
Cr (125 μm thick, electroplated on AISI 1095 steel[a])	6590 ± 284		

[a]Hardness, 3500 ± 451 MPa.

2.2. Specimen preparation

Cold-worked aluminum, copper and AISI 1095 steel rods 2.54 cm and 0.635 cm in diameter were used to prepare the specimens. Disks (2.54 cm in diameter and of about the same thickness) and pins (0.635 cm in diameter with hemispherical tips of the same diameter) were cut and machined from the cold-worked rods. Before annealing, the aluminum disks were polished with 600 grit SiC abrasive paper and the copper disks with 240, 320 and 600 grit SiC. The annealed aluminum and copper specimens were polished with 0.3 μm α-Al_2O_3 and 0.05 μm γ-Al_2O_3 to obtain a very smooth surface finish. The specimens finished with alumina were cleaned with warm water and soap, rinsed with distilled water and methanol, dried in air and stored in a desiccator with Ca_2SO_4 at room temperature to protect them from water vapor.

The steel specimens were polished with an abrasive cloth and mineral oil to obtain a smooth surface. Then they were cleaned with warm water and soap, rinsed with methanol and electroplated with chromium, approximately 125 μm thick. The electroplated chromium disks were polished with 320 and 600 grit SiC abrasive paper and 0.3 μm α-Al_2O_3, while the pins were polished with 0.3 μm α-Al_2O_3. All the specimens were then cleaned, as for the aluminum and copper specimens, and stored in a desiccator with Ca_2SO_4 at room temperature.

2.3. Experimental apparatus

Lubricated sliding tests were conducted in air at room temperature using a pin-on-disk tester (Fig. 1). The disks were mounted on a metal plate which was rotated at 4.5 rad s^{-1} (43 rev min^{-1}) and the pin was held stationary in a holder attached to a strain ring. A Plexiglas container was used as a reservoir for the lubricant. At the end of each experiment the loose wear debris and contaminated oil were removed with warm water and methanol. A normal load of 2 N (204 gf) was used for all the experiments, while the sliding velocity was varied between 0.6 and 4.3 cm s^{-1}. These experimental conditions were chosen so that hydrodynamic effects due to light loads

Fig. 1. Experimental apparatus.

TABLE 2

Test conditions

Load	2 N (204 gf)
Angular speed	4.5 rad s^{-1}
Tangential speed	0.6 - 4.3 cm s^{-1}
Distance slid	0.03 - 100 m
Lubricant	Mineral oil
Temperature	≈294 K
Relative humidity	20% - 30%

and/or high sliding speeds did not occur. The experimental conditions are listed in Table 2. The pin and disk specimens used in each test were identical.

2.4. Wear measurements

Because of the very low wear rates, a surface profilometer was used to trace the profile of the worn surfaces in a direction normal to the sliding direction. In order to obtain accurate estimates for the wear volume of the disk specimens at least four profiles, depending on the scatter, were obtained at different locations. The wear volume of each pin was calculated from the diameter of the circular (approximately) worn surface measured with an optical microscope and the radius of the hemispherical tips. The experimental friction and wear data were assumed to follow a normal distribution.

Special attention was devoted to the changes in the surface topography with sliding distance. Thus micrographs of several wear tracks were obtained

for different sliding distances using a scanning electron microscope. An energy-dispersive X-ray analyzer was used after each experiment with chromium to check whether the AISI 1095 steel subsurface was exposed during the wear test.

3. Experimental results

Figure 2 shows some typical profiles of aluminum worn surfaces for various sliding distances. It can be seen that the surface roughness and the width of the wear track increase with sliding distance until a steady state is reached and then they remain almost constant. In Fig. 3 some characteristic surface profiles of copper surfaces are shown. Again, the depth of the wear grooves and the width of the wear track increase with sliding. However, the depth and width of the wear grooves are much smaller than those on the aluminum surfaces. Profiles of worn chromium surfaces are shown in Fig. 4.

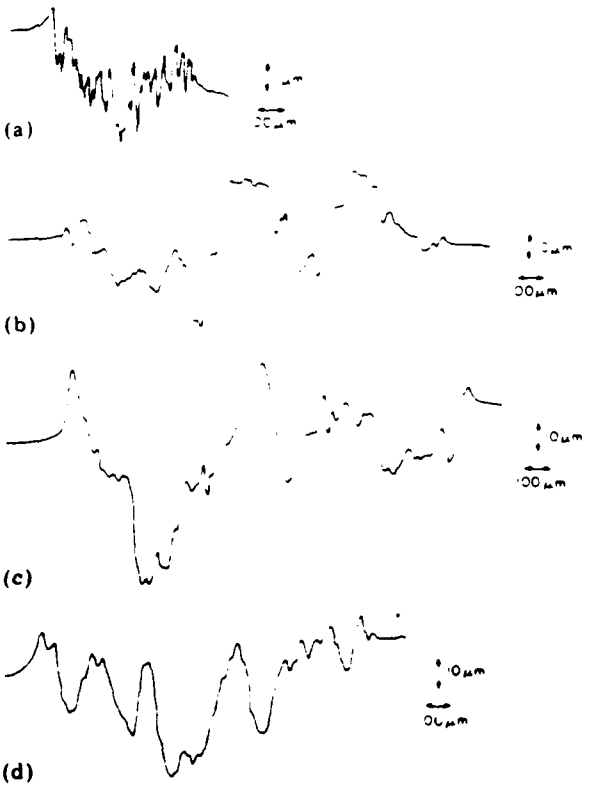

Fig. 2. Surface profiles of the aluminum disk specimens for various sliding distances (lubricated experiment; normal load, 2 N): (a) 0.22 m (10 rev); (b) 7.5 m (260 rev); (c) 60 m (1935 rev); (d) 78 m (2064 rev).

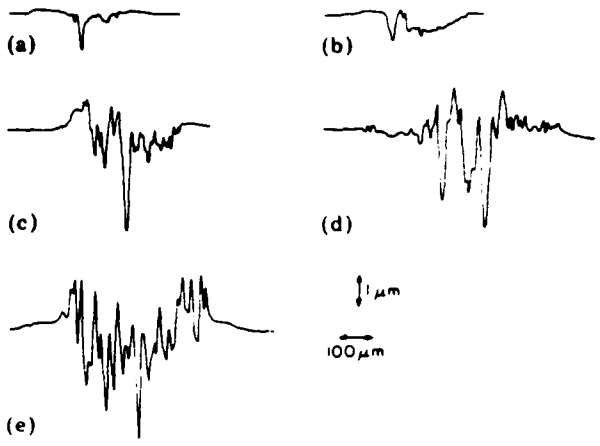

Fig. 3. Surface profiles of the copper disk specimens for various sliding distances (lubricated experiment; normal load, 2N): (a) 0.4 m (10 rev); (b) 3 m (205 rev); (c) 17.5 m (965 rev); (d) 22.5 m (1862 rev); (e) 44 m (1950 rev).

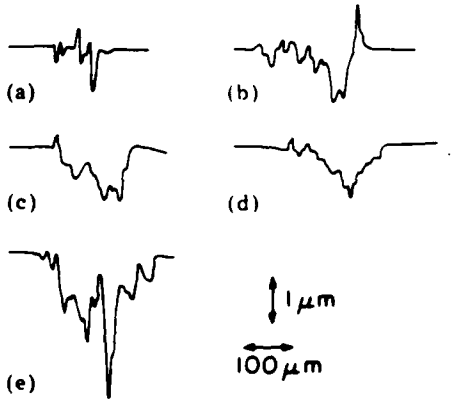

Fig. 4. Surface profiles of the chromium disk specimens for various sliding distances (lubricated experiment; normal load, 2 N): (a) 0.37 m (10 rev); (b) 16 m (440 rev); (c) 30.5 m (1080 rev); (d) 36.2 m (896 rev); (e) 54.4 m (1920 rev).

It can be seen that although the surface topography of the chromium surfaces changes with the distance slid, it does not undergo drastic transitions such as the aluminum and copper surfaces do. Moreover, the depth of the wear grooves and the width of the wear track appear to be much smaller. The surface profiles shown in Figs. 2 - 4 demonstrate that the depth and the width of the wear grooves decrease as the hardness of the surfaces increases.

Table 3 lists the steady state coefficients of friction, the calculated total wear rates and the total wear coefficients, together with their standard deviations, for the materials tested. Aluminum has a coefficient of friction of 0.2 and a wear rate of the order of 10^{-8} cm^3 cm^{-1}, while copper and

TABLE 3

Experimental results[a]

Material	*Coefficient of friction (steady state)*	*Wear rate* ($cm^3\ cm^{-1}$)	*Wear coefficient*	
			Based on annealed hardness	*Based on cold-worked hardness*[b]
Pure Al	0.20 ± 0.02	$(4.3 \pm 2.1) \times 10^{-8}$	$(1.2 \pm 0.6) \times 10^{-3}$	$(2.3 \pm 1.2) \times 10^{-3}$
OFHC Cu	0.17 ± 0.02	$(2.0 \pm 1.1) \times 10^{-9}$	$(1.5 \pm 0.9) \times 10^{-4}$	$(4.0 \pm 2.4) \times 10^{-4}$
Electroplated Cr	0.15 ± 0.01	$(6.6 \pm 2.2) \times 10^{-10}$	$(6.5 \pm 2.1) \times 10^{-4}$	$(8.7 \pm 2.8) \times 10^{-4}$

[a] Normal load, 2 N.
[b] Hardnesses: Al, 343 MPa; Cu, 1372 MPa; Cr, 8820 MPa.

chromium have lower friction coefficients, 0.17 and 0.15 respectively, and wear rates of the order of 10^{-9} cm^3 cm^{-1} and 10^{-10} cm^3 cm^{-1} respectively. The coefficients of friction are similar to those reported in the literature. The results also indicate that the hardness of the sliding surfaces plays an important role in boundary lubrication as well.

Although all the surfaces were highly polished and carefully cleaned before each experiment, ploughing grooves and wear debris formed on the surfaces. More grooves and wear debris were formed as sliding continued. The wear particles either became loose and were removed by the lubricant or adhered to one of the surfaces, ploughing the counterface as they slid on each other. Figure 5(a) and its higher magnification (Fig. 5(b)) show the material which adhered on a chromium pin after sliding on a chromium disk for 0.37 m. The wear debris entrapped at the interface is under a triaxial state of stress and thus can plough and cut the surfaces, forming microchips and new wear debris. Accordingly, the analysis presented later is based on

Fig. 5. (a) Worn surface of a chromium pin (lubricated test; normal load, 2 N; distance slid, 0.37 m (10 rev)). (b) Higher magnification of (a). The arrows show the sliding direction.

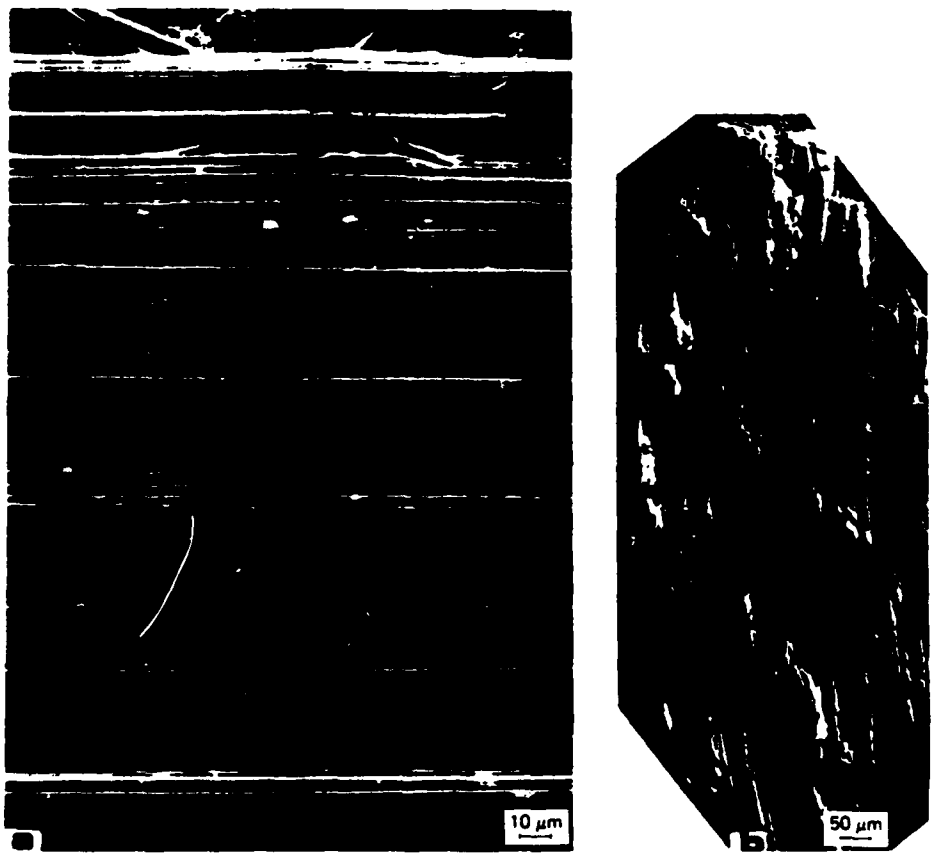

Fig. 6. Wear tracks of the aluminum surfaces (lubricated experiment; normal load, 2 N; distance slid, 0.22 m (10 rev)): (a) disk; (b) pin.

the shape of the wear grooves formed, assuming that the wear particles are rigid in contrast with the plastically deforming surfaces. Some characteristic micrographs of aluminum, copper and chromium surfaces, obtained after 10 rev of sliding, are shown in Figs. 6 - 8.

Figure 6 shows the surface topography of aluminum specimens after 10 rev (0.22 m). Numerous ploughing grooves and wear debris can be observed, especially on the disk surface, and extensive plastic deformation of the pin surface. Figure 7 shows wear tracks of copper specimens obtained after 10 rev (0.4 m). As for aluminum, wear grooves and wear debris have formed on both surfaces. (Figure 7(b) clearly shows two large wear particles which adhered to the pin surface.) Ploughing grooves and wear particle formation can be observed on chromium surfaces after 10 rev (0.37 m) of sliding (Fig. 8). However, the width of the wear track and the number of ploughing grooves are significantly less than those of aluminum and copper surfaces (Figs. 6 and 7). A comparison of the worn surfaces after 10 rev

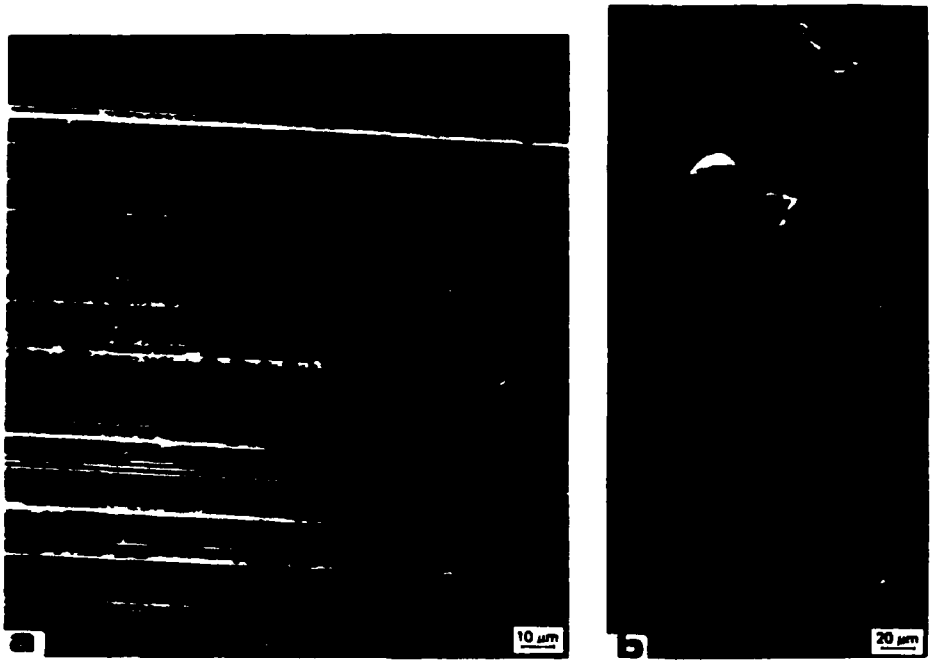

Fig. 7. Wear tracks of the copper surfaces (lubricated experiment; normal load, 2 N; distance slid, 0.4 m (10 rev)): (a) disk; (b) pin.

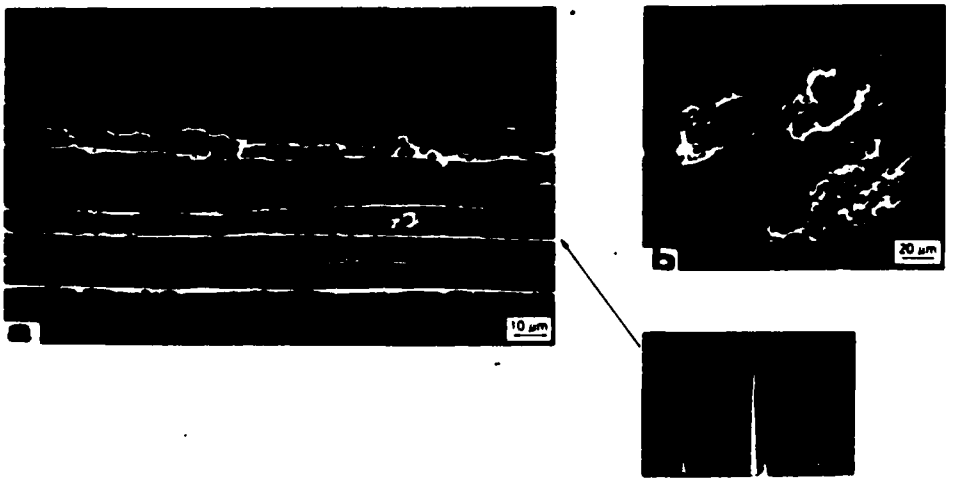

Fig. 8. Wear tracks of the chromium surfaces (lubricated experiment; normal load, 2 N; distance slid, 0.37 m (10 rev)): (a) disk; (b) pin.

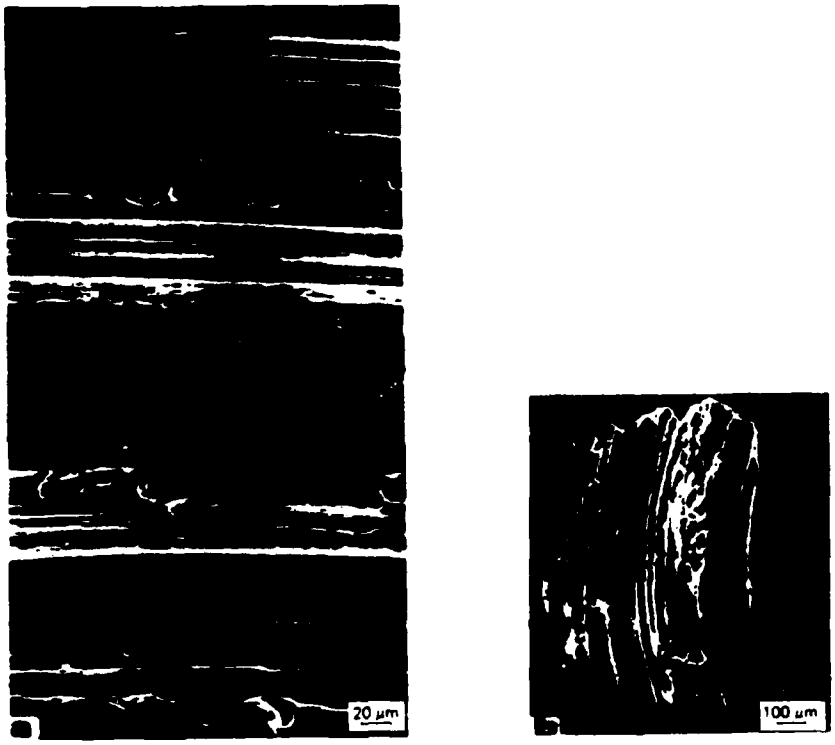

Fig. 9. Wear tracks of the aluminum surfaces (lubricated experiment; normal load, 2 N; distance slid, 83.6 m (2150 rev)): (a) disk; (b) pin.

shows that plastic deformation and wear groove formation on the surfaces can be reduced if the hardness of the sliding pair is increased.

Similar observations were made for the surface topographies after long sliding distances. For instance, Figs. 9 and 10 show the worn surfaces of aluminum and chromium specimens after 2150 rev (83.6 m) and 1900 rev (85.2 m) respectively. It is clear that plastic deformation and wear groove and wear particle formation occurred on all the surfaces, although the hardness of the materials was substantially different.

The experimental results of this investigation illustrate the role of the wear debris in boundary lubrication. The formation of ploughing grooves on highly polished and well-cleaned surfaces immediately after sliding is initiated can be explained only from the ploughing action of the entrapped wear debris. When sliding commences some of the asperity junctions deform plastically and eventually fracture, producing small wear particles and thus initiating an abrasive-type wear mechanism. The wear particles adhere to or indent one of the sliding surfaces and, as a result, ploughing or microcutting of the opposite surface occurs. The observed ploughing grooves and the microcutting action of the wear debris demonstrate that under boundary-

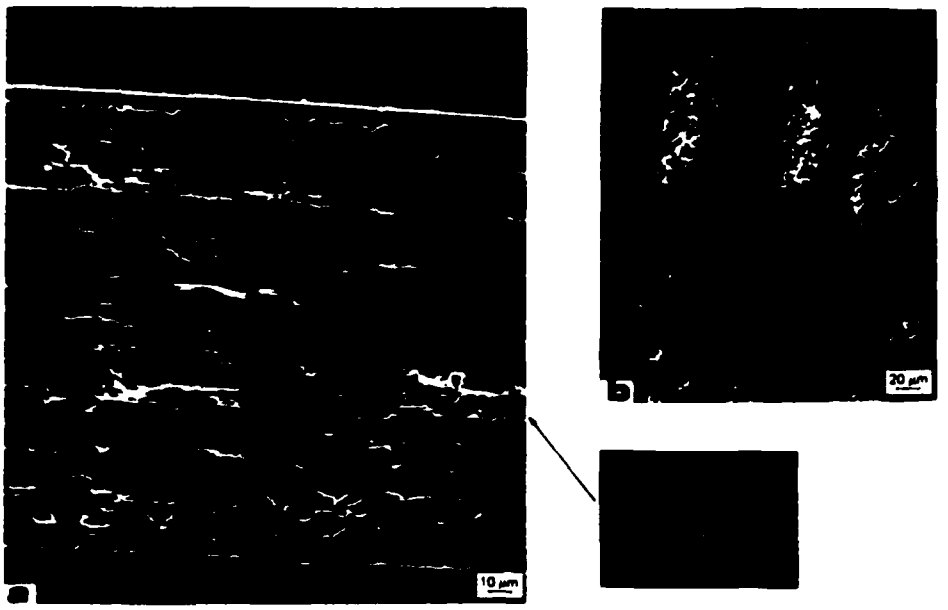

Fig. 10. Wear tracks of the chromium surfaces (lubricated experiment; normal load, 2 N; distance slid, 85.2 m (1900 rev)): (a) disk; (b) pin.

lubricated conditions the primary wear mechanism is an abrasive-type wear mechanism and that adhesion has a secondary contribution to the total wear.

4. Analysis and discussion of the wear mechanism

The experimental work of this investigation clearly demonstrates the important role of the wear debris in the wear of boundary-lubricated surfaces. During sliding, wear particles are formed some of which become entrapped at the sliding interface while the rest are removed by the lubricant. The entrapped wear debris can plough and cut the surfaces as they slide on each other, resulting in groove and microchip formation. Ploughing and microcutting of the surfaces can also result from asperities formed during fragmentation of the ridges along the ploughing grooves. In order to study the ploughing action of the wear particles (or surface asperities) in boundary lubrication it may be assumed that a plane strain slip line solution approximates the ploughing situation fairly well.

It should be noted that there are similarities of metal flow between grinding and abrasion during sliding. Thus the slip line fields proposed for grinding may be adopted for analyzing abrasion as well. A great deal of effort has been devoted in the past to obtain analytical solutions for such complex problems as those in machining operations. However, most of the slip line analyses were performed in an attempt to obtain analytical solutions primarily for machining operations (*e.g.* cutting, drawing, extrusion and

grinding) and very little was done to analyze the abrasion of metals in sliding wear.

On the basis of the ideal plastic behavior of an isotropic material deforming in plane strain, Lortz [18] developed a slip line model for ploughing and cutting conditions. The proposed model accounts for the formation of a dead zone between the plastically deformed material and the penetrating spherical indenter, the interfacial friction conditions and the transition from ploughing to cutting conditions with the formation of a quasi-continuous chip. Although the suggested model seems to be in fair qualitative agreement with the experimental observations (*e.g.* dead zone and chip formation and the shape of the plastic zone) analytical solutions were not obtained and thus comparison with other models and available experimental results is impossible. However, Lortz's analysis sheds much light on the most essential characteristics that a slip line field appropriate for ploughing and cutting conditions must account for.

Rowe and Wetton [19] developed a model for grinding based on the slip line approach, which can also be used to analyze abrasion in sliding if modified to account for interfacial friction. The model predicts a transition from continuous to discontinuous chip formation when the absolute value of the negative rake angle increases up to a critical value. On the basis of the assumed slip line field they derived a semi-empirical expression for the rake angle as a function of the depth of penetration and the height of the material displaced ahead of the truncated wedge. Good correlation was found between the theoretical magnitudes of the critical rake angle and the experimental results obtained from experiments conducted with large-scale model grits sliding on plasticine.

Several slip line solutions for two-dimensional machining were also proposed and discussed by Kudo [20] and some characteristic phenomena observed in actual machining were explained quantitatively under the assumption of a rigid perfectly plastic model. Although most of the proposed models may be appropriate for cutting conditions with positive rake angle tools, the discussed slip line fields for machining with negative rake angles, involving a built-up edge (dead zone) and a pre-pile-up (ridge), were found to be kinematically incompatible (*i.e.* all the velocity boundary conditions were not satisfied simultaneously). Consequently, the accuracy of the suggested slip line models for negative rake angles appears to be fortuitous.

Recently, Challen and Oxley [21] analyzed the friction and wear phenomena on the basis of three different slip line fields, namely the rubbing, wear and cutting models. The rubbing model, however, cannot be employed for analyzing wear because it does not account for material removal. The wear model was proposed for the wear of relatively smooth surfaces but the proposed slip line field does not satisfy the kinematic constraints on the problem. For rough surfaces the cutting model was proposed. This model is kinematically admissible but it assumes that plastic deformation takes place abruptly at a single shear plane and, moreover, it does not account for the plastically deformed material sufficiently ahead of and below the shear plane.

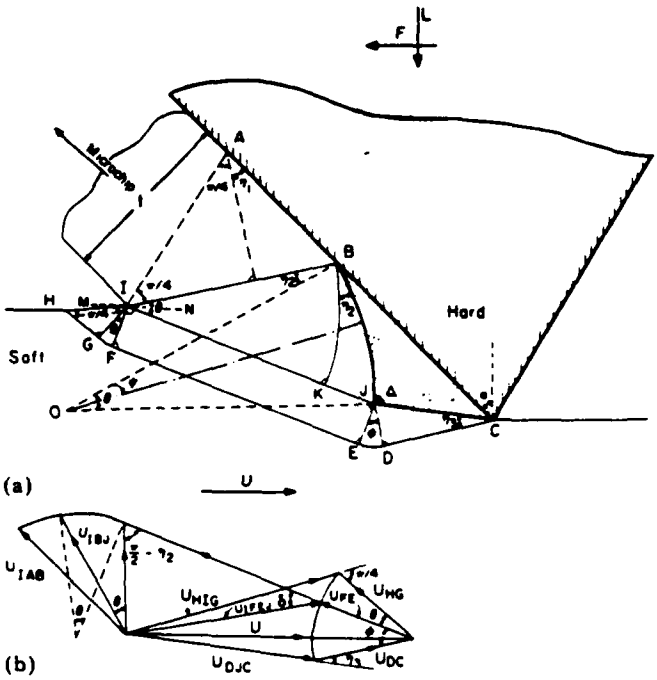

Fig. 11. (a) Slip line field and (b) hodograph.

The slip line model used in this paper is shown in Fig. 11 and is based on the work of Abebe and Appl [22]. Figure 11(a) shows a hard asperity (or wear particle) sliding and cutting a softer material which deforms plastically resulting in microchip formation. The proposed slip line field is kinematically compatible (Fig. 11(b)).

For the geometry shown in Fig. 11(a) the volume wear rate V can be written as

$$V = tU_{AB} \tag{1}$$

where t is the microchip thickness and U_{AB} is the relative velocity between the microchip and the hard asperity.

The microchip thickness t is given by

$$t = \mathrm{AI}\sin\left(\frac{\pi}{4} + \eta_1\right)$$

or

$$t = \mathrm{AB}\,2^{1/2}\cos\eta_1 \sin\left(\frac{\pi}{4} + \eta_1\right) \tag{2}$$

Substituting into eqn. (2) the expression for AB, as given by the first of eqns. (A7), the thickness t may be rewritten as (Appendix A)

$$t = \mathrm{JC}\,\frac{\cos\eta_1\cos(\eta_2+\theta/2)\sin(\beta+\Delta-\alpha)}{\sin\theta\sin(\beta-\alpha-\theta/2)} \tag{3}$$

where the angles β, Δ and θ are given by eqns. (A9), (A10) and (A13) respectively in Appendix A.

Volume conservation requires that the velocity normal to IB must be the same in both fields AIB and JIB. Thus

$$U^{\mathrm{IB}}_{\mathrm{AIB}} = U^{\mathrm{IB}}_{\mathrm{JIB}}\,\frac{\cos\eta_2}{\cos\eta_1}$$

or

$$U^{\mathrm{IB}}_{\mathrm{AIB}} = U^{\mathrm{IJ}}_{\mathrm{JIB}}\,\frac{\cos(\eta_2-\theta/2)\cos\eta_2}{\cos(\eta_2+\theta/2)\cos\eta_1}$$

or

$$U^{\mathrm{IB}}_{\mathrm{AIB}} = U\,\frac{\sin(\eta_1+\theta-\alpha)\cos(\eta_2-\theta/2)}{\cos\eta_1\cos(\eta_2+\theta/2)} \tag{4}$$

where $U^{\mathrm{IB}}_{\mathrm{AIB}} = U_{\mathrm{AB}}$, and $U^{\mathrm{IB}}_{\mathrm{JIB}}$ and $U^{\mathrm{IJ}}_{\mathrm{JIB}}$ are the velocities in JIB on the β lines IB and IJ respectively.

Substituting eqns. (3) and (4) into eqn. (1), the volume wear rate V can be expressed as

$$V = \mathrm{JC}\,\frac{\sin(\eta_1+\theta-\alpha)\cos(\eta_2-\theta/2)\sin(\beta+\Delta-\alpha)}{\sin\theta\sin(\beta-\alpha-\theta/2)}\,U \tag{5}$$

Using eqn. (5) for the volume wear rate, the wear coefficient K can be written as

$$K = \frac{3HV}{LS} = \mathrm{JC}\,\frac{3H}{L}\,\frac{\sin(\eta_1+\theta-\alpha)\cos(\eta_2-\theta/2)\sin(\beta+\Delta-\alpha)}{\sin\theta\sin(\beta-\alpha-\theta/2)} \tag{6}$$

Substituting eqn. (A8) into eqn. (6) and assuming that $H = 6k$, where k is the shear strength, the wear coefficient can be expressed as

$$K = 18\,\frac{\sin(\eta_1+\theta-\alpha)\cos(\eta_2-\theta/2)}{\sin\theta}\left[\frac{2^{1/2}\cos(\eta_2+\theta/2)\cos(\pi/4+\eta_1-\alpha)}{\sin\theta} - \right.$$

$$-\{1+\sin(2\eta_2)\}\sin\left(\beta-2\alpha-\frac{\theta}{2}\right)+\frac{\theta\cos(\beta-2\alpha)}{\sin(\theta/2)}-$$

$$-\{2-\cos(2\eta_2)\}\cos\left(\beta-2\alpha-\frac{\theta}{2}\right)+$$

$$\left.+\frac{\sin(\beta-\alpha-\theta/2)}{\sin(\beta+\Delta-\alpha)}\{(1+2\theta+2\phi)\sin(\beta+\Delta-2\alpha)+\cos(\beta+\Delta-2\alpha-2\eta_3)\}\right]^{-1} \tag{7}$$

It can be seen that the wear coefficient as given by eqn. (7) is a function of the semi-asperity angle α, the shape of the plastic zone and the interfacial shear strength s_j, along AB, BJ and JC, which is a function of the "friction" angles η_j (eqn. (A2)).

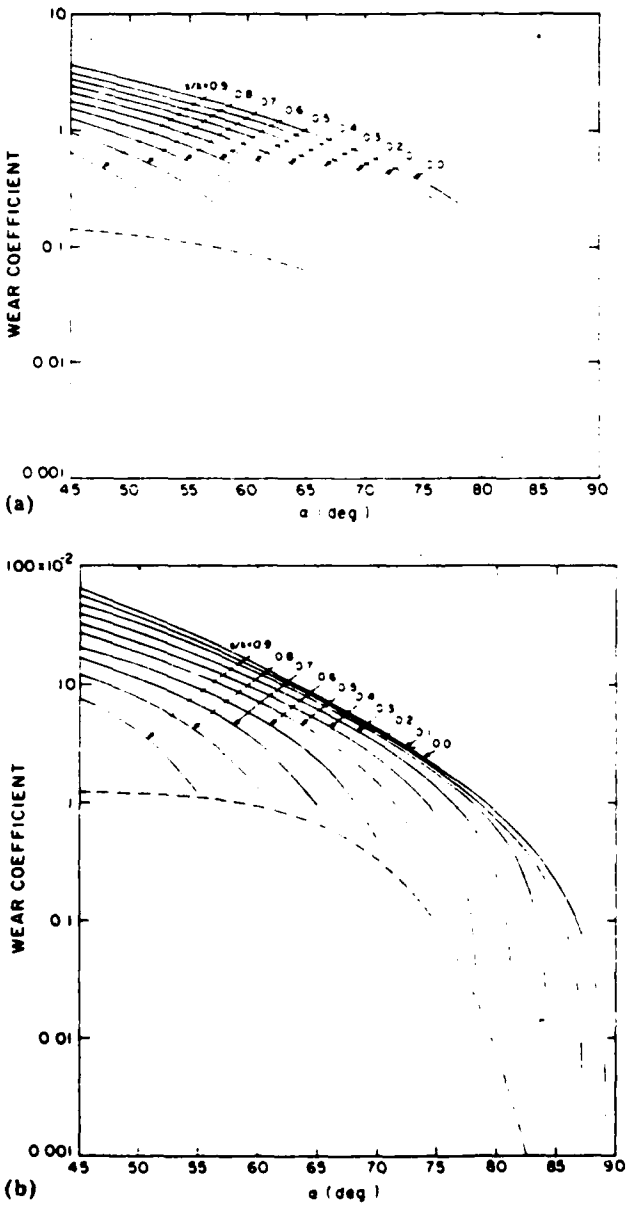

Fig. 12. Slip line solutions for the wear coefficient as a function of the semi-asperity angle α for different interfacial friction conditions: (a) maximum; (b) minimum.

Figures 12(a) and 12(b) show the maximum and minimum magnitudes of the wear coefficient as a function of the angle α when the same friction conditions prevail along the boundaries AB, BJ and JC, *i.e.* $\eta_1 = \eta_2 = \eta_3$. The figure shows that the wear coefficient decreases when the angle α increases. In the case of very sharp asperities (or wear particles) the wear coefficient assumes values of the order of unity while in the case of very blunt asperities it reduces significantly to small magnitudes of the order of $10^{-5} \cdot 10^{-4}$. The results also illustrate the importance of the interfacial shear strength s on the magnitude of the wear coefficient. For a given semi-asperity angle α the wear coefficient increases when the interfacial shear strength decreases and obtains a maximum in the case of "frictionless" interfacial conditions (*i.e.* when $s = 0$). (Incidentally, this provides important insight into abrasive machining: sharp abrasives and lubricants should be used to maximize the material removal rate.) In the particular case of "sticking" at the interface, *i.e.* when $s/k = 1$, the slip line shown in Fig. 11 is not valid. Under boundary-lubricated conditions, however, sticking is unlikely to occur and the ratio s/k assumes values of about 0.1.

Solutions for the wear coefficient may be obtained as long as the geometric conditions, eqns. (A10) - (A14), are satisfied. The broken curves in Figs. 12(a) and 12(b) indicate the limit of the solutions obtained from the proposed slip line field (Fig. 11). Outside the broken curves different slip line fields must be generated. However, under lubricated sliding conditions, the curves for $s/k = 0$, 0.1, 0.2 and 0.3 may be the appropriate curves. Under these interfacial friction conditions solutions for the wear coefficient have been obtained for a large range of the semi-asperity angles α.

Measurements based on the topography of the worn surfaces indicated large variations in the magnitude of the semi-included angle of the surface grooves. This implies that the sharpness of the surface asperities and the entrapped wear debris in general varies over a large range of values. Because the magnitude of the wear coefficient is a strong function of α, as shown in Figs. 12(a) and 12(b), the calculation of wear coefficients on the basis of the mean value of α may not give a realistic estimate. Sharp asperities and acicular wear particles contribute more to wear than do shallow asperities and smooth wear particles. Figure 13 shows the percentage of the grooves with semi-included angles less than α as a function of α. The data points correspond to measurements taken from lubricated worn surfaces obtained from experiments conducted for various sliding distances, but always after the steady state coefficient of friction was reached. It can be seen that the cumulative distribution is different for the materials tested and that the mean value of α shifts towards $\alpha = 90°$ as the material hardness is increased. It is necessary, therefore, that eqn. (7) be modified accordingly to account for the wide variation in α.

Moreover, the analysis presented so far was based on a two-dimensional slip line field analysis. Although this type of analysis is appropriate for predicting forces accurately, it overestimates the volume wear rate because it assumes that all the material that has been ploughed is removed completely.

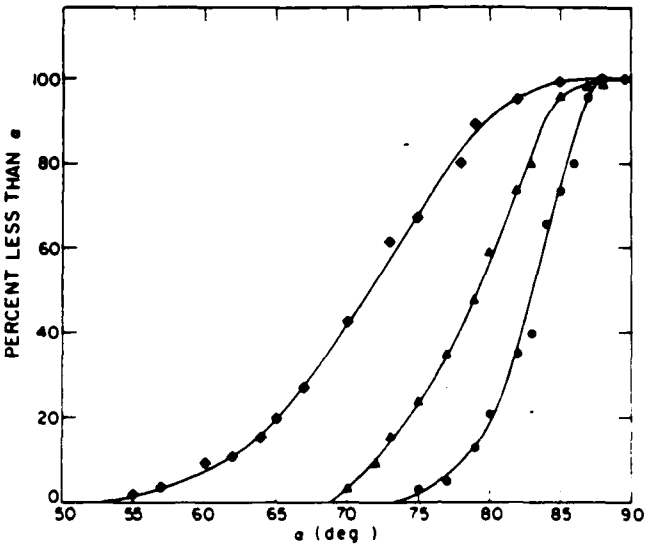

Fig. 13. The percentage of grooves with a semi-included angle less than α as a function of α: ♦, pure aluminum; ▲, OFHC copper; ●, electroplated chromium.

It is well known, however, that only a small proportion of the ploughed material is removed and that the rest deforms plastically resulting in ridge formation. Goddard *et al.* [23] conducted dry sliding experiments of various metals on abrasive papers and observed that less than 10% of the groove volume was removed as wear debris. Avient *et al.* [24] conducted similar experiments and concluded that most of the energy was expended in ploughing and only 10% of the groove volume was removed completely from the surfaces. Stroud and Wilman [25] slid silver on emery paper (mean particle diameter, 5 μm) and estimated the proportion of the total groove volume removed to be about 10%. Experiments conducted by Sin *et al.* [26] with conical diamond tools sliding on AISI 1095 steel showed that the ratio of the volume removed to the calculated groove volume approaches values well below 0.1 for attack angles less than 20°, *i.e.* for $\alpha > 70°$ (Fig. 14). Thus a second modification of the derived expression for the wear coefficient is appropriate to account for the proportion of the groove volume removed.

It can be assumed that the formation of grooves of semi-included angle α is due to the ploughing action of surface asperities (and/or wear particles) with semi-asperity angles α. The normal load dL carried by the asperities of the same angle α is a fraction of the total normal load L and can be expressed as

$$dL = Lf(\alpha)\, d\alpha \tag{8}$$

where $f(\alpha)$ represents the probability density function of asperities with semi-asperity angle α and thus satisfies the following relation:

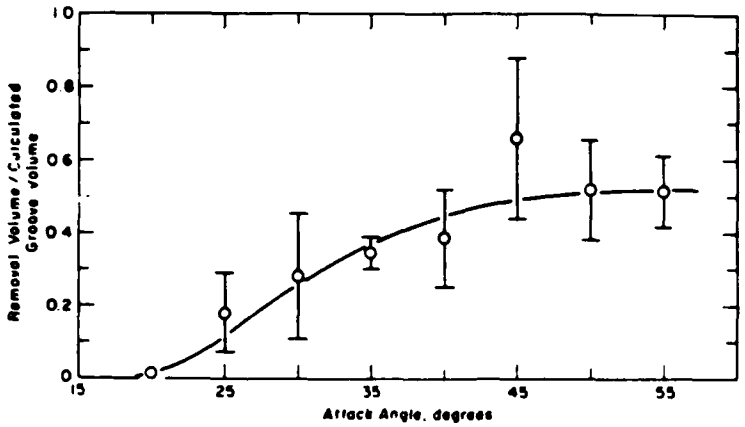

Fig. 14. Ratio of the groove volume removed to the calculated groove volume as a function of the attack angle for AISI 1095 steel [26] (attack angle, $90^\circ - \alpha$).

$$\int_0^{\pi/2} f(\alpha)\, d\alpha = 1$$

The theoretical volume wear rate dV_{th} can be expressed as

$$dV_{th} = K_{th}(\alpha, s/k, \theta, \ldots) \frac{dL\, S}{3H} \tag{9}$$

where $K_{th}(\alpha, s/k, \theta, \ldots)$ represents the theoretical wear coefficient given by eqn. (7).

Substitution of eqn. (8) into eqn. (9) yields

$$dV_{th} = K_{th}(\alpha, s/k, \theta, \ldots) \frac{LS}{3H} f(\alpha)\, d\alpha \tag{10}$$

If dV_a is the actual volume wear rate obtained from grooves with the same semi-included angle α, then

$$dV_a = \xi(\alpha)\, dV_{th} \tag{11}$$

where $\xi(\alpha)$ represents the proportion of the theoretical volume that actually is removed.

If eqns. (10) and (11) are combined the following expression for the actual volume wear rate dV_a is obtained:

$$dV_a = \xi(\alpha) K_{th}(\alpha, s/k, \theta, \ldots) \frac{LS}{3H} f(\alpha)\, d\alpha \tag{12}$$

Integration of eqn. (12) produces the total actual wear volume V_a

$$V_a = \frac{LS}{3H} \int_0^{\pi/2} \xi(\alpha) K_{th}(\alpha, s/k, \theta, \ldots) f(\alpha)\, d\alpha \tag{13}$$

Hence, the actual wear coefficient K_a can be obtained from eqn. (13) by using $K_a = V_a(3H/LS)$ as

$$K_a = \int_0^{\pi/2} \xi(\alpha) K_{th}(\alpha, s/k, \theta, \ldots) f(\alpha)\, d\alpha \tag{14}$$

The probability density function $f(\alpha)$ can be expressed in terms of the fraction $\Delta N/\Delta\alpha$, which represents the asperities of semi-asperity angle α in the range $\Delta\alpha$, and the total number N_T of asperities as follows:

$$\begin{aligned} f(\alpha) &= \frac{d}{d\alpha}\left\{\frac{N(\alpha)}{N_T}\right\} \\ &= \frac{1}{N_T}\frac{dN(\alpha)}{d\alpha} \\ &\approx \frac{1}{N_T}\frac{\Delta N(\alpha)}{\Delta\alpha} \end{aligned} \tag{15}$$

Thus, using eqns. (14) and (15), the actual wear coefficient K_a can be written as

$$K_a \approx \int_0^{\pi/2} \xi(\alpha) K_{th}(\alpha, s/k, \theta, \ldots) \frac{1}{N_T}\frac{\Delta N(\alpha)}{\Delta\alpha}\, d\alpha \tag{16}$$

Table 4 lists the experimental wear coefficients for the tested materials together with the theoretical wear coefficients obtained by numerically integrating eqn. (16). Since appreciable work hardening occurs during the first few revolutions of sliding, the fully cold-worked hardness was used in the calculations of the experimental wear coefficients. The minimum and maximum values of the theoretical wear coefficient K_{th} used in eqn. (16)

TABLE 4

Experimental and theoretical wear coefficients

Material	*Experimental wear coefficient*[a]	*Theoretical wear coefficient*[b]		*Theoretical wear coefficient*[c]	
		Minimum	*Maximum*	*Minimum*	*Maximum*
Pure Al	$(2.3 \pm 1.2) \times 10^{-3}$	4.8×10^{-2}	5.5×10^{-1}	7.7×10^{-3}	7.3×10^{-2}
OFHC Cu	$(4.0 \pm 2.4) \times 10^{-4}$	9.7×10^{-3}	1.6×10^{-2}	9.2×10^{-5}	1.5×10^{-4}
Electroplated Cr	$(8.7 \pm 2.8) \times 10^{-4}$	3.3×10^{-3}	5.5×10^{-2}	2.6×10^{-5}	5.1×10^{-4}

[a] Based on the cold-worked hardness.
[b] For $s/k = 0.1$ and $\xi(\alpha) = 1$.
[c] For $s/k = 0.1$ and $0.005 < \xi(\alpha) < 0.3$.

were obtained for the case that $s/k = 0.1$, which is a reasonable approximation for boundary-lubricated surfaces. The theoretical wear coefficients listed in Table 4 were obtained for $\xi(\alpha) = 1$ and for $\xi(\alpha)$ values in the range 0.005 - 0.3, obtained from Fig. 14 by extrapolation. The agreement between experimental and theoretical wear coefficients is reasonably close.

Figures 12 and 13 clearly show that the wear of boundary-lubricated surfaces can be reduced significantly if hard materials are used. Coating the sliding surfaces with hard layers (*e.g.* oxides and nitrides) may prevent ploughing, thus minimizing the abrasive-type wear mechanism. Indeed, experimental work in progress with titanium nitride (TiN) layers of different thicknesses deposited onto pure titanium and AISI 1095 steel has shown that the wear of the lubricated surfaces was virtually insignificant. Under these conditions most of the solid–solid contacts deform only elastically and the wear is practically zero.

5. Conclusions

On the basis of the experimental results and the plane strain slip line analysis of the present work the following conclusions may be drawn regarding the wear of boundary-lubricated metal surfaces.

(1) During lubricated sliding, wear particles are formed which become entrapped at the interface resulting in ploughing and microcutting of the surfaces.

(2) The magnitude of the experimental coefficient of friction obtained under these ploughing conditions was between 0.1 and 0.2, which is typical of boundary-lubricated sliding.

(3) The predominant steady state mechanism of material removal is an abrasive-type wear mechanism.

(4) On the basis of the slip line analysis and the statistics of the surface topography, an expression for the wear coefficient was obtained. The wear coefficient was found to be a function of the sharpness of the surface asperities and the entrapped wear debris, the interfacial shear strength (lubricant effect) and the shape of the plastic zone.

Acknowledgments

The work presented in this paper was sponsored by the Office of Naval Research under Contract N00014-82-K-0520. The authors are grateful to Dr. A. W. Ruff and Dr. R. S. Miller for their personal support and encouragement.

References

1 E. Rabinowicz, *Friction and Wear of Materials*, Wiley, New York, 1965, pp. 198 - 220.

2 M. B. Peterson, Mechanisms of wear. In F. F. Ling, E. E. Klaus and R. S. Fein (eds.), *Boundary Lubrication: An Appraisal of World Literature*, American Society of Mechanical Engineers, New York, 1969, pp. 25 - 34.

3 W. E. Campbell, Boundary lubrication. In F. F. Ling, E. E. Klaus and R. S. Fein (eds.), *Boundary Lubrication: An Appraisal of World Literature*, American Society of Mechanical Engineers, New York, 1969, pp. 87 - 117.

4 C. N. Rowe, Lubricated wear. In E. R. Booser (ed.), *CRC Handbook of Lubrication, Theory and Practice of Tribology*, Vol. II, *Theory and Design*, CRC Press, Boca Raton, FL, 1984, pp. 209 - 225.

5 J. T. Burwell and C. D. Strang, On the empirical law of adhesive wear, *J. Appl. Phys.*, *23* (1952) 18 - 28.

6 E. Rabinowicz, The relation between friction and wear for boundary-lubricated surfaces, *Proc. Phys. Soc. London, Sect. B*, *68* (1955) 603 - 608.

7 E. Rabinowicz, *Friction and Wear of Materials*, Wiley, New York, 1965, Section 8.3.

8 J. F. Archard, Contact and rubbing of flat surfaces, *J. Appl. Phys.*, *24* (1953) 981 - 988.

9 F. P. Bowden, J. N. Gregory and D. Tabor, Lubrication of metal surfaces by fatty acids, *Nature (London)*, *156* (1945) 97 - 101.

10 F. P. Bowden and D. Tabor, *The Friction and Lubrication of Solids*, Clarendon, Oxford, 1958, pp. 219 - 227.

11 C. N. Rowe, Some aspects of the heat of adsorption in the function of a boundary lubricant, *ASLE Trans.*, *9* (1966) 101 - 111.

12 S. Jahanmir, On the wear mechanisms and the wear equations. In N. P. Suh and N. Saka (eds.), *Fundamentals of Tribology*, Massachusetts Institute of Technology Press, Cambridge, MA, 1980, pp. 455 - 467.

13 K. Komvopoulos, N. Saka and N. P. Suh, The mechanism of friction in boundary lubrication, *J. Tribol.*, *107* (1985) 452 - 462.

14 S. Jahanmir, Wear of AISI 4340 steel under boundary lubrication. In S. K. Rhee, A. W. Ruff and K. C. Ludema (eds.), *Proc. Int. Conf. on Wear of Materials, San Francisco, CA, March 30 - April 1, 1981*, American Society of Mechanical Engineers, New York, 1981, pp. 648 - 655.

15 S. Jahanmir, Wear mechanisms of boundary-lubricated surfaces, *Wear*, *73* (1981) 169 - 184.

16 N. P. Suh, Wear mechanisms: an assessment of the state of knowledge. In N. P. Suh and N. Saka (eds.), *Fundamentals of Tribology*, Massachusetts Institute of Technology Press, Cambridge, MA, 1980, pp. 443 - 453.

17 P. Heilmann, J. Don, T. C. Sun, D. A. Rigney and W. A. Glaeser, Sliding wear and transfer, *Wear*, *91* (1983) 171 - 190.

18 W. Lortz, A model of the cutting mechanism in grinding, *Wear*, *53* (1979) 115 - 128.

19 G. W. Rowe and A. G. Wetton, Theoretical considerations in the grinding of metals, *J. Inst. Met.*, *97* (1969) 193 - 200.

20 H. Kudo, Some new slip-line solutions for two-dimensional steady-state machining, *Int. J. Mech. Sci.*, *7* (1965) 43 - 55.

21 J. M. Challen and P. L. B. Oxley, An explanation of the different regimes of friction and wear using asperity deformation models, *Wear*, *53* (1979) 229 - 243.

22 M. Abebe and F. C. Appl, A slip-line solution for negative rake angle cutting, *Proc. 9th North Am. Manufacturing Research Conf., Pennsylvania State University, University Park, PA, May 19 - 22, 1981*, Society of Manufacturing Engineers, Dearborn, MI, 1981, pp. 341 - 348.

23 J. Goddard, H. J. Harker and H. Wilman, A theory of the abrasion of solids such as metals, *Nature (London)*, *184* (1959) 333 - 335.

24 B. W. E. Avient, J. Goddard and H. Wilman, An experimental study of friction and wear during abrasion of metals, *Proc. R. Soc. London, Ser. A*, *258* (1960) 159 - 180.

25 M. F. Stroud and H. Wilman, The proportion of the groove volume removed as wear in abrasion of metals, *Br. J. Appl. Phys.*, *13* (1962) 173 - 178.

26 H. Sin, N. Saka and N. P. Suh, Abrasive wear mechanisms and the grit size effect, *Wear*, *55* (1979) 163 - 190.

Appendix A

A.1. A slip line analysis for ploughing

Figure 11 shows a slip line field, which is based on the work of Abebe and Appl [A1], with the corresponding velocity field (hodograph) for a hard asperity (or wear particle) cutting a softer surface which is moving with a relative velocity U. Along each α and β line the equilibrium and yield conditions are satisfied. The hydrostatic pressure p and the shear angle Φ are given for each slip line from Henky's equations [A2, A3]

$$p + 2k\Phi = C_1 \qquad (\alpha \text{ line})$$

and (A1)

$$p - 2k\Phi = C_2 \qquad (\beta \text{ line})$$

where C_1 and C_2 are constants. On the basis of eqns. (A1) and Mohr's circle the stresses in each field can be obtained. The triangular fields AIB, IGH and JDC and the rectangular field IFEJ consist of straight α and β lines; therefore the hydrostatic pressure remains constant in each of these fields. However, the sectors GIF, BIK and EJD and the field KBJ are networks of straight and circular orthogonal α and β lines; therefore the hydrostatic pressure is constant only along the same radial line.

Since there are no normal or tangential stresses at the surfaces HI and IA (stress-free surfaces), the α and β lines meet these surfaces at 45°. The angles η_1, η_2 and η_3 that the α and β lines make with the interface ABJC depend on the interfacial shear strength s_j. Hence, from Mohr's circle, the following relations are derived:

$$s_j = k\cos(2\eta_j)$$

or

$$\eta_j = \frac{1}{2}\cos^{-1}\left(\frac{s_j}{k}\right) \qquad j = 1, 2, 3 \qquad \text{(A2)}$$

where 1, 2 and 3 represent the boundaries AB, BJ and JC respectively.

From the given boundary conditions, *i.e.* stress-free surfaces and eqn. (A2), and from Henky's equations and Mohr's circle, the normal and tangential stresses, σ_n and σ_t respectively, along the interface ABJC are as follows: along interface AB,

$$\sigma_n^{AB} = k\{1 + \sin(2\eta_1)\}; \qquad \sigma_t^{AB} = k\cos(2\eta_1) \qquad \text{(A3)}$$

along interface BJ,

$$\sigma_n^{BJ} = k\{1 + 2\psi + \sin(2\eta_2)\}; \qquad \sigma_t^{BJ} = k\cos(2\eta_2) \qquad \text{(A4)}$$

and along interface JC,

$$\sigma_n^{JC} = k\{1 + 2\theta + 2\phi + \sin(2\eta_3)\}; \qquad \sigma_t^{JC} = -k\cos(2\eta_3) \qquad \text{(A5)}$$

The vertical and horizontal forces can be expressed in terms of the slip line angles, the semi-asperity angle α and the interfacial "friction" conditions given by eqn. (A2). The normal force L is given by

$$L = \mathrm{AB}(\sigma_n^{\mathrm{AB}} \sin\alpha + \sigma_t^{\mathrm{AB}} \cos\alpha) +$$

$$+ \mathrm{OB}\left[\int_0^{\theta} \{\sigma_n^{\mathrm{BJ}} \sin(\eta_2 - \eta_1 + \alpha - \psi) + \sigma_t^{\mathrm{BJ}} \cos(\eta_2 - \eta_1 + \alpha - \psi)\}\, \mathrm{d}\psi\right] +$$

$$+ \mathrm{JC}\{\sigma_n^{\mathrm{JC}} \sin(\pi - \Delta - \eta_1 + \eta_2 - \theta + \alpha) - \sigma_t^{\mathrm{JC}} \cos(\pi - \Delta - \eta_1 + \eta_2 - \theta + \alpha)\} \tag{A6}$$

The lengths of AB and OB are related to the length JC through the following trigonometric relations:

$$\mathrm{AB} = \mathrm{JC}\, \frac{\cos(\eta_2 + \theta/2) \sin(\eta_1 - \eta_2 + \theta + \Delta)}{2^{1/2} \cos(\pi/4 - \eta_1) \sin\theta \sin(\eta_1 - \eta_2 + \theta/2)}$$

$$\mathrm{OB} = \mathrm{JC}\, \frac{\cos(\theta/2) \sin(\eta_1 - \eta_2 + \theta + \Delta)}{\sin\theta \sin(\eta_1 - \eta_2 + \theta/2)} \tag{A7}$$

Substitution of eqns. (A3) - (A5) and (A7) into eqn. (A6) and summation gives the following expression for the normal force L:

$$L = \mathrm{JC}k\left\{\frac{\sin(\beta + \Delta - \alpha)}{\sin(\beta - \alpha - \theta/2)}\left[\frac{2^{1/2} \cos(\eta_2 + \theta/2) \cos(\pi/4 + \eta_1 - \alpha)}{\sin\theta} -\right.\right.$$

$$- \{1 + \sin(2\eta_2)\} \sin(\beta - 2\alpha - \theta/2) + \frac{\theta \cos(\beta - 2\alpha)}{\sin(\theta/2)} -$$

$$\left. - \{2 - \cos(2\eta_2)\} \cos(\beta - 2\alpha - \theta/2)\right] + (1 + 2\theta + 2\phi) \sin(\beta + \Delta - 2\alpha) +$$

$$\left. + \cos(\beta + \Delta - 2\alpha - 2\eta_3)\right\} \tag{A8}$$

where

$$\beta = \eta_1 - \eta_2 + \theta + \alpha \tag{A9}$$

At point J the summation of all the angles must be equal to 2π. This condition yields

$$\Delta = \frac{\pi}{2} + \eta_2 + \eta_3 - \phi \tag{A10}$$

Along the discontinuity β line HGFEDC the velocity must be the same. Hence

$$U_{\mathrm{HG}} = U_{\mathrm{DC}}$$

or

$$\phi = \eta_1 + \eta_3 + \theta - \alpha - \sin^{-1}\{2^{1/2}\sin(\pi/4 + \alpha - \eta_1 - 2\theta)\sin\eta_3\} \quad \text{(A11)}$$

and

$$U_{EF} = U_{HG}$$

or

$$\delta = \eta_1 + \theta - \alpha + \tan^{-1}\left\{\frac{2^{1/2}\sin(\pi/4 + \alpha - \eta_1 - 2\theta)\sin(\eta_1 + \theta - \alpha)}{1 - 2^{1/2}\sin(\pi/4 + \alpha - \eta_1 - 2\theta)\cos(\eta_1 + \theta - \alpha)}\right\} \quad \text{(A12)}$$

In order for a microchip to form the material should flow plastically around I. For this flow to happen the angles $H\hat{I}M$, $B\hat{I}N$ and $J\hat{I}N$ must be non-zero. From these constraints the range of θ yields

$$\alpha - \eta_1 < \theta < \frac{1}{2}\left(\frac{\pi}{4} + \alpha - \eta_1\right)$$

and (A13)

$$\theta < \pi/4$$

For a dead zone to form the angle $B\hat{C}J$ must be non-zero, *i.e.*

$$\phi + \frac{\pi}{2} - \eta_1 - \eta_3 > \theta \quad \text{(A14)}$$

These geometric conditions, *i.e.* eqns. (A10) - (A14), must be satisfied in addition to the equilibrium conditions for the slip line field shown in Fig. 11(a) to be valid. The relations (A13) indicate that there can be an infinite number of solutions within the limits set by the relations. However, in the present study solutions were obtained for all the allowed values of θ, set by the relations (A13), and the maximum and minimum wear coefficients were obtained as a function of α and s/k.

References for Appendix A

A1 M. Abebe and F. C. Appl, A slip-line solution for negative rake angle cutting, *Proc. 9th North Am. Manufacturing Research Conf., Pennsylvania State University, University Park, PA, May 19 - 22, 1981*, Society of Manufacturing Engineers, Dearborn, MI, 1981, pp. 341 - 348.

A2 R. Hill, *The Mathematical Theory of Plasticity*, Oxford University Press, London, 1967, pp. 128 - 149.

A3 L. M. Kachanov, *Fundamentals of the Theory of Plasticity*, Mir, Moscow, 1974, pp. 148 - 184.

Appendix B: Nomenclature

C_1, C_2	constants
f	probability density function of grooves (or asperities)
H	hardness

k	shear strength
K, K_{th}	theoretical wear coefficients
K_a	actual wear coefficient
L	total normal load
N	number of grooves (or asperities)
N_T	total number of grooves (or asperities)
p	hydrostatic pressure
s, s_j	interfacial shear strength
S	distance slid
t	microchip thickness
U	velocity
V, V_{th}	theoretical volume wear rate
V_a	actual volume wear rate
α	semi-asperity angle
δ	angle in the hodograph
η_1, η_2, η_3	"friction" angles
θ	angle in the slip line field
ξ	ratio of the volume removed to the calculated wear volume
σ_n	normal stress
σ_t	tangential stress
ϕ	angle in the slip line field
Φ	shear angle in Henky's equations

Subscripts

a	actual
th	theoretical